Durability of GFRP Bars Bond to Concrete under Different Loading and Environmental Conditions

by

Juliana R. Alves

A Thesis submitted to the Faculty of Graduate Studies of

The University of Manitoba

in partial fulfilment of the requirements of the degree of

MASTER OF SCIENCE

Department of Civil Engineering

University of Manitoba

Winnipeg

THE UNIVERSITY OF MANITOBA

FACULTY OF GRADUATE STUDIES

*****

COPYRIGHT PERMISSION

Durability of GFRP Bars Bond to Concrete Under Different Loading and Environmental Conditions

By

Juliana R. Alves

A Thesis/Practicum submitted to the Faculty of Graduate Studies of The University of Manitoba in partial fulfillment of the requirement of the degree

Of

Master of Science

ACKNOWLEDGMENTS

First and foremost I offer my sincerest gratitude to my supervisor, Professor Ehab El-Salakawy, Ph.D., P.Eng., Canada Research Chair in Advanced Composite Materials and Monitoring of Civil Infrastructures in the Department of Civil Engineering at the University of Manitoba, for his encouragement, guidance, support and friendship from the initial to the final moments of my master program.

I am indebted to many of my colleagues, who made this thesis possible by extensively and untiringly helping me throughout my experimental program and theoretical courses. I am heartily thankful to all of them.

I owe my deepest gratitude to Dr. Amr ElRagaby, P.Eng., for his guidance during my work in the laboratory and writing this thesis.

The financial support provided by the Natural Science and Engineering Research Council of Canada (NSERC) through Discovery and the Canada Research Chairs programs is gratefully acknowledged.

I would like to thank Mr. Karl Truderung, P.Eng., and Lafarge Canada Inc., for gently providing material for my research.

I am grateful to the technical staff at the McQuade Heavy Structures Laboratory, Mr. Chad Klowak, P.Eng., and Mr. Grant Whiteside, for their help during the construction and testing of specimens.

I would like to express my sincerest gratitude to Mr. Felipe Tabet, who during the entire Master program provided priceless advices and companionship.

I would like to thank my family for their encouragement and support, which provided the necessary strength to achieve everything in my life. Without their support nothing would be possible.

Finally, to God,

"The LORD is my shepherd; I shall not want

He maketh me to lie down in green pastures: he leadeth me beside the still waters

He restoreth my soul: he leadeth me in the paths of righteousness for his name's sake.

Yea, though I walk through the valley of the shadow of death, I will fear no evil: for thou art with me; thy rod and thy staff they comfort me.

Thou preparest a table before me in the presence of mine enemies: thou anointest my head with oil; my cup runneth over

Surely goodness and mercy shall follow me all the days of my life: and I will dwell in the house of the LORD for ever." Psalm 23

"A righteous man has regard for the life of his animal"

Proverbs 12:10

In memory of my beloved cat "Pretinho" (1987-2009)

ABSTRACT

In the last decade, the non-corrodible fibre reinforced polymer (FRP) reinforcing bars have been increasingly used as main reinforcement for concrete structures in harsh environments. Also, due to its lower cost compared to other types of FRP bars, glass FRP (GFRP) bars are more attractive to the construction industry especially for implementation in bridge deck slabs. Since bridges directly sustain repeated moving wheel loads they are more susceptible to fatigue effects. Furthermore, bridge deck slabs are the bridge components which are the most exposed to temperature-induced stresses, which can be a major concern in regions of drastic temperature changes such as freeze-thaw cycles. FRP-reinforced concrete elements are subjected to greater damage due to temperature changes because of the mismatched thermal properties between FRP bars and concrete. In addition, sustained loads may also damage the bond between FRP bars and concrete and can lead to an unexpected increase of the required anchoring length. This research investigates the influence of freeze-thaw cycles along with sustained axial load, fatigue loading or a combination of both conditionings on the bond characteristics and behaviour of GFRP bars embedded in concrete. An FRP-reinforced concrete specimen was developed to apply axial load to FRP bars within the concrete environment. A total of thirty-six specimens were constructed and tested. The test parameters included bar diameter, concrete cover thickness and loading and/or environmental conditioning. After conditioning, each specimen was sectioned into two halves for pullout testing. Test results are presented in terms of bond-slip relationships and ultimate pullout strength. Development lengths are calculated considering the obtained bond strength values, and compared with standards.

Keywords: GFRP reinforcement; Bond Strength; Concentric and Eccentric Pullout Test; Freeze/Thaw cycles, Fatigue loading, Sustained loading

TABLE OF CONTENTS

Acknowledgments i

Abstract iv

Table of Contents v

List of Tables viii

List of Figures x

List of Symbols xiv

List of Abbreviations xvi

CHAPTER 1: INTRODUCTION 1

1.1.Overview 1

1.2.Research Objectives and Originality 3

1.3.Methodology 5

1.4.Thesis Outline 5

CHAPTER 2: LITERATURE REVIEW 6

2.1. Introduction to FRP Composite Materials 6

2.1.1. Constituent materials 6

2.1.1.1. Matrix 7

2.1.1.2. Fibre 8

2.1.2. General overview of FRP bars 9

2.2. Bond of FRP Bars 12

2.2.1. Definition of bond 12

2.2.2. Mechanisms of bond transfer 16

2.2.3. Techniques to improve bond resistance 17

2.2.4. Parameters influencing bond strength 19

2.2.4.1. Effect of confining pressure 20

2.2.4.2. Effect of bar diameter 21

2.3. Methods for Bond Evaluation 22

2.3.1. Mechanisms of bond failure 29

2.4. Durability Issues 33

2.4.1. Creep, relaxation and sustained loads 35

2.4.2. Freeze-thaw cycles 37

2.4.3. Fatigue loading 38

2.4.4. Freeze-thaw cycles along with sustained load 39

2.5. Code Review 40

2.5.1. Concrete cover 40

2.5.2. Fatigue levels 41

2.5.3. Sustained loads level 41

2.5.4. Development length 42

CHAPTER 3: EXPERIMENTAL PROGRAM 46

3.1. General 46

3.2. Material Properties 47

3.3. Details of Specimens 50

3.4. Test Parameters 56

3.5. Construction and Curing of Specimens 58

3.6. Conditioning 59

3. 6.1. Sustained loading 59

3. 6.2. Freeze-thaw cycles 62

3. 6.3. Fatigue loading 64

3.7. Test set-up and procedure 65

CHAPTER 4: ANALYSIS OF EXPERIMENTAL RESULTS 67

4.1. Pullout Results 67

4.2. Failure Modes 91

4.3. Development Length Analysis 99

CHAPTER 5: SUMMARY AND CONCLUSIONS 110

5.1. Summary 110

5.2. Conclusions 111

5.3. Recommendations for Future Work 116

REFERENCES 117

APPENDICES 126

Appendix A – Temperature and Strains due to Freeze-Thaw Conditioning A-1

Appendix B - Analytical Investigation B-1

LIST OF TABLES

TABLE 2.1: Mechanical properties of resins 7

TABLE 2.2: Mechanical properties of fibres 8

TABLE 2.3: Physical properties of fibres 9

TABLE 2.4: Mechanical properties of FRP and steel bars 10

TABLE 2.5: Linear coefficients of thermal expansion 11

TABLE 2.6: Concrete clear cover specification 40

TABLE 2.7: Fatigue limits 41

TABLE 2.8: Modification factors 45

TABLE 3.1: Proportions of concrete mixture for 1 m^3 47

TABLE 3.2: Properties of GFRP bars 49

TABLE 3.3: Test parameters 56

TABLE 4.1: Summary of results from Series I 84

TABLE 4.2: Summary of results from Series II 85

TABLE 4.3: Summary of results from Series III 85

TABLE 4.4: Summary of results from Series IV 86

TABLE 4.5: Summary of results 87

TABLE 4.6: Summary of increase and residual strains per specimen 89

TABLE 4.7: Average of increase and residual strains 90

TABLE 4.8: Mode of failure of concentric specimens in Series I 94

TABLE 4.9: Summary of failure modes 94

TABLE 4.10: Summary of development lengths for Series I to IV 99

TABLE 4.11: Analysis of development length for Series II and IV 104

TABLE A.1: Cylinders: Series I A-5

TABLE A.2: Cylinders: Series II A-5

TABLE A.3: Cylinders: Series III A-5

TABLE A.4: Cylinders: Series IV A-6

TABLE B.1: Calculated bond strength: Series I B-3

TABLE B.2: Calculated bond strength: Series II B-4

TABLE B.3: Calculated bond strength: Series III B-6

TABLE B.4: Calculated bond strength: Series IV B-7

LIST OF FIGURES

Fig. 2.1: Stress versus strain relationship for GFRP and steel bars 9

Fig. 2.2: Equilibrium of forces 12

Fig. 2.3: Stress field in static pullout tests 13

Fig. 2.4: Beam: stress distribution in steel, in concrete and bond stress 15

Fig. 2.5: Splice: detail of the bond distribution 15

Fig. 2.6: Pullout specimen: stress in steel (left) and bond stress (right) 15

Fig. 2.7: Standard pullout specimen 23

Fig. 2.8: Pullout test layout 1 24

Fig. 2.9: Pullout test layout 2 24

Fig. 2.10: Pullout test: stress configuration 25

Fig. 2.11: Difference between loaded and free-end slip 27

Fig. 2.12: Bond stress versus free-end slip curve of monotonically loaded bars 28

Fig. 3.1: Experimental program scheme 46

Fig. 3.2: GFRP bar 48

Fig. 3.3: Series I: specimen details 51

Fig. 3.4: Series II to IV: specimen details 53

Fig. 3.5: Series II to IV: specimen construction 55

Fig. 3.6: Concrete mixer 58

Fig. 3.7: Material preparation 58

Fig. 3.8: Detail of steel anchors and bond breakers in Series I 59

Fig. 3.9: Curing process, with wet burlap sheets 59

Fig. 3.10: Sustained loading set-up: side view 60

Fig. 3.11: Sustained loading set-up: top view and specimen under sustained load 60

Fig. 3.12: Details of prestressing 61

Fig. 3.13: Specimens inside environmental chamber 63

Fig. 3.14: Details of fatigue test 64

Fig. 3.15: Details of pullout test set-up 65

Fig. 4.1: Effect of conditioning: bar No. 16 and concrete clear cover of 1.5 d_b 68

Fig. 4.2: Effect of conditioning: bar No. 16 and concrete clear cover of 2.0 d_b 69

Fig. 4.3: Effect of conditioning: bar No. 16 and concrete clear cover of 2.5 d_b 69

Fig. 4.4: Effect of conditioning: bar No. 19 and concrete clear cover of 1.5 d_b 70

Fig. 4.5: Effect of conditioning: bar No. 19 and concrete clear cover of 2.0 d_b 70

Fig. 4.6: Effect of conditioning: bar No. 19 and concrete clear cover of 2.5 d_b 71

Fig. 4.7: Effect of bar diameter: Series I and concrete clear cover of 1.5 d_b 72

Fig. 4.8: Effect of bar diameter: Series I and concrete clear cover of 2.0 d_b 72

Fig. 4.9: Effect of bar diameter: Series I and concrete clear cover of 2.5 d_b 73

Fig. 4.10: Effect of bar diameter: Series II and concrete clear cover of 1.5 d_b 73

Fig. 4.11: Effect of bar diameter: Series II and concrete clear cover of 2.0 d_b 74

Fig. 4.12: Effect of bar diameter: Series II and concrete clear cover of 2.5 d_b 74

Fig. 4.13: Effect of bar diameter: Series III and concrete clear cover of 1.5 d_b 75

Fig. 4.14: Effect of bar diameter: Series III and concrete clear cover of 2.0 d_b 75

Fig. 4.15: Effect of bar diameter: Series III and concrete clear cover of 2.5 d_b 76

Fig. 4.16: Effect of bar diameter: Series IV and concrete clear cover of 1.5 d_b 76

Fig. 4.17: Effect of bar diameter: Series IV and concrete clear cover of 2.0 d_b 77

Fig. 4.18: Effect of bar diameter: Series IV and concrete clear cover of 2.5 d_b 77

Fig. 4.19: Average bond strength versus concrete clear cover; bar No.16; for the centric placement of the bar, two out of three points where considered 78

Fig. 4.20: Average bond stress versus concrete clear cover (d_b); bar No.19; for the centric placement of the bar, two out of three points where considered 79

Fig. 4.21: Bond strength versus concrete clear cover – all series 81

Fig. 4.22: Average peak slip 82

Fig. 4.23: Average increase and residual strains in specimens 88

Fig. 4.24: Mode of failure of specimens is Series I 92

Fig. 4.25: Failure mode of specimens with bar No. 16 95

Fig. 4.26: Mode of failure of specimens with bar No. 19 96

Fig. 4.27: After pullout test: sand-coating detachment 98

Fig. 4.28: Development length versus concrete clear cover; Series II and bar No. 16 101

Fig. 4.29: Development length versus concrete clear cover; Series IV and bar No. 16 101

Fig. 4.30: Development length versus concrete clear cover; Series II and bar No. 19 102

Fig. 4.31: Development length versus concrete clear cover; Series IV and bar No. 19 103

Fig. 4.32: Factor k_6 versus concrete clear cover: Series II 105

Fig. 4.33: Factor k_6 versus concrete clear cover: Series IV 105

Fig. 4.34: Development length versus concrete clear cover: Series II and bar No. 16 106

Fig. 4.35: Development length versus concrete clear cover: Series IV and bar No. 16 107

Fig. 4.36: Development length versus concrete clear cover: Series II and bar No. 19 107

Fig. 4.37: Development length versus concrete clear cover: Series IV and bar No. 19 108

Fig. 4.38: Development length versus concrete clear cover: Series IV and bar No. 19 109

Fig. A.1: Specimen behaviour under freeze-thaw cycles at 21 to 26 days of conditioning A-1

Fig. A.2: Concrete deterioration: Series III A-2

Fig. A.3: Concrete deterioration: Series IV A-3

Fig. A.4: Cylinders deterioration A-4

Fig. A.5: Testing of conditioned cylinders A-4

Fig. B.1: Stresses at failure; plastic stage B-1

Fig. B.2: Stresses at failure – simplified model; partly cracked behaviour B-2

Fig. B.3: Crack pattern of specimens in Series I B-3

Fig. B.4: Crack pattern of specimens in Series II B-4

Fig. B.5: Crack pattern of specimens in Series III: bar No. 16 B-5

Fig. B.6: Crack pattern of specimens in Series III: bar No. 19 B-5

Fig. B.7: Crack pattern of specimens in Series IV B-7

LIST OF SYMBOLS

A_b	Area of the bar (mm^2)
A_{frp}	Area of the FRP bar (mm^2)
A_{tr}	Area of transverse reinforcement (mm^2)
C	Concrete cover (mm)
c_y	Concrete clear cover (mm)
d_b	Bar diameter (mm)
E_{frp}	Modulus of elasticity of the FRP bar (GPa)
E_s	Modulus of elasticity of the steel bar (GPa)
f'_c	Concrete compressive strength (MPa)
f_{cr}	Concrete tensile/rupture strength (MPa)
f_{frp}	Stress in the FRP bar (MPa)
$f_{frp,u}$	Tensile strength of FRP bar (MPa)
f_{radial}	Radial force acting in the GFRP bar (kN)
f_s	Stress in steel
f_y	Yielding stress of a steel bar (MPa)
jd	Internal lever arm (mm)
l_e	Embedment length, part of the bar embedded in concrete (mm)

l_d	Development length (mm)
P	Axial load acting in the bar (kN)
V	Shear force (kN)
α	Angle between the compressive strut and the bar
ΔM	Change in bending moment (kN.m)
μ	Actual bond stress (MPa)
μ_{avg}	Average bond stress (MPa)
$\mu\varepsilon$	Micro-strain
μ_{frp}	Bond strength of the FRP bar (MPa)
τ	Bond strength (MPa)

LIST OF ABBREVIATIONS

AFRP	Aramid Fibre Reinforced Polymer
CFRP	Carbon Fibre Reinforced Polymer
CTE	Coefficient of Thermal Expansion
FRP	Fibre Reinforced Polymer
GFRP	Glass Fibre Reinforced Polymer
LE	Loaded-end

CHAPTER 1: INTRODUCTION

1.1. Overview

The use of Fibre Reinforced Polymer (FRP) bars instead of regular steel reinforcing bars would be beneficial where steel bars perform poorly, such as in aggressive environments encountered in bridge deck slabs or marine structures. Although some solutions have been developed to improve steel resistance to chemicals, such as: epoxy coating, polymer concrete and cathodic protection, none is a permanent solution (Adimi et al. 2000). The main reason to replace steel bars by FRP lays in the fact that such bars are non-corrodible. Other advantages of FRP bars include: low weight, high tensile strength and magnetic neutrality. However, FRP can still be deteriorated by other factors such as physical factors (moisture and temperature) or chemicals (alkaline, salts and acids) (ISIS Canada 2006).

The FRP bars differ from the regular steel reinforcing bars in many aspects. First, FRP bars are a composite material, non-homogeneous. It presents an elastic stress-strain curve up to rupture differing from steel reinforcement where a yield plateau presents considerable warning prior to failure. For this reason, FRP reinforced concrete elements are actually designed to fail by crushing of concrete, because failure by bar rupture would be sudden/brittle and, consequently, dangerous. Another important issue regarding FRP reinforced concrete elements is the mismatching of Coefficients of Thermal Expansion (CTE) and the Poisson ratios which may lead to initiation of longitudinal cracks accompanied by partial or complete loss of bond strength (ISIS Canada 2007).

One of the design assumptions of reinforced-concrete sections is perfect bond. Bond strength is affecting both ultimate and service design, as it is related to the capacity of the section as well as cracking width and spacing (both related to the effects of tension-stiffening). Also, the premises of perfect bond are not only related to flexural elements but are also related to the shear, torsion and punching mechanisms. Therefore, bond is of utmost importance and its properties should be guaranteed whatever loading or environmental conditions are present (Cosenza et al. 1997; Pecce et al. 2001; Edwards and Yannopoulos 1978).

Whether or not FRP bars can be designed for their full tensile capacity depends largely on the bond behaviour at the interface between the FRP bar and the concrete. The bond behaviour, as it will be further discussed in the following chapters, is influenced by a large range of factors, such as: bar composition (fibre and resin), surface conditions and loading history.

Research work done to date covers mainly the bond strength under static/monotonic load, with bond strengths achieving smaller, equal or even higher values than the steel reinforcement (Katz 2000; Shahidi et al. 2006; Mashima and Iwamoto 2004; Katz et al. 1999; Larralde and Silva-Rodriguez 1993; Faoro 1996). However, there is still a need of understanding the effects of freeze-thaw cycles, wet-dry cycles, high and low temperatures, chemical attacks, as well as loading effects such as fatigue, low cycles-high stress and high cycle-low stress tests, with constant and variable stress ranges, impact loads, and sustained loads, among others.

1.2. Research Objectives and Originality

In past decades, the research community concentrated on studying the mechanical properties and structural performance of FRP materials. Nowadays, properties such as the tensile strength, and modulus of elasticity, among others are well understood and attention has been focused on the long-term behaviour and durability issues, such as: pH variation, fatigue resistance and temperature issues. Understanding the behaviour of the bar or reinforced element when subjected to different types of environmental and/or loading conditions is of great interest for the engineering community. A better understanding will lead to safer yet economical designs.

To address these new necessities, this research program was designed to further evaluate the bond properties of glass FRP bars to concrete under harsh environmental and/or loading conditionings.

The main objectives of this research work are to investigate the residual bond properties and behaviour of GFRP bars embedded in concrete after being subjected to the following:

I. Simultaneous effects of freeze-thaw cycles and sustained loads;

II. Fatigue loading;

III. Combined effect of freeze-thaw cycles and sustained loading and then fatigue loading.

The specific objectives of this research are to investigate:

a. The influence of concrete cover (1.5, 2.0 and 2.5 d_b) on bond resistance and the splitting failure mechanisms through testing eccentric pullout specimens;

b. The influence of bar diameter (No. 16 and No. 19) on bond strength;

c. The deterioration of the bond properties of the GFRP bar when subjected to fatigue loading (1,000,000 cycles);

d. The degradation of the concrete-GFRP bar interface due to the freeze-thaw cycles (250 cycles) along with sustained loads (30% of ultimate tensile strength);

e. The creep behaviour of the GFRP bar due to constant exposure to a high level of sustained load (30% of ultimate tensile strength).

1.3. Methodology

To be able to achieve the above objectives, an experimental program was designed. The experimental program is composed of four Series: (I) Static pullout, (II) Fatigue loading; (III) Freeze-thaw cycles simultaneously with sustained loads and (IV) Freeze-thaw cycles along with sustained loads followed by fatigue loading. A total of thirty six (36) specimens were constructed and tested. In each of the four series, the variables are the concrete cover and GFRP bar diameter.

1.4. Thesis Outline

Chapter I presents a brief overview of the topic, along with the motivation for the research, the objectives and the methodology.

In Chapter II, a literature review is introduced, where the FRP materials and their bond properties are extensively reviewed.

Chapter III presents the experimental program. It shows a detailed description of the specimens, its dimensions and construction, the environmental conditioning as well as the loading scheme and the instrumentation.

In Chapter IV, an analysis of the experimental results is performed. The influence of the parameters, environmental conditioning and loading program is evaluated. In addition, a comparison with FRP code predictions such as ACI 440-06, CAN/CSA-S806-02 and CAN/CSA-S6-06 is presented

Chapter V presents the conclusions that can be drawn from this study.

CHAPTER 2: LITERATURE REVIEW

2.1. Introduction to FRP Composite Materials

2.1.1. Constituent materials

FRP materials are composed of fibres and a binding matrix. It may also contain other constituents such as fillers and/or additives. The main role of the resin is to provide protection against mechanical and environmental actions, to transfer the stress between fibres, avoid buckling of individual fibres and to compensate for the different expansion ratios in the fibres.

As for the fibres, their main function is to provide strength and stiffness, and to carry load (Faoro 1996; ISIS Canada 2007). While, the resin is responsible for the transverse properties of the FRP bar, such as the transverse Coefficient of Thermal Expansion (CTE), the fibres are responsible for the longitudinal properties (ISIS Canada 2007).

Fillers can be added to achieve better performance of the FRP bar, such as: to improve mechanical properties, to reduce shrinkage and cracking, to improve the transfer of load, to improve chemical resistance, among others. Common types of fillers are: clay, silica, and mica (ACI Committee 440 1996).

Additives can be introduced in the FRP bar as a way to: control the rate of curing, to reduce the shrinkage during curing, improve weathering resistance, reduce the viscosity of the resin, etc (ACI Committee 440 1996).

2.1.1.1. Matrix

The matrix choice is of great importance for bond issues, since it appears that it is the resin that controls the bond behaviour and not the fibre (Al-Zahrani et al. 1999). Matrices are very susceptible to deterioration, which may occur due to temperature or chemical attack.

A matrix resin can be either thermoplastic or thermosetting. The former is not desired in the construction industry since it has the property to be softened under heat encountered in normal fire conditions. On the other hand, in the case of thermosetting resins, once it has been hardened it cannot be softened under usual fire temperature encountered in construction. As it is an irreversible process, any fold or hooks necessary in reinforced concrete should be ordered with the manufacturer. Also, thermosetting resins present better creep and stress relaxation behaviour than thermoplastic resins. There are three major thermosetting resins which are currently being used in the composition of FRP bars: polyester, vinyl ester and epoxy (ACI Committee 440 1996).

The stress versus strain curve for a matrix is a nonlinear curve. Table 2.1 presents the mechanical properties of thermosetting resins.

TABLE 2.1: Mechanical properties of resins

Resin	Tensile strength (MPa)	Modulus of elasticity (GPa)
Polyester	34.50-103.50	2.10-3.45
Vinylester	73.00-81.00	3.00-3.35
Epoxy	55.00-130.00	2.75-4.10

2.1.1.2. Fibres

Fibres are composed of oxides. Of importance for the construction industry, there are three major types of fibres: aramid, carbon and glass. Each type of fibres has its subdivisions. As the present research was prepared with Glass Fibre Reinforced Polymer (GFRP) bars focus will be given to this type of fibre. The following types of glass fibres are available:

- Type AR (alkali resistance)
- Type C (chemical)
- Type E (electric)
- Type S (strength)

Fibres alone present a linear elastic stress-strain relationship. Each type of fibre presents advantages and disadvantages. The reason why the scientific community is focusing on the glass fibre is because of its lower cost, relative to the other types of fibres. Table 2.2 presents a comparison between mechanical properties of the types of fibre. Table 2.3 brings a comparison in the chemical resistance.

TABLE 2.2: Mechanical properties of fibres

Fibre type	Tensile strength (MPa)	Modulus of elasticity (GPa)
Carbon (PAN, High strength)	3500	200-240
Aramid (Kevlar 49)	2800	130
E-glass	3500-3600	74-75
S-glass	4900	87

TABLE 2.3: Physical properties of fibres

Fibre type	Acid resistance	Alkali resistance	Organic resistance
Carbon (PAN, High strength)	Good	Excellent	Excellent
Aramid (Kevlar 49)	Poor	Good	Excellent
E-glass	Poor	Fair	Excellent
S-glass	Good	Poor	N/A

2.1.2. General overview of FRP bars

There are various types of FRP bars, with differing surface patterns. The production of FRP bars can be manufactured through one of the following: Pultrusion, Filament winding or Bag Moulding (ASM International 1987 & 1988).

The stress-strain relationship for FRP bars is linear up to failure and is located in between the curves for fibres alone and resins alone (see Fig. 2.1). Table 2.4 shows the mechanical properties of typical FRP bars (ACI Committee 440 1996).

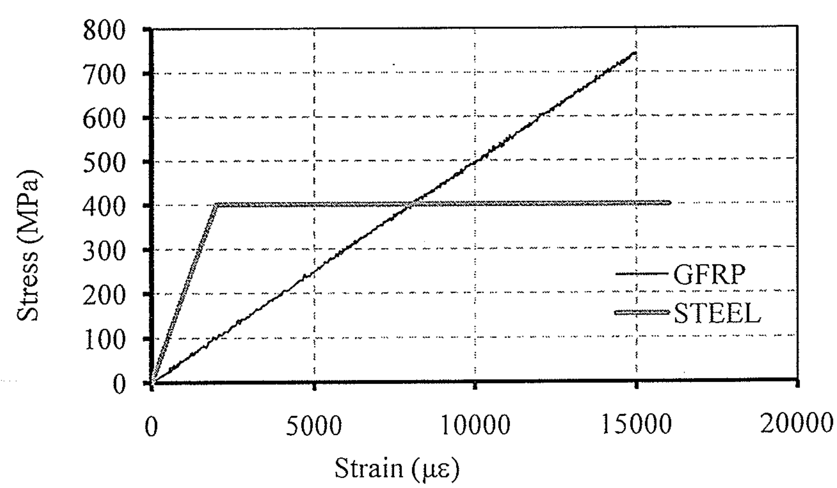

Fig. 2.1: Stress versus strain relationship for GFRP and steel bars

TABLE 2.4: Mechanical properties of FRP and steel bars

Bar	Ultimate strength (MPa)	Elastic modulus (GPa)	Rupture strain (%)
Steel	483-690	200	> 6.0 to 12.0
AFRP	1720-2540	41-125	1.9 to 4.4
CFRP	600-3690	120-580	0.5 to 1.7
GFRP	483-1600	35-51	1.2 to 3.1

In comparison with the regular steel deformed bars, the modulus of elasticity of a GFRP bar is very small. This difference will lead to higher elongation of the GFRP bar under the same tensile stress as steel bar (Pecce et al. 2001).

Unlike conventional steel reinforcement, the stiffness of FRP bars under tension and compression differs; the stiffness of FRP bars in compression depends primarily on the bar type and diameter, among other things. The compressive modulus of elasticity is smaller than the tensile one (ACI Committee 440 1996).

An important property of FRP bars is the Coefficient of Thermal Expansion (CTE). In the transverse direction, it is dependent on the resin type, while in the longitudinal direction, it is a property of the fibre. There is a significant difference in the coefficient for concrete and the FRP bar, especially in the transverse direction which can achieve 2 to 8 times the concrete value. When there is a temperature fluctuation, thermal stresses will arise in the concrete in both the axial and radial directions, which may lead to splitting cracks in the concrete cover, following the longitudinal reinforcement. The presence of spirals glued to the surface of the

FRP bar decreases the transverse CTE (Gentry and Husain 1999; Aiello 1999; Galati et al. 2005). Table 2.5 lists the CTEs for different types of bar (ISIS Canada 2007).

TABLE 2.5: Linear coefficients of thermal expansion (x10^{-6}/°C)

Direction	Steel	AFRP	CFRP	GFRP	Concrete
Longitudinal	11.7	-6 to -2	-1 to 0	6 to 10	10- 12
Transverse	11.7	60 to 80	22 to 23	21 to 23	10-12

2.2. Bond of FRP Bars

2.2.1. Definition of bond

The basis of reinforced concrete is that tensile stresses will be transferred from the concrete to the reinforcement through shear stresses in the concrete/bar interface. The forces are transferred by inclined compressive struts. The tangent component, a shear stress, is denominated bond. The radial components, which are compressive stresses, are balanced by circumferential tensile stresses in the concrete around the bar and may give rise to splitting forces (MacGregor 2005; Tepfers 1983; Abrishami and Mitchel 1993, Park and Paulay 1975).

For bond stresses to exist, there must be a variation in the bar stress. Figure 2.2 presents a portion of a bar embedded in concrete. The following equation for the shear stress can be written considering the equilibrium of the stresses:

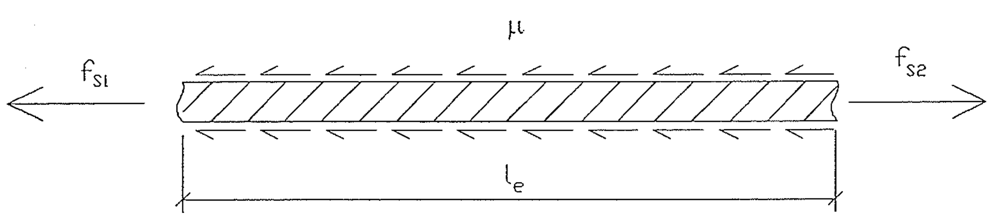

Fig. 2.2: Equilibrium of forces

$$(f_{s2} - f_{s1}).\frac{\pi.d_b^2}{4} = \mu_{avg}.(\pi.d_b).l_e$$ **Equation 2-1**

Where μ_{avg} is the average bond stress and d_b is the bar diameter. Considering an infinitesimal length of dx, we have:

$$\frac{df}{dx} = \frac{4.\mu}{d_b}$$ **Equation 2-2**

In this equation μ is the actual bond stress. The radial stress can be written as:

$$f_{radial} = \mu.\tan\alpha$$ **Equation 2-3**

Where, α is the angle between the inclined compressive strut and the GFRP bar (see Fig. 2.3). This angle is about 45° for steel bars (Tepfers 1983) and ranges between 30 to 45° for GFRP bars (Tepfers et al. 1998).

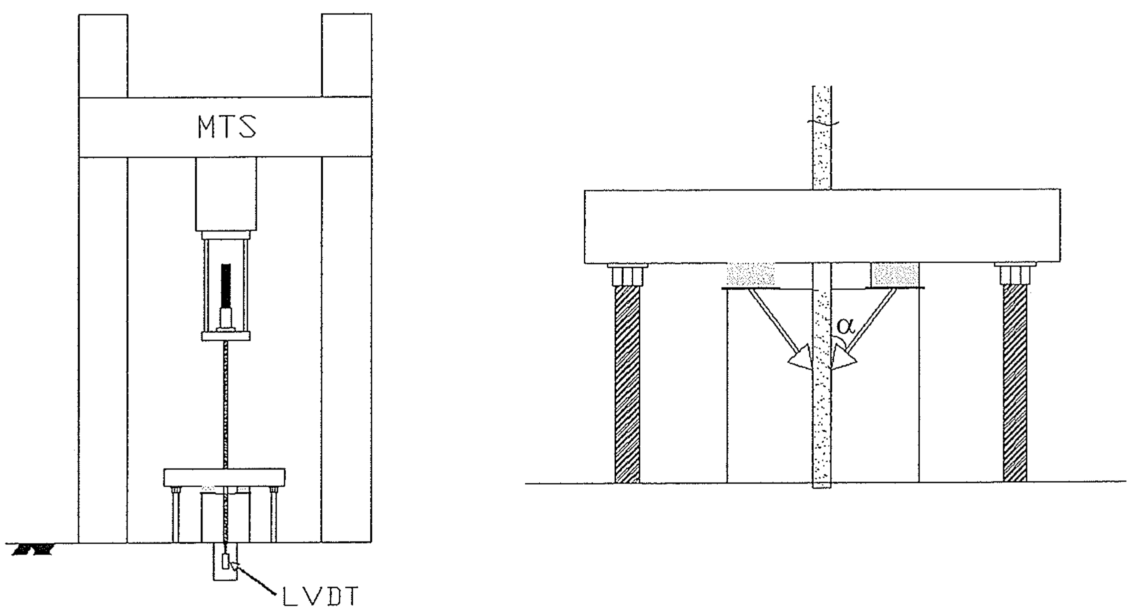

(a) Static pullout test (b) Detail of compressive strut

Fig. 2.3: Stress field in static pullout tests

Considering that the force in the bar varies with the applied moment, we have:

$$\frac{\Delta M}{\Delta x} = (\pi.d_b).\mu_{avg}.(jd) \qquad \textbf{Equation 2-4}$$

Here *(jd)* is the internal lever arm, between the compression and tension forces. It is interesting to note that the bond stress is proportional to the slope of the moment diagram. As known from statics, shear force is the change in the moment along the length, so we can also write the previous equation as,

$$\mu_{avg} = \frac{V}{(\pi.d_b).(jd)} \qquad \textbf{Equation 2-5}$$

Between two cracks, the force in the bar does not change, therefore the $\frac{df}{dx} = 0$ and, so, $\mu = 0$. The true shear stress distribution is normally referred to in-and-out stress since it transfers the stress into the bar and back again to the concrete. Figure 2.4 show the stress distribution in a simply-supported beam, with two concentrated loads. Figure 2.5 presents the stress distribution for a splice test and Figure 2.6 presents the stress distribution for a pullout test (MacGregor 2005).

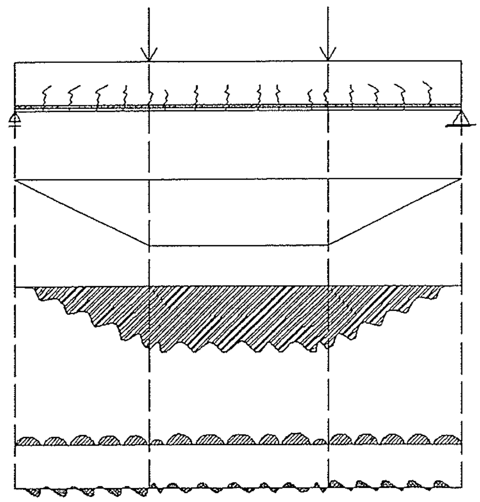

Fig. 2.4: Beam: stress distribution in steel, in concrete and bond stress

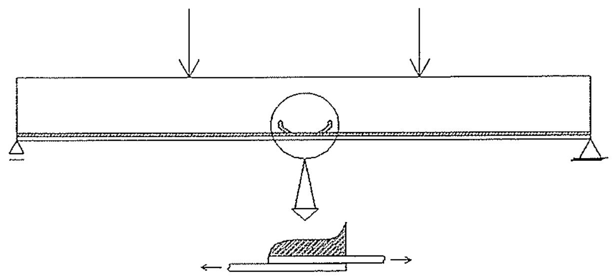

Fig. 2.5: Splice: detail of the bond distribution

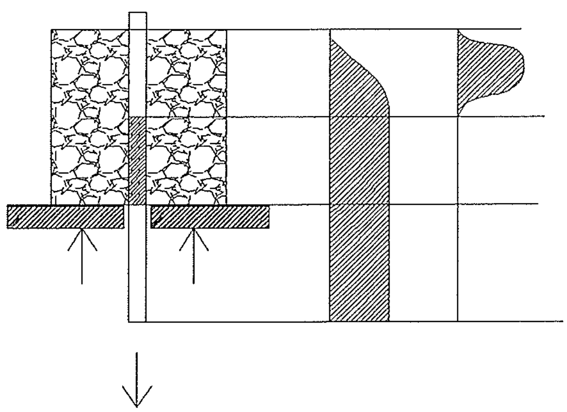

Fig. 2.6: Pullout specimen: stress in steel (left) and bond stress (right)

2.2.2. Mechanisms of bond transfer

There are three main bond components: chemical adhesion, friction and interlock/bearing. Although during the pullout test the chemical bond (adhesion) is the main mechanism of stress transfer at the very beginning, it is very low and rapidly lost. In the following stage stress transfer is achieved through friction and interlocking mechanisms (Cosenza et al. 1997).

For this reason, there are two main types of bond-resistance mechanisms for FRP bars, namely: friction resistance (where the friction resistance is more active than the interlocking one) and bearing resistance (where the interlocking mechanism is predominant). Bond mechanisms are very dependent on the type of resin, shape of the bar, and surface pattern, among others (Cosenza et al. 1997).

In smooth bars and bars without any deformations, two types of stress transfer mechanisms can be seen: adhesion (firstly) and friction (secondly). As there are no ribs or indentations, no interlocking mechanism develops along the bar. The bond strength for these bars is mainly controlled by the resin type, as the concrete mechanical properties are negligible. This type of bar presents weak adhesion to the concrete (Cosenza et al 1997; Katz 2000).

For bars containing deformations (ribbed, braided, indented, twisted strands, glued spirals) the interlocking mechanism will be activated. However, the way it is activated depends on geometry (dimension and spacing of ribs), concrete properties and the characteristics of the reinforcement (Cosenza et al. 1997).

2.2.3. Techniques to improve bond resistance

There are two main types of process to improve bond properties of the FRP bars: deforming the outer surface, or roughening it. Commonly used deformations are: ribs, indentations, twisted strands, and spirals glued to bars.

In those techniques which involve adding materials to the surface of the bar, such as applying sand, or a helical wrap of fibres, the bond resistance achieved is related to the quality of the material added. If the material added has the same properties as the core, good bond resistance will be developed with good quality material. If a stronger material is used, good bond resistance is obtained. However, if a weaker material is applied, small values of bond resistance are observed.

Applying sand to the FRP bar surface greatly enhances its bond strength, leading to an increase of up to 400% with respect to smooth bars, and achieving values that are similar or even higher than the regular steel reinforcement (Cosenza et al. 1997). The sand-coating not only increases the bond resistance but also the initial stiffness (Cosenza et al. 1996). This is also beneficial when using high-strength concrete since it increases the cracked moment of inertia, I_{cr}, and reduces crack widths, which are indications of better bond performance (ACI Committee 440 1996). Another interesting fact of the sand-coating is that the sand-coated FRP bar will be able to sustain the peak load for a considerable slip (Katz 2000). The drawback of using sand coating to improve the bond resistance is the brittle failure, which is due to sudden detachment of the sand layer leading to immediate loss of bond (Cosenza et al. 1996).

Benmokrane et al. (1996) found that applying deformations by double wrapping of helical fibres around the rod greatly improved the bond properties, while bars containing glued spirals or twisted bars showed low bond strength, similar to smooth bars (Cosenza et al. 1996; Cosenza et al. 1997; Malvar 1995).

Bond strength of deformed bars is very dependent on the pattern of the deformations. It was found that deep indentations deviates the longitudinal fibres causing a decrease in the tensile strength. In the research by Malvar (1995), the author indicates that small deformations of about 5% of the bar diameter are enough to develop bond strengths as high as the values obtained for steel bars. Also, deformations obtained by stressing external helicoidal fibres or strands present reliable bond strength (Malvar 1995).

In the case of deformed bars, adding sand will also increase the bond strength and also will make the failure more brittle, as in the case of smooth bars. The values of bond strength obtained by deformed sand-coated bars are higher, even greater than the steel bars, but accompanied by much higher peak slips (Cosenza et al. 1997).

The disadvantage of promoting deformations in the surface of the bar is that such irregularities give rise to stress concentrations which may lead to premature cracks and multi-axial stresses under fatigue loading, greatly damaging the bond behaviour of FRP bars (ACI Committee 440 1996).

2.2.4. Parameters influencing bond strength

The bond behaviour of FRP bars is influenced by many factors such as the adhesion, surface pattern and shape of the deformations. Factors such as the pressure surrounding the FRP bar due to shrinkage of concrete and swelling of FRP due to temperature and moisture also influence the bond resistance (Cosenza et al. 1997).

The effect of the following parameters will be discussed in the following subsections:

- Confining pressure (concrete cover);
- Bar diameter

Other factors also influence the bond resistance, such as:

- shape of the bar (circular, square or rectangular) (Achillides and Pilakoutas 2004),
- position during concrete casting (Chaallal and Benmokrane 1993; Esfahani et al. 2005, Rossetti and Galeota 1995),
- surface deformation geometry (Achillides and Pilakoutas 2004; Al-Zahrani et al. 1999; Malvar et al. 2003),
- concrete compressive strength (Achillides and Pilakoutas 2004; Tastani et al. 2005; Pecce et al. 2001; Nanni et al. 1995; Cosenza et al. 1996),
- embedment length (Wambeke and Shield 2006; Focacci et al. 2000; Ehsani et al. 1996; Benmokrane et al. 2002; Tepfers et al. 2000; Tepfers et al. 1998; Nanni et al. 1995; Makitani el al. 2000; Achillides and Pilakoutas 2004; Al-Zahrani et al. 1999; Larralde 1993; Pecce et al. 2001; Chaallal and Benmokrane 1993), and
- type of fibre and resin (ACI Committee 440 1996; Cosenza et al. 1997).

2.2.4.1. Effect of confining pressure

The confining mechanism may be provided by confining steel rings (Malvar et al. 2003; Cosenza et al. 1997; Malvar 1995; Tastani et al. 1984), stirrups or helix (Aly 2007) or only by providing adequate concrete cover. Only the latter will be discussed since it is directly related to the proposed research.

Tepfers et al. (1998) tested concentric and eccentric pullout specimens using sand-coated GFRP bars with helical wraps. The embedment length was 75 mm, which represented 4.68 d_b for the bar No. 16 (15.9-mm diameter) and 3.00 d_b for the bar No. 25 (25-mm diameter). For the concentric specimens, bond breakers where present, while for eccentric specimens, the full embedded length was in contact with the concrete. Concrete covers of 1.0, 1.5 and 2.0 d_b where investigated. The results presented an increase of bond strength with increasing concrete cover up the value of 2.0 d_b and then with the concentric placement of the bar, the bond strength was reduced to approximately 30% to 50% in comparison with the values obtained for the concrete cover of 2.0d_b.

Esfahani et al. (2005) tested pullout specimens using sand-coated GFRP bars with an embedment length of 6.25d_b (no bond breakers where present) and concrete clear covers of 1.25d_b and 3.125d_b. An increase in the bond strength with increasing concrete cover in eccentric pullout specimens was observed.

Weber (2005) also tested concentric and eccentric pullout specimens with GFRP containing trapezoidal ribs in its surface for bond enhancement. The embedment length was 5d_b and only one concrete cover, 1.25d_b, was investigated. The author concluded that increasing the concrete cover led to enhancing the bond strength.

In the research by Galati et al. (2005), the effect of concrete cover on the bond strength of sand-coated GFRP bars with helical wraps was investigated. In addition to concentric specimens, concrete clear covers of $2.00d_b$ and $3.00d_b$ were evaluated for an embedment length of $8d_b$. The concentric placement of the bar produced the smallest value of bond strength.

2.2.4.2. Effect of bar diameter

Larger size bars produce smaller bond stress and it also loses its adhesive bond earlier than small size bars (in the case of sand-coated GFRP bars). Benmokrane et al. (1996), Larralde and Silva-Rodriguez (1993), Nanni et al. (1995) and Tepfers et al. (1998) studied the effect of bar diameter in the bond resistance of GFRP bars with different surface patterns. The results presented an increase in the bond stress with decreasing bar diameter.

For small embedment lengths, the bond stress is considered uniform and can be described by the following equations (CSA 2002).

$$\tau_{avg} = \frac{P}{\pi . d_b . l_e}$$ **Equation 2-6**

$$\tau_{avg} = \frac{d_b . f_{frp}}{4 . l_e}$$ **Equation 2-7**

Therefore, in order to achieve the same bond stress, larger bar diameters need longer embedment lengths (Achillides and Pilakoutas 2004). It is clear from the above presented equations that, similar to steel, if the bar diameter decreases the bond stress increases.

2.3. Methods for Bond Evaluation

There are several methods to evaluate bond strength of reinforcement: eccentric or concentric pullout, beam, beam end, direct tension, splice, and ring pullout tests among others (Nanni et al. 1995). Each of these tests presents different bond strength values due to the difference in loading and stress field in the concrete surrounding the bar, which is a very important issue.

The pullout test provides the least realistic values of bond resistance. However, the pullout test presents the following advantages: the specimen is small, the testing method is simple and no special equipment is needed. The pullout test offers an economical and simple solution to evaluate bond performance. For experiments that are focused on observing the influence of a test parameter in relation to a control, this simple test method provides very reasonable results.

One of the reasons for the higher bond values encountered in pullout tests is the state of stress in the concrete surrounding the bar. In a pullout specimen, the concrete is in compression, which is the most favourable state of stress in terms of bond resistance. A compression state provides confinement and avoids micro cracks around the bar, somehow diminishing the splitting tendency and allowing the development of high values of bond resistance (Tastani et al. 2005). However, this compressive stress is very small, on the order of 0.2 MPa and has insignificant effect on the bar bond strength, especially for FRP bars without deformations, which are not affected by the concrete compressive strength (Nanni et al. 1995).

In the present research the pullout test was chosen to evaluate the bond strength between the GFRP bar and the concrete. The standard bond specimen described in the CAN/CSA-S806-02 standard (CSA 2002) was considered for the concentric pullout specimen. Figure 2.7 presents the concentric specimen as specified in CAN/CSA-S806-02 (CSA 2002).

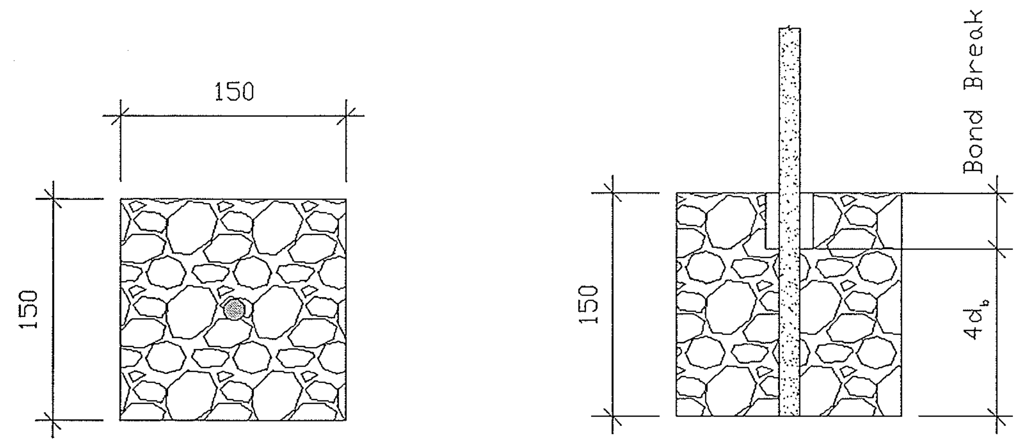

(a) Top view (b) Lateral cut

Fig. 2.7: Standard pullout specimen

Larger size cubes may be used when dealing with larger diameter rods, in order to minimize splitting of concrete due to smaller cover than the minimum. When the cover size is less than 5 or 6 times the bar diameter, splitting of concrete may be a problem (CSA 2002).

The PVC tube is used to minimize the stress concentration in the concrete on the loaded-end side due to the loading plate, through preventing bonding. Instead of a PVC tube, the bar can be wrapped with a cling film or with several layers of tape (Achillides and Pilakoutas 2004).

Between the concrete and the reaction plate, a wood plate or neoprene rubber can be used. This plate is used to guarantee good contact between the concrete (which may include non-uniformities) and to the reaction plate, thus avoiding introduction of accidental bending moment or movements caused by local crushing of concrete (Achillides and Pilakoutas 2004). Figures 2.8 and 2.9 present two ways to perform the pullout test.

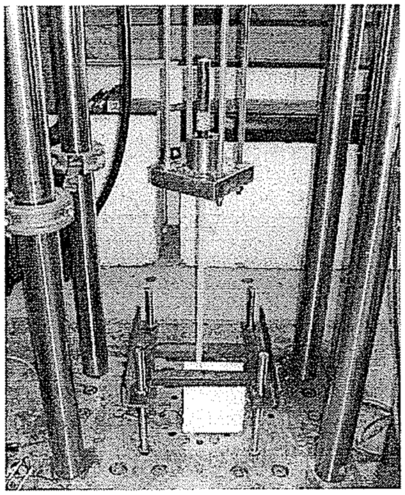

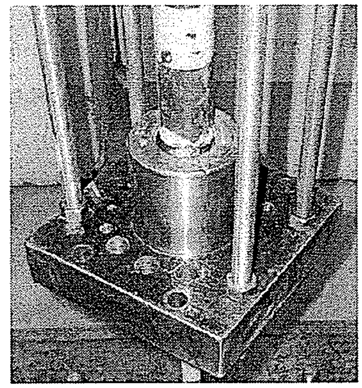

(a) Test set-up (b) Detail of grip

Fig. 2.8: Pullout test layout 1

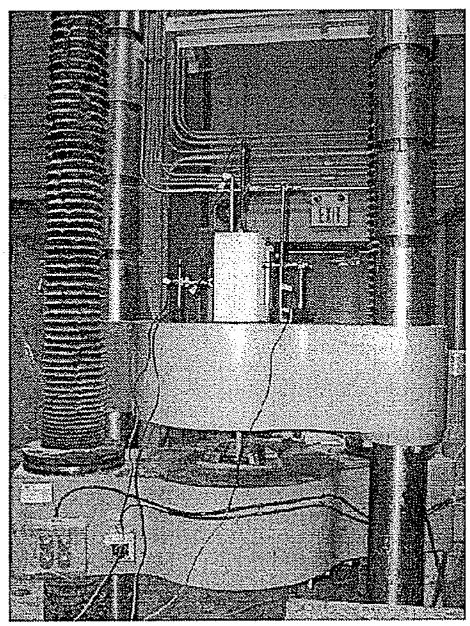

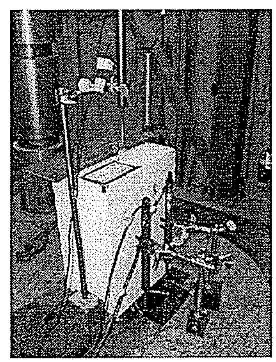

(b) Instrumentation

(a) Test set-up (b) Steel plates - grips

Fig. 2.9: Pullout test layout 2

The average bond stress is calculated considering the assumption of uniform bond stress distribution, accordingly with the CAN/CSA-S806-02 (CSA 2002), as:

$$\tau = \frac{P}{\pi . d_b . l_e} \qquad \textbf{Equation 2-8}$$

Where, P is the maximum pullout force, d_b is the bar diameter and l_e is the embedment length. If thought to be wrongly representing the bonding behaviour of the rod, the embedment length can be taken greater than four times the diameter.

Figure 2.10 presents the state of stress when an eccentric or a concentric pullout test is conducted.

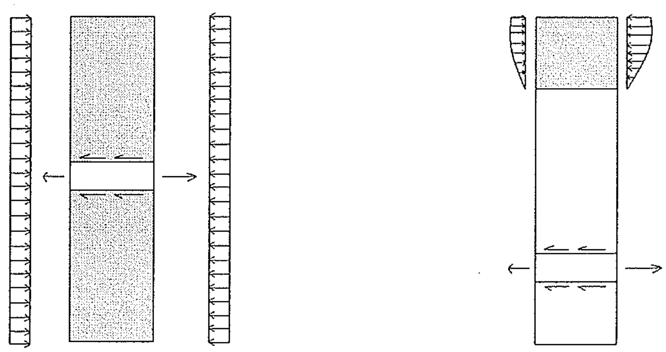

(a) Concentric test (b) Eccentric test

Fig. 2.10: Pullout test: stress configuration; the grey color represents the compressed concrete (Tastani et al. 2005)

Depending on the test performed to investigate bond, a variety of curves can be extracted from the experiments, such as:

- Bond stress versus slip (at free or loaded-end);
- Slip versus number of cycles;
- Slip versus time .

The output from a monotonic pullout test is basically the bond stress versus slip curve, at both the free-end and loaded-end.

Unlike the regular steel bars, in FRP bars there is a difference in the bond stress versus loaded-end slip and the bond stress versus free-end slip curves. Such differences are due to the non-linear distribution of the bond stress and the slip along the embedment length. The difference between the slip at the free and loaded end represents the elongation of the bar, which is due to the low modulus of elasticity of the FRP bar (Pecce et al. 2001; Al-Zahrani et al. 1999). In the case of failure by rupture of the FRP bar, no slip is recorded at the free-end (Pecce et al. 2001).

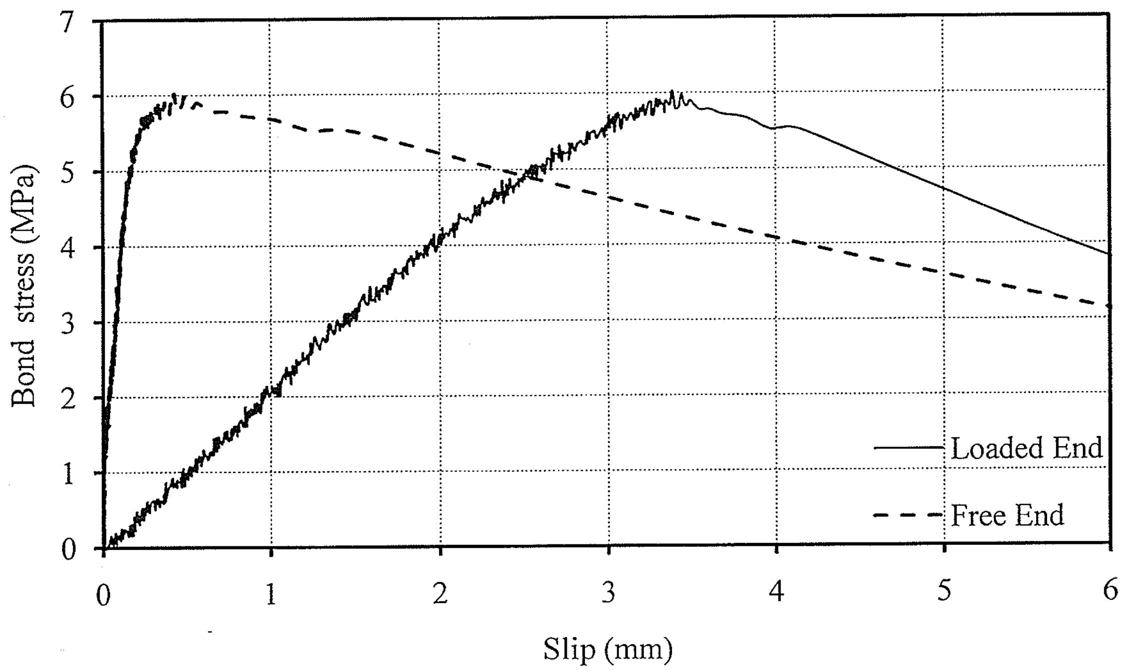

Fig. 2.11: Difference between loaded and free-end slip

The loaded-end slips as soon as the chemical adhesion is lost. The chemical adhesion can be estimated, as proposed by Achillides and Pilakoutas (2004), by analysing the bond stress versus slip curve. The point at which the bond modulus rapidly decreases is the one where the chemical bond is lost. According to Achillides and Pilakoutas (2004), this adhesion resistance seems to depend only on the bar diameter, and is not influenced by either the type of fibre or concrete used.

He and Sun (2006) investigated the bond behaviour using static pullout specimens with GFRP bars containing helically wound glass fibre strands. The authors identified that during the monotonic loading process there are four visible phases. The first one is characterized by a small slippage. In this phase chemical adhesion is gradually lost. The second phase is characterized by a large slippage; in this phase the curve becomes non linear. It then reaches its ultimate stress. In the third phase there is a sudden fall in the bond stress accompanied by a large slippage. In this phase, there is a linear descending line. The fourth phase is called residual, where the bond stress is residual, and almost constant. Figure 2.12 presents a scheme of the phases (He and Sun 2006).

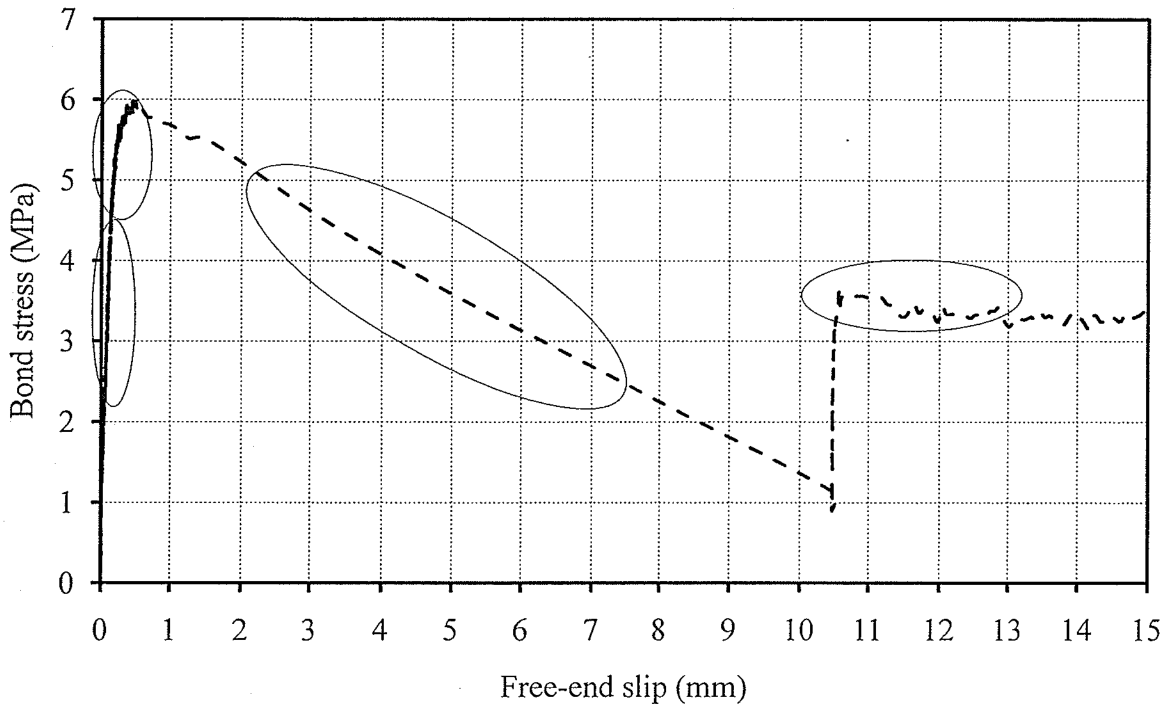

Fig. 2.12: Bond stress versus free-end slip curve of monotonically loaded bars

2.3.1. Mechanisms of bond failure

Unlike steel reinforcement, FRP bars present different modes of failure. As reported by Tastani et al. (1984), the following types of failure were observed in pullout specimens under monotonic load,

- Pullout failure : The bar is pulled out of the concrete, with little to no damage in the concrete matrix.

- Splitting failure : Splitting of the concrete element or concrete cover leading to loss of bond resistance.

- Failure with cone detachment : The bar is pulled out of the concrete bringing along a concrete cone. In this case the concrete element dimensions are not enough to provide the necessary anchorage.

- Bar Rupture (FRP) : The bar achieves its tensile strength, and bar rupture is achieved without bond failure. In this case, the embedment length is equal or greater than the development length. No slip is recorded at the free-end.

The pullout failure can be given by either crushing of concrete between the deformations or shearing off the bar deformations. In the case of regular steel bars, the failure is always caused by shearing off the concrete between the deformations, without any damage to the bar. For FRP bars, if the concrete compressive strength is: lower than 15 MPa failure will come by crushing of the concrete between the deformations; if it is between 15 and 50 MPa, both damage to the FRP bar and concrete will be visible, and if it is greater than 60 MPa the deformations in the FRP bar will be sheared off with negligible damage to the concrete (Pecce et al. 2001).

In a pullout failure, the maximum bond stress and also the bond damage move in the direction of the free-end in a progressive manner (Benmokrane et al. 1996). Adding sand to the surface of the FRP bar makes the pullout failure more brittle, since the bond failure will be given by sudden detachment of the sand surface layer (Cosenza et al. 1997).

As the surface of the FRP bar is softer than the steel bar, it doesn't create local stress concentrations at contact points, which often delays the appearance of cover splitting cracks along the bar. However, the necessary load to cause the crack pattern from the ultimate splitting failure is dependent on the surface type of the FRP bar (Tepfers 2003).

In the experiments of Tepfers (2004), the author noticed that depending on the splitting pattern of the concrete cover, a complete or partial loss of bond was observed. In the case of one crack in the smallest direction, the bond resistance was lost, but when a V-shape crack pattern occurred then the bond resistance was partially lost and there was still a residual resistance, which means that a V-shape pattern resists higher splitting forces.

In the case of steel reinforcing bars, according to Tepfers (1983), the cracking of concrete cover doesn't mean necessarily that bond capacity is exhausted. The author states that although the load can still be raised it will be accompanied by increase in slip. The bond stresses become uniformly distributed where the crack is open. In the case of FRP bars, like steel bars, the cracking of the concrete cover promotes an increase in slip along with loss of bond resistance (Tepfers 2003).

If extra confinement is provided, such as an external jacket, the failure becomes more ductile and a pullout failure is probably going to take place instead of a splitting failure (Tastani et al. 1984; Pecce et al. 2001).

The load which will cause the splitting of the concrete cover can be estimated by the theory of the thick-walled concrete ring, first described by Timoshenko in "Theory of Elasticity" (1970), then used by Tepfers to investigate splices of steel bars (Tepfers 1973) and pullout specimens with GFRP bars (Tepfers et al. 1998). There are three stages, which can be considered to describe the concrete behaviour: elastic, plastic and partly cracked stages. A brief explanation is given as follows:

- **Elastic**: The concrete is considered as acting elastically. Once the tensile strength of the concrete is achieved in the surface of the bar, it is considered that the crack will immediately propagate and all bond resistance will be lost.
- **Plastic:** The concrete is considered as acting plastically. In this stage, in order for a crack to appear, it is necessary that an even distribution of stresses in the whole length of the concrete cover be equal to the tensile strength of concrete.
- **Partly Cracked:** This stage considers that after the start of the crack in the surface of the bar, there will still be some resistance of the cover. Failure through propagation of the crack will come sometime after the start of the crack and before the stresses become even in the whole length of the cover.

In Tepfers et al. (1998), the author concluded that the appearance of a crack in the cover can be estimated to be between the cases of partly cracked elastic and plastic stages. The angle of action was found to be 30° for sand-coated GFRP bars with helical wraps, while for the case of steel bars it was 45°.

In Tepfers (1983 & 2004), the author proposed three equations to predict the splitting load: load at which the concrete cover will split. These equations are written based on the behaviour of the concrete and on the theory of thick-walled concrete ring,

Elastic Stage:
$$\frac{\tau}{f_{cr}} = \frac{1}{\tan\alpha}.\left[\frac{\left(c_y + \frac{d_b}{2}\right)^2 - \left(\frac{d_b}{2}\right)^2}{\left(c_y + \frac{d_b}{2}\right)^2 + \left(\frac{d_b}{2}\right)^2}\right]$$
Equation 2-9

Partly Cracked Stage:
$$\frac{\tau}{f_{cr}} = \frac{\left(c_y + \frac{d_b}{2}\right)}{1.664.d_b.\tan\alpha}$$
Equation 2-10

Plastic Stage:
$$\frac{\tau}{f_{cr}} = \frac{2.c_y}{d_b.\tan\alpha}$$
Equation 2-11

Tepfers (2004) concluded that for thinner concrete covers the results of splitting load were closer to the plastic stage, while for thicker covers the results grouped better around the partly cracked stage. Accordingly to the author this is expected, because when dimensions increase the plasticization becomes less pronounced (Tepfers 1983 & 2004).

2.4. Durability Issues

Nowadays the durability of FRP bars and FRP reinforced concrete elements is the most important issue regarding FRP usage in civil engineering. All the physical properties of the bar are now well defined. The next step is to better understand the long term behaviour and durability of the FRP reinforcement, to know whether or not it can be used in the construction field with long-term security.

The following issues are related to the durability of the FRP,

- Creep, relaxation and sustained loads;
- Freeze-thaw cycles;
- Fatigue loading;
- Thermal effects;
- Wet and dry cycles;
- pH variation and alkaline environment.

From the above listed issues, only the first three will be investigated in detail, since they are directly related to this study. The remaining will be briefly described as follows.

Thermal effects include the influence of high and low temperatures at curing or testing, as well as temperature fluctuations and fire conditions, in the bond resistance mechanisms and behaviour.

Katz et al. (1999) tested pullout specimens at high temperatures, as high as 250°C. They concluded that high temperatures are very degrading to the bond properties. The authors also highlight the concrete behaviour under such high temperatures.

The effects of curing at high temperatures on the bond resistance was evaluated in the research of Cosenza et al. (1997), Bank et al. (1998) and Galati et al. (2005). All researchers observed significant losses in bond resistance and/or increase in peak slip values.

Katz (2000) studied the effects of curing at high temperatures and/or fatigue loading conditions. The author observed that such conditions, individually or combined, significantly degraded the bond resistance.

Aiello et al. (1999) studied the cracking of the concrete cover when the specimen was submitted to a thermal load. Thermal steps were from 5 to 10°C. The experimental results indicated the through cracks (or splitting cracks) were observed for temperatures ranging between 40 and 45°C. According to Gentry and Husain (1999), the use of large covers and wide spacing is expected to diminish the possibility of cracking due to thermal loads.

No research to-date has been reported that explores wet-dry cycles for internally FRP reinforced concrete elements with bond resistance.

Al-Dulaijan et al. (1996) investigated the effect of high pH and high temperature curing in the bond strength using direct pullout specimens. The author observed a reduction in the bond strength ranging from 14% to 37%. Also increase in the free-end slip of more than 100% was observed. The authors concluded that there was a significant degradation in the bond resistance due to the high pH and temperature conditioning (also, Bank et al. 1998).

Won and Park (2006) investigated the effect of the following conditions in the residual bond strength of different types of bars through testing pullout specimens: alkaline exposure, acid, salt, deionized water, repeated wet-dry cycles, long-term oven drying, repeated freeze and thaw cycles, sulphate solution immersion and calcium immersion. The authors concluded that all conditions promoted a decrease in the residual bond resistance of all types of bars.

2.4.1. Creep, relaxation and sustained loads

FRP bars are more susceptible to creep and stress relaxation since polymers are visco-elastic materials. Therefore, once load is applied, there will be an immediate elastic deformation followed by a slow viscous deformation. So, if a structure is subjected to sustained load it may fail under lower loads than the static strength (ACI Committee 440 1996).

The effects of such properties become even more worrisome when the bar is subjected to moisture and/or temperature, which will accelerate the process (Micelli and Nanni 2004). However, these time-dependent behaviours are also present under room temperature (Adimi et al. 1998).

Regarding the type of fibre, accordingly to researches, the most susceptible fibre to suffer creep rupture is the glass fibre, followed by the aramid and carbon fibre. The creep behaviour will be influenced by the orientation and by the volume of fibres (ACI Committee 440 1996; ISIS Canada 2007).

Tests in GFRP reinforced beams performed by Laoubi et al. (2006), found no significant difference when comparing beams submitted to sustained loads at room temperature to the results of control specimens. The authors also concluded that the equation from the ACI 440.1R-06 (2006) for the long-term deflection due to creep and shrinkage highly over-estimates the deflections.

Hattori et al. (1995) investigated the creep behaviour of AFRP bars and CFRP cables, in comparison with mild steel bars. Pullout cubes of 100 mm and beam specimens of 100 (width) x 200 (height) x 1500 mm were used. Regular static pullout tests, creep pullout tests and flexural creep tests were performed. The free-end slip, as well as the progress of deflection was recorded over time to evaluate the effects of bond creep. The aramid bars presented values of free-end slip larger than the steel bar and the CFRP cable in the pullout creep test. However, the tensile strain of the FRP bar didn't change in the pullout creep test. It was concluded, in the flexural creep test, that the effect of bond creep was negligible and the creep of the concrete in compression controlled the increase in deflection, as in steel.

Shahidi et al. (2006) studied the effects of sustained load in pullout specimens. The authors studied three types of bars: sand-coated GFRP with helical lugs, indented CFRP bars and CFRP strands. The Pullout specimens consisted of 150 mm diameter cylinders 100 mm long with an embedment length of $5d_b$. The level of sustained load was between 60%-90% of the maximum static pullout load for the FRP bars and between 14%-90% of the maximum static pullout load for the steel bars. Experiments took from 9 to 12 months. The authors reported that both the GFRP and the CFRP bars under sustained load presented high free-end slip; higher than for steel bar. The slippage for these two types of bars didn't stabilize, but kept increasing continuously. The CFRP strands showed acceptable values of free-end slip compared with the regular steel bars and the slippage achieved a stable condition after 100 days, 50 days less than that required by the steel bar.

2.4.2. Freeze-thaw cycles

Temperature fluctuations are a very important issue for FRP bars since the coefficients of thermal expansion of the concrete and the FRP bars are different. Also, the temperature distribution along the cross section of the bar is non-linear (Koller et al. 2007).

When dealing with steel reinforcement, freeze-thaw cycles is a very important issue in the durability and service life of the reinforced concrete element. Under such temperature variations cracks are produced, which enlarge the possibility of water or fluid penetration. When the water penetrates the concrete and the temperature falls, the water will expand and introduce forces to the surrounding concrete or in the interface bar-concrete, thereby damaging the bond resistance by promoting corrosion of the steel section.

Mashima and Iwamoto (2004) studied the effects of different numbers of freeze-thaw cycles, ranging from 50 to 600 cycles based on the ASTM C 666 on the bond resistance of FRP bars. The authors concluded that freeze-thaw cycles didn't influence the bond strength of GFRP and CFRP bars. However, the bond strength of AFRP bars decreased with the increase in the numbers of freeze-thaw cycles.

Won and Park (2006) investigated the effect of 300 freeze-thaw cycles in the bond strength of hybrid GFRP bars with helical wraps using pullout specimens. The embedment length was $5d_b$. The authors concluded that the conditioning promoted a 20% decreased in the bond resistance of the GFRP bars.

Laoubi et al. (2006) investigated the influence of freeze-thaw cycles in the ultimate capacity and deflection of GFRP reinforced beams. The authors concluded that no significant difference was observed in the behaviour of conditioned and unconditioned beams.

2.4.3. Fatigue loading

Fatigue strength of FRP composites is directly related to the type of fibre. The number of cycles to failure is attributed to many variables such as: stress level, stress rate, loading history, material composition (type of fibre, matrix), and environmental conditions, among others (Koller et al. 2007).

Katz (2000) studied the effects of 450,000 cycles of fatigue load on the bond strength of GFRP bars with different surface conditions within a concrete environment. The author observed that the reduction in the bond varied from 19% to 80% depending on the surface conditions. The GFRP bars with smooth surface made of polyester resin suffered the highest loss in bond strength, while bars containing sand-coating and helical wraps made of vinyl ester resin presented the lowest. It was also observed by Katz (2000) that bars containing helical wraps failed during the repeated loading phase. It seems that the helical wrap initiates the failure, as failure zones were located immediately below the wrap.

He and Sun (2006) performed cyclic pullout tests, where a tensile cyclic load was applied to a GFRP bar containing helically wound glass strands in a pullout specimen. Monotonic pullout tests were performed for comparison. The specimens subjected to fatigue loading showed up to 40% smaller bond resistance and up to 6 times higher peak slip than those specimens without any loading history.

Bakis et al. (1998) investigated the influence of cyclic load on the bond behaviour of GFRP reinforced beams. Bars with difference surface patterns were investigated. The authors reported that cumulative slip increased with increase in the peak load or with increase in the number of cycles, regardless of the surface pattern. It was reported that the cycled beams presented higher bond strength than the virgin specimens; and also larger free-end slips. The author speculated that the increase in the bond strength was due to better interlocking mechanisms developed due to previous slipping under tension. So, the bar under tension would diminish its size due to the Poisson's effect and slip into a smaller place, where the interlocking mechanisms would be more efficient once the bar was unloaded and returned to its regular size.

2.4.4. Freeze-thaw cycles along with sustained load

When considering the combination of thermal load and service load, an even more worrisome conditions arise. With the service load, the anchored tension bars will introduce extra stresses in the surround concrete, which would already be stressed by the thermal load. The combined effects cannot be predicted since the Poisson ratio and the transverse coefficient of thermal expansion act in opposite directions when high temperatures are applied along with service loads which cause tension in the FRP bars. For bars under compression the picture is even less clear since the Poisson effect will expand the bar, further damaging the interface between concrete and bar (Aiello et al. 2001).

Laoubi et al. (2006) evaluated the influence of freeze-thaw cycles combined with sustained load in the deflection of GFRP reinforced beams. The difference in capacity and deflection was insignificant.

2.5. Code Review

In this section a general overview of concrete cover, sustained and fatigue levels and development lengths is made.

2.5.1. Concrete cover

The ISIS Design Manual No. 3 (ISIS Canada 2007) recommends the use of the clear covers suggested by the CHBDC, CAN/CSA-S6-06 (CSA 2006), given in the following table.

TABLE 2.6: Concrete clear cover specification (ISIS Canada 2007)

Type of exposure	Beam	Slab
Internal	Max (2.5d_b or 40 mm)	Max (2.5d_b or 20 mm)
External	Max (2.5d_b or 50 mm)	Max (2.5d_b or 30 mm)

The CAN/CSA-S6 code (CSA 2000 & 2006) suggests a minimum clear cover for FRP bars of 35 mm with a construction tolerance of $\pm$ 10 mm in the case of bridge decks.

The CAN/CSA-S806-02 code (CSA 2002) does not mention a minimum or maximum clear cover; it only suggests that the distance from the bottom to the centre of the bar should be less than 50 mm. The ACI 440.1R-06 (ACI Committee 440 2006) only provides a maximum limit of 3.5d_b.

2.5.2. Fatigue levels

The ACI 440.1R-06 (ACI Committee 2006) limits the fatigue stress to the values shown in Table 2.7 (Note: an environmental factor, $CE = 0.7$, is considered in the ACI 440.1R-06 (ACI Committee 440 2006) but not considered in the CSA codes).

TABLE 2.7: Fatigue limits (ACI Committee 440 2006)

GFRP	AFRP	CFRP
$0.20f_{frp,u}$	$0.30f_{frp,u}$	$0.55f_{frp,u}$

According to CAN/CSA-S6-06 (CSA 2006), the fatigue limit for GFRP bars is 25% of the bars guarantee tensile strength of the bar, considering factored loads.

2.5.3. Sustained load levels

The CAN/CSA-S806-02 (CSA 2002) states that when FRP bars are used as reinforcement for structural elements, the tensile stress in the FRP fibre under sustained factored loads should not exceed 30% of its tensile failure stress.

The ACI 440.1R (2006) provides sustained stress levels, which are the same as the fatigue limits, given by Table 2.7.

The ISIS Manual No. 3 (ISIS Canada 2007) states that, when GFRP reinforcement is used for structural purposes, the tensile stress in the fibre under sustained factored loads shall not exceed 30% of its tensile failure stress.

2.5.4. Development length

The development length is the minimum length in which the bar can achieve its ultimate strength. From mechanics the following equation can be written,

$$l_d.\pi.d_b.\mu_{frp} = A_{frp}.f_{frp,u}$$ **Equation 2-12**

The normal force in the bar is described as the area of the bar (A_{frp}) times the tensile strength of the bar ($f_{frp,u}$); l_d stands for development length; μ_{frp} is the average bond stress and d_b is the bar diameter.

The ISIS Design Manual No. 3 (ISIS Canada 2007) indicates the following equation for the development length, which is the one provided by the CHBDC (2006), which is the same as CHBDC (2000), (CAN/CSA-S6 2000 & 2006):

$$l_d = 0.45.\frac{k_1.k_4}{\left(d_{cs} + k_{tr}.\dfrac{E_{frp}}{E_s}\right)}.\left(\frac{f_{frp,u}}{f_{cr}}\right).A_{frp}$$ **Equation 2-13**

Where,

$$k_{tr} = 0.45\frac{A_{tr}f_y}{10.5sn}$$ **Equation 2-14**

The factor k_1 is referred to as the bar location factor; it has the value of 1.3 for horizontal reinforcement placed so that more than 300 mm of fresh concrete is cast below the bar; in all other cases it has the value of 1.0. The bar surface factor k_4 represents the ratio of bond strength of FRP to that of steel bar having the same cross-sectional area, but not greater than 1.0. In the absence of manufacturer or test data a value of $k_4 = 0.8$ may be used. The factor k_{tr} is the transverse reinforcement index specified in clause 8.15.2.2 of CHBDC (2006); d_{cs} is the smallest of the distance from the closest concrete surface to the centre of the bar being developed or 2/3 of the centre-to-centre spacing of bars being developed (mm), with the following restraining,

$$\left(d_{cs} + k_{tr}.\frac{E_{frp}}{E_s}\right) \leq 2.5.d_b$$ **Equation 2-15**

The development suggested by ACI 440.1R-06 (2006) is given by:

$$l_d = \frac{\alpha \dfrac{f_{fr}}{0.083\sqrt{f_c^{'}}} - 340}{13.6 + \dfrac{C}{d_b}} d_b$$ **Equation 2-16**

Where, α is the bar location factor. It takes the value of 1.5 for bar containing more than 300 mm of concrete below it and 1.0 in the other cases; d_b stands for bar diameter and the ratio C/d_b should not be taken higher than 3.5; f_{fr} is the smallest of f_{fu} , f_{fe} or f_f, which are given by,

$$f_{fe} = \frac{0.083\sqrt{f_c^{'}}}{\alpha}\left(13.6\frac{l_e}{d_b} + \frac{C}{d_b}\frac{l_e}{d_b} + 340\right) \leq f_{fu}$$ **Equation 2-17**

$$f_f = \left(\sqrt{\frac{\left(E_f \varepsilon_{cu}\right)^2}{4} + \frac{0.85\beta_1 f_c^{'}}{\rho_f} E_f \varepsilon_{cu}} - 0.5 E_f \varepsilon_{cu}\right) \leq f_{fu}$$ **Equation 2-18**

In the above equations, E_f is the modulus of elasticity of the FRP bar, l_e is the length of the bar embedded, ε_{cu} is the ultimate strain in the concrete, ρ_f is the ratio of reinforcement and β_l is the factor for the concrete stress block.

The minimum development length suggested by ISIS Design Manual No. 3 (ISIS Canada 2001) is to be larger of 20 d_b or 380 mm; as proposed by Challal and Benmokrane (1993).

The CAN/CSA-S806-02 (2002) recommends as a normal requirement the following expression:

$$l_d = 1.15.\frac{k_1.k_2.k_3.k_4.k_5}{d_{cs}}.\frac{f_{frp,u}}{\sqrt{f_c^{'}}}.A_b$$ **Equation 2-19**

In the above equation the k-factors are modification factors. Table 2.8 presents the values for those coefficients.

TABLE 2.8: Modification factors

k_1	Bar location factor	= 1.3 for horizontal reinforcement placed so that more than 300 mm of fresh concrete is cast in the member below the development length or splice.
		= 1.0 for all other cases.
k_2	Concrete density factor	= 1.3 for structural low-density concrete.
		= 1.2 for structural semi-low-density concrete.
		= 1.0 for normal density concrete.
k_3	Bar size factor	= 0.8 for $A_b \leq 300$ mm.
		= 1.0 for $A_b > 300$ mm.
k_4	Bar fibre factor	= 1.0 for CFRP and GFRP.
		= 1.25 for AFRP.
k_5	Bar surface profile factor	= 1.00 for spiral roughened or sand-coated surfaces.
		= 1.05 for spiral pattern surfaces.
		= 1.00 for braided surfaces.
		= 1.05 for ribbed surfaces.
		= 1.80 for indented surfaces.

CHAPTER 3: EXPERIMENTAL PROGRAM

3.1. General

The experimental program is divided into four series: (I) Static pullout; (II) Fatigue loading; (III) Freeze-thaw cycles along with sustained loads; (IV) Freeze-thaw cycles along with sustained loads followed by fatigue loading. The following flow chart outlines the experimental program.

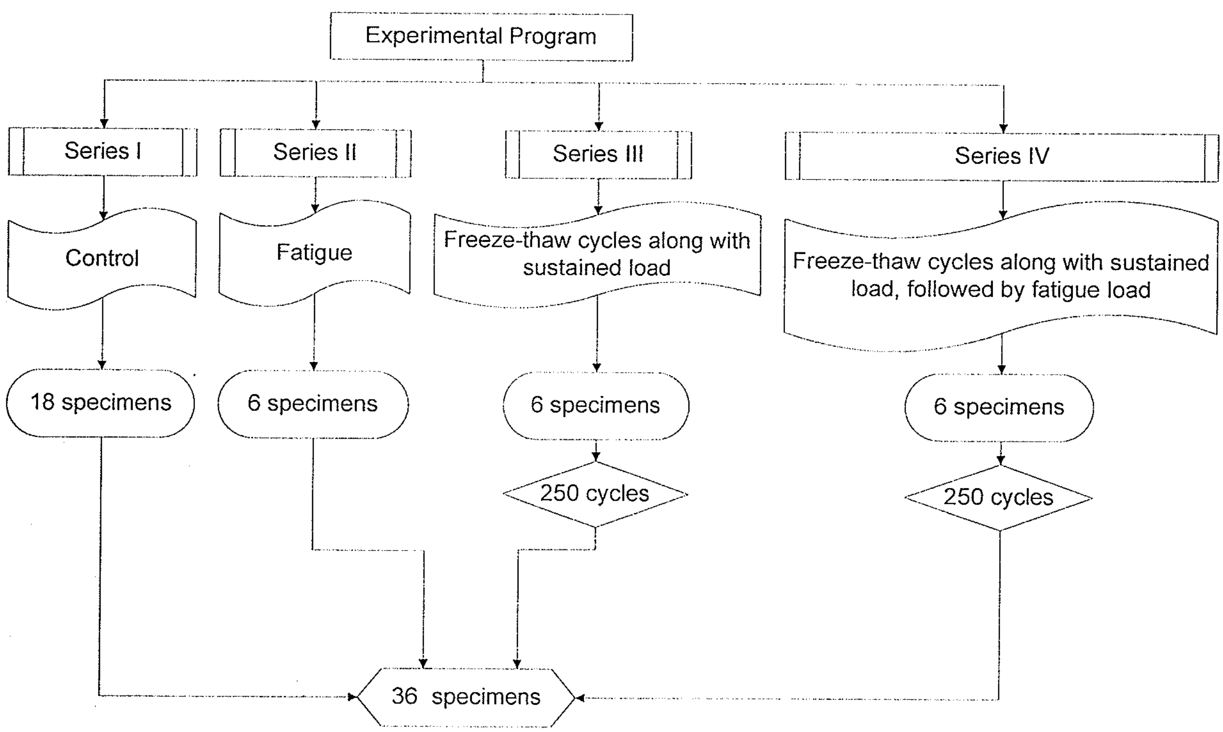

Fig. 3.1: Experimental program scheme

3.2. Material Properties

The materials used in this work are: concrete and sand-coated glass FRP bars commercially known as V-ROD™ (Pultrall Inc. 2007).

The specimens were fabricated using normal weight concrete with an average 28-day compressive strength of 50 MPa. In case of Series I to III, the anchor blocks were fabricated using normal weight concrete with an average 28-day compressive concrete strength of 55 MPa. At least twelve 100 by 200 mm and six 150 by 300 mm cylinders were prepared for each concrete batch to evaluate the compressive and tensile strength of concrete.

All the concrete used was mixed in the McQuade Heavy Structures Laboratory in the University of Manitoba using a mechanical mixer for quality control of the concrete. Table 3.1 presents the concrete mixture used in the specimens.

TABLE 3.1: Proportions of concrete mixture for 1 m^3

Material	50 MPa	55 MPa
	Quantity or ratio	Quantity or ratio
Cement (Type I) (kg)	488	540
Aggregate (10 mm) (kg)*	527	527
Fine aggregate (kg)*	598	515
Water/Cement ratio	0.42	0.40

Note.: * Properly dried for, at least, 24 hrs

The GFRP bars were composed of E-glass fibres with a minimum volume fraction of 65%, and as a bonding matrix a modified vinyl ester resin is used with a maximum volume of 35%. The surface of the bars is covered with sand to enhance bond behaviour (V-ROD – Product Guide Specification 2007).

Two bar sizes were used: No.16 (15.9-mm diameter) and No.19 (18.8-mm diameter). Table 3.2 present the properties of the GFRP bars, given by the manufacturer.

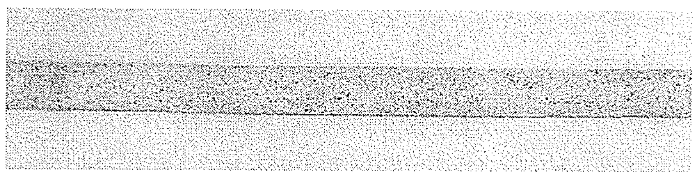

Fig. 3.2: GFRP bar

TABLE 3.2: Properties of GFRP bars (Pultrall Inc. 2007)

Bar size (mm)	Nominal d_b (mm)	Area (mm^2)	Weight (g/m)	Modulus of elasticity (MPa)	Guaranteed tensile strength (MPa)	Coefficient of thermal expansion (at $10^{-6}/^{o}C$)	
						Longitudinal	Transverse
No.16	15.9	198.0	425.5	48.2	683	6.4	29.1
No.19	19.1	285.0	614.5	47.6	656	6.0	29.0

3.3. Details of Specimens

The concentric static pullout test is used to assess the bond characteristics of the used GFRP bars as well as to provide a datum for the other test specimens using a standard procedure provided by CAN/CSA-S806-02 (CSA 2002). These specimens were used as control specimens along with the eccentric static pullout specimens.

The concentric static pullout specimen consists of a 200 mm side length concrete cube and a central GFRP bar with a $5d_b$ embedment length. Bond breakers were used in the loading end of the bar to avoid any interference from the bearing plates. The dimensions of the concrete cube were chosen to avoid splitting of the concrete. Steel pipes were used as anchors, and were cast with grout prior to the casting of the specimens. The eccentric static pullout specimen is very similar to the concentric one. It consists of a 200-mm side length concrete cube with a $5d_b$ embedment length, but eccentric placement of the bar.

No instrumentation was attached to the specimens in Series I. Details of the specimens are presented in Figure 3.3.

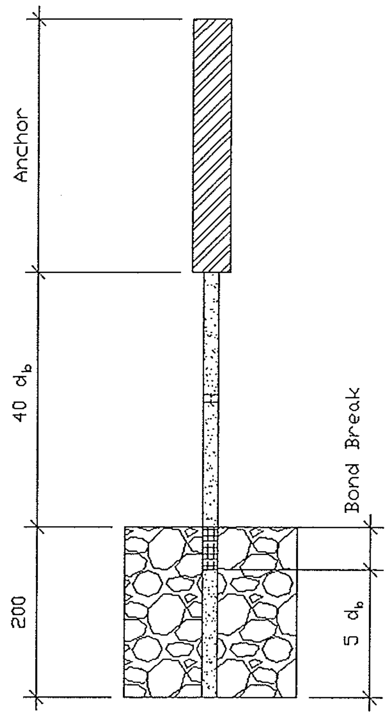

(a) Concentric

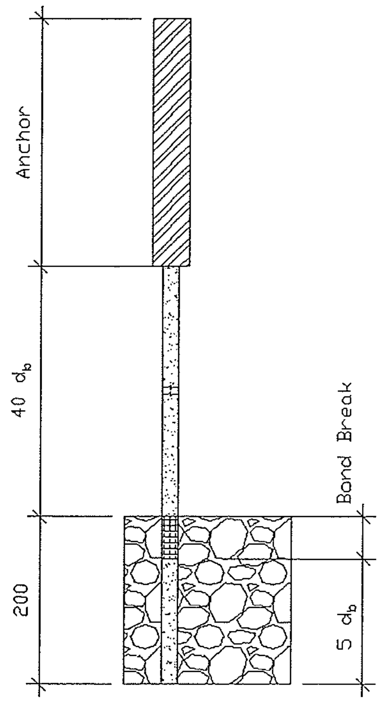

(b) Eccentric

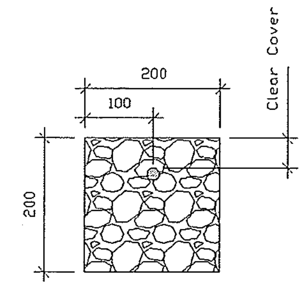

(c) Plan view 1

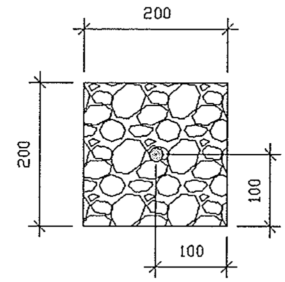

(c) Plan view 2

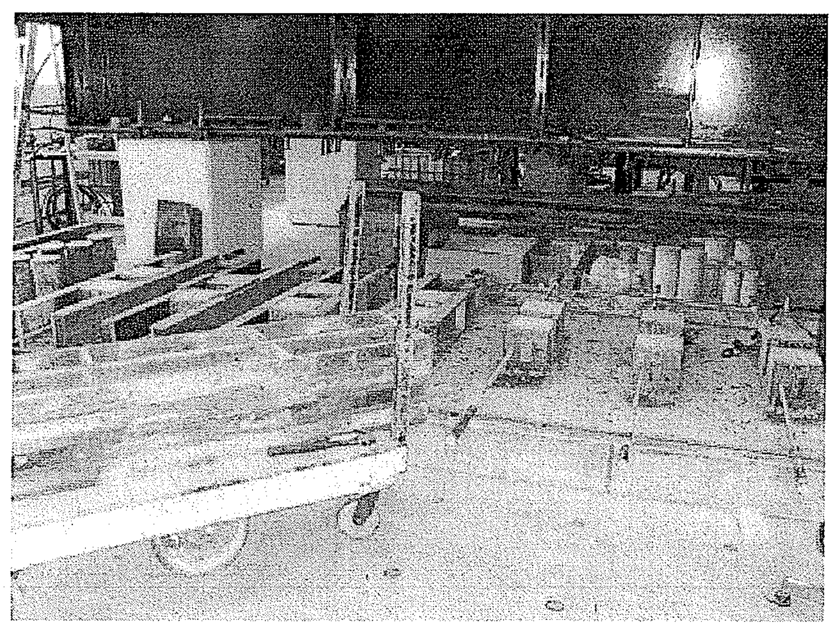

(d) Construction

Fig. 3.3: Series I: specimen details

The FRP specimens of Series II to IV have the same geometry as those of Series I. The specimen consists of three concrete blocks: the test portion, (the middle block) and two end anchor blocks. The three portions were connected together by the GFRP bar. The specimen was designed so that it would be able to carry fatigue and /or sustained loading without premature failure.

The middle block was a 200 mm wide, by 200 mm deep by 405 mm long prism. These dimensions were selected such that after conditioning, each specimen was split into two 200 mm side length cube specimens for static pullout test (considering a 5 mm clearance for the cutting saw). The end anchors were 200 mm wide by 507.5 mm long with a variable depth, depending on the concrete clear cover chosen for the middle block. The GFRP bar was always eccentric in the middle block, while the end anchors were always adjusted to be concentric with respect to the GFRP bar. Bond breakers were placed as shown in the Figure 3.4. Two U-Shaped steel grids were used to reinforce the end anchors, to further eliminate the possibility of concrete splitting during conditioning and testing. Each anchor contained six 16 mm-diameter thread rods placed perpendicular to the axis of the GFRP bar to apply the necessary loads.

A strain gauge was attached to the GFRP bars in all specimens of Series III and IV. Also, a thermocouple was attached to the GFRP bars in four specimens: S.FT.16.15, S.FT.19.25, S.FT.F.16.15 and S.FT.F.19.25, which represented the specimens with the smallest and largest concrete covers of each series. These thermocouples were attached to verify the temperature inside the specimens during the freeze-thaw cycles. Details of the specimens in Series II to IV are presented in Figures 3.4 and 3.5. It should be noted that specimens of Series II had neither strain gauges nor thermocouples.

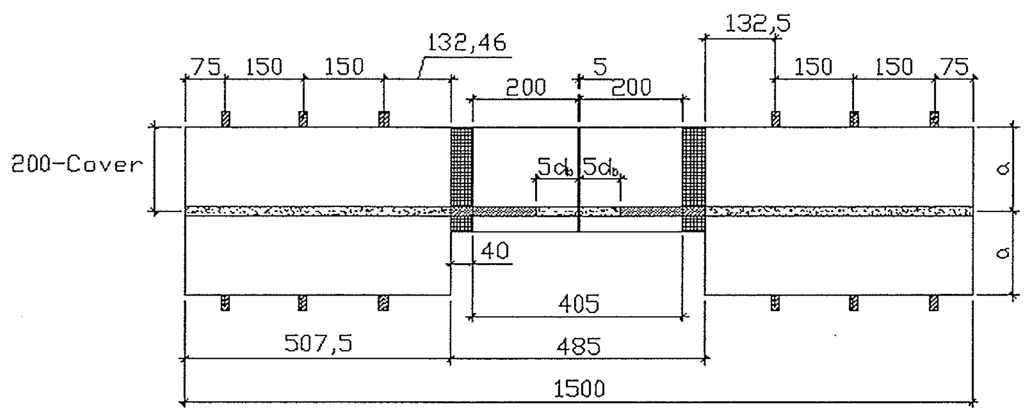

(a) Plan view

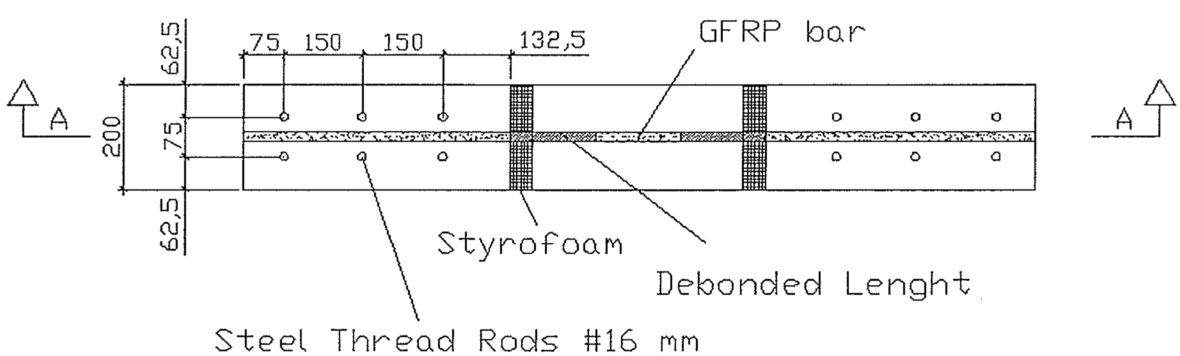

(b) Elevation

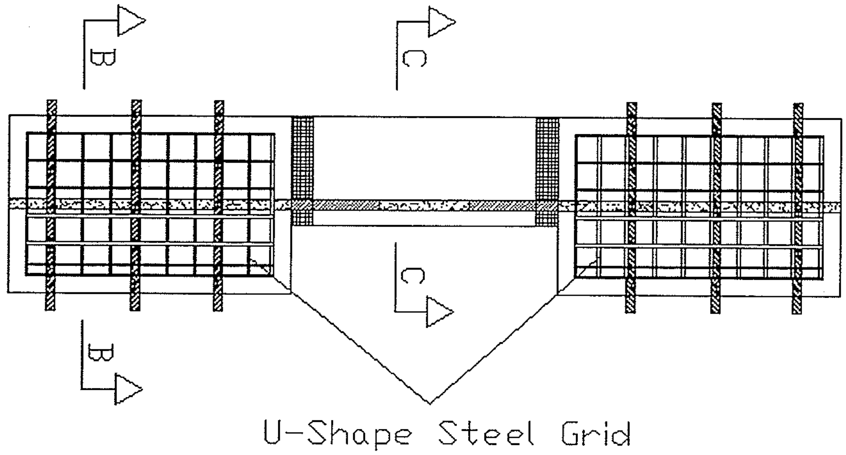

(c) Section A-A

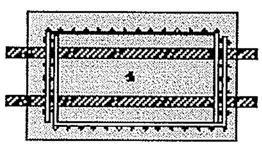

(d) Section B-B

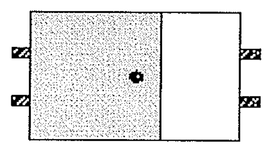

(e) Section C-C

Fig. 3.4: Series II to IV: specimen details

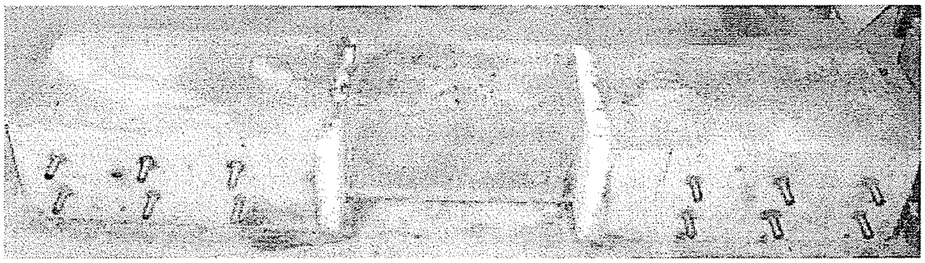

(a) Specimen

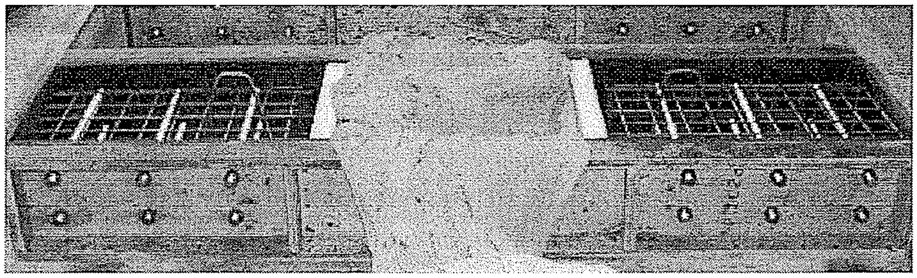

(b) Form work

Fig. 3.5: Series II to IV: specimen construction

3.4. Test Parameters

The table below presents the specimens parameters.

TABLE 3.3: Test parameters

Specimens	Name*	Compressive Strength (MPa)	Sustained load	Freeze-thaw cycles	Fatigue load
Series I	C.16	50	No pre-conditioning	No pre-conditioning	No pre-conditioning
	C.19				
	E.16.15				
	E.16.20				
	E.16.25				
	E.19.15				
	E.19.20				
	E.19.25				
Series II	F.16.15	50	No pre-conditioning	No pre-conditioning	1,000,000 cycles at 1.5 Hz and 25% of GTS*
	F.16.20				
	F.16.25				
	F.19.15				
	F.19.20				
	F.19.25				
Series III	S.FT.16.15	50	30% of GTS*	250	No pre-conditioning
	S.FT.16.20				
	S.FT.16.25				
	S.FT.19.15				
	S.FT.19.20				
	S.FT.19.25				
Series IV	S.FT.F.16.15	50	30% of GTS*	250	1,000,000 cycles at 1.5 Hz and 25% of GTS*
	S.FT.F.16.20				
	S.FT.F.16.25				
	S.FT.F.19.15				
	S.FT.F.19.20				
	S.FT.F.19.25				

*Note: GTS stands for guaranteed tensile strength of the GFRP bar

Notes: *C – refers to the concentric specimens and E – refers to the eccentric specimens; S – stands for sustained load, FT – freeze-thaw cycles, F – fatigue load, the first two numbers represent the bar diameter (No.16 or No.19), the following two numbers stands for the concrete clear cover (1.5, 2.0 or 2.5d_b). So, for example, S.FT.F.16.15 stands for a specimen subjected to sustained load, to freeze-thaw cycles, followed by fatigue loading, considering bar diameter No. 16 mm and concrete clear cover of 1.5d_b; C.16 stands for concentric specimen with bar diameter No. 16 mm; and E.19.25 refers to the eccentric specimens with bar diameter No. 19 mm and concrete clear cover of 2.5d_b.

3.5. Construction and Curing of Specimens

All the specimens were constructed using wood formwork. As previously mentioned, all concrete mixes were prepared by the author using a mechanical mixer (see Fig. 3.5). Figure 3.7 illustrates the process of dividing the materials into 3 or 4 "batches", since the amount of concrete was relatively large for the mixer. After all the formwork was assembled, the concrete was cast. The following day, the formwork was disassembled and the curing process started. Curing was provided by wrapping the specimens with wet burlap and a plastic sheet to avoid evaporation losses. The curing process continued for 7 days.

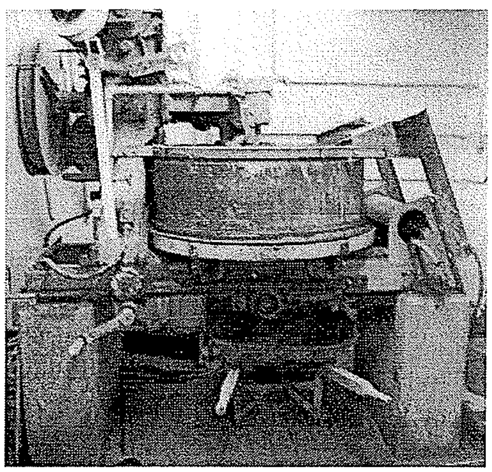

Fig. 3.6: Concrete mixer

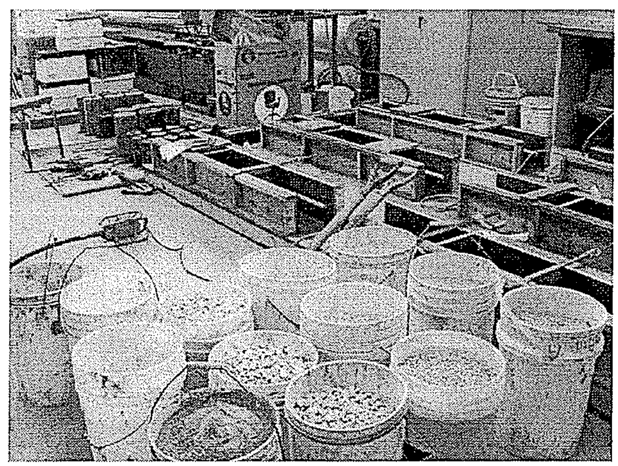

Fig. 3.7: Material preparation

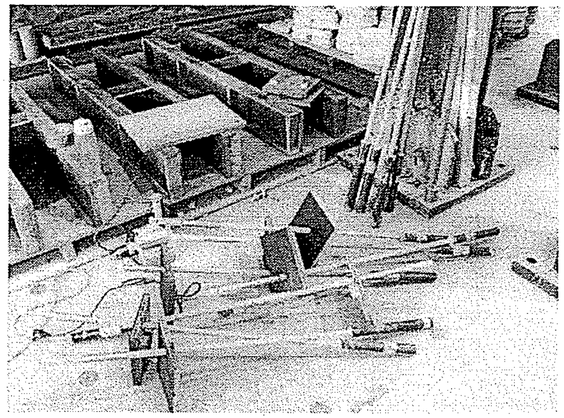

Fig. 3.8: Detail of steel anchors and bond breakers in Series I

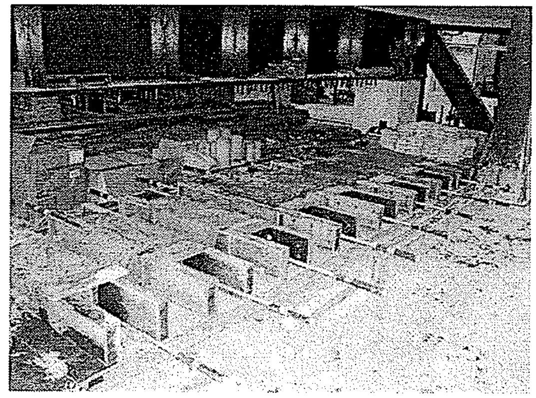

Fig. 3.9: Curing process, with wet burlap sheets

3.6. Conditioning

For the specimens subjected to combined conditioning, the order of conditioning was sustained load, followed by freeze-thaw cycles, and then fatigue loading, where applicable.

3.6.1. Sustained loading

A sustained load of 30% of the guaranteed tensile strength (GTS) of the GFRP bar was applied to the specimens of Series III and IV. This value is the maximum limit of sustained load on GFRP bars permitted by the CAN/CSA-S806-02 (CSA 2002). The sustained load was applied to the specimen through a prestressing bed. A set of steel plates was used to apply the load. Steel angles and two 38-mm diameter thread rods were used to hold the anchors in place, thus sustaining the load. To avoid relative movement between concrete and the steel angles, nuts were used on both sides of the angles, as shown in detail in Figure 3.12. During prestressing, the load was monitored by a load cell, while the strains in the GFRP bars were monitored by a strain gauge.

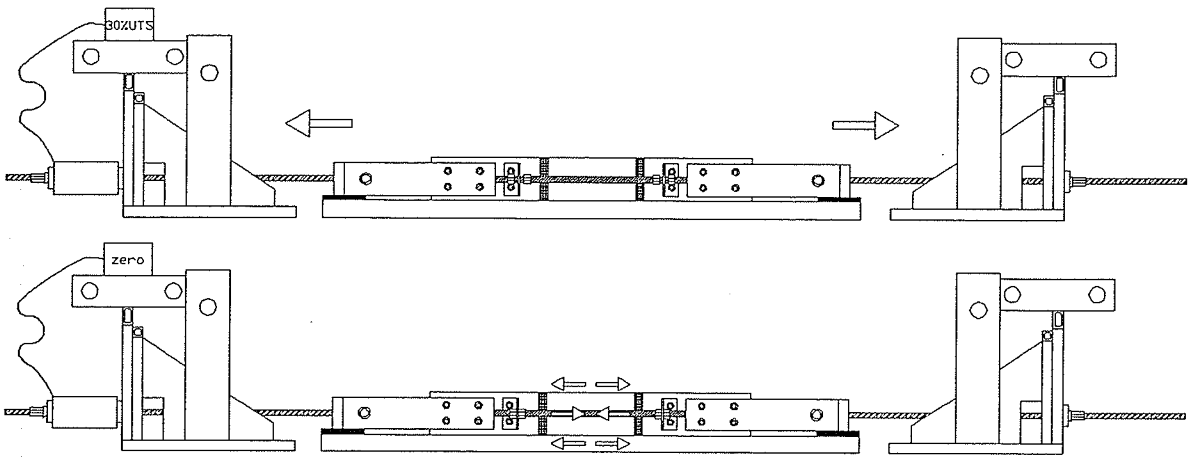

Fig. 3.10: Sustained loading set-up: elevation

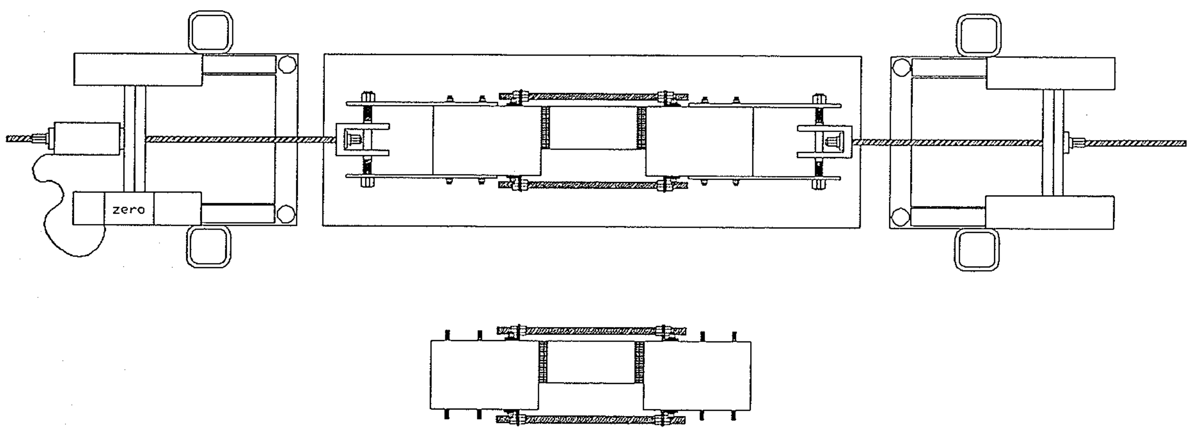

Fig. 3.11: Sustained loading set-up: plan view and specimen under sustained load

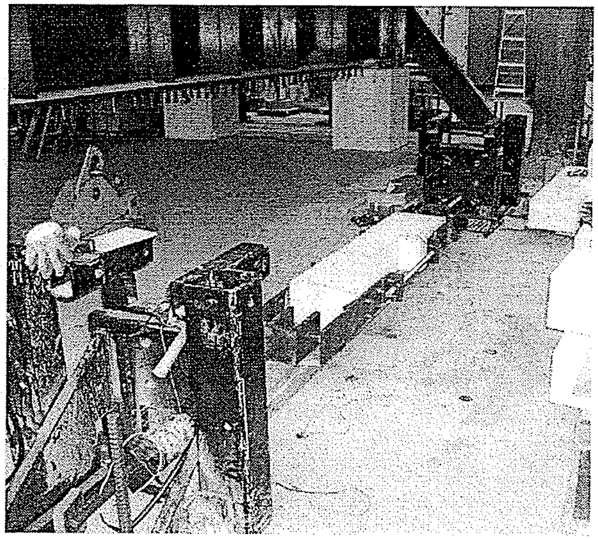

(a) Diagonal view of the prestressing bed

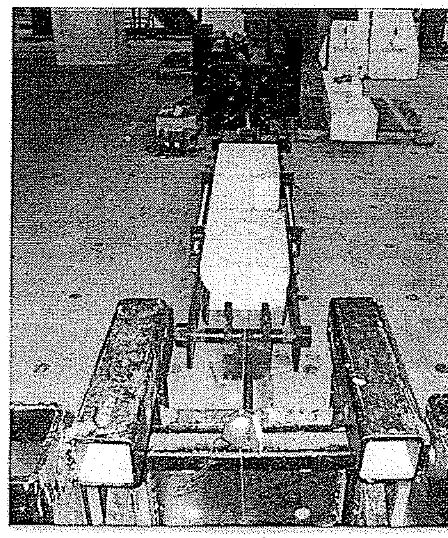

(b) Longitudinal view of the prestressing bed

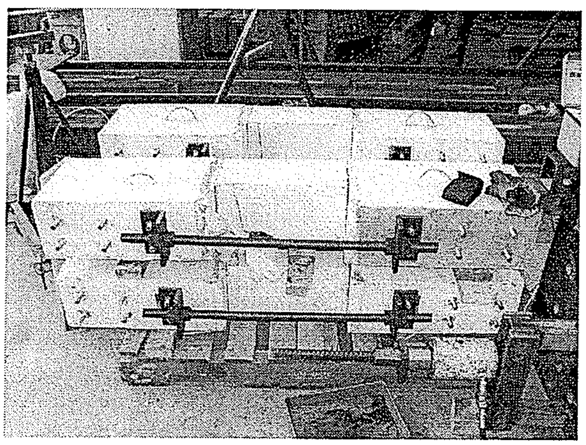

(c) Specimens under sustained load

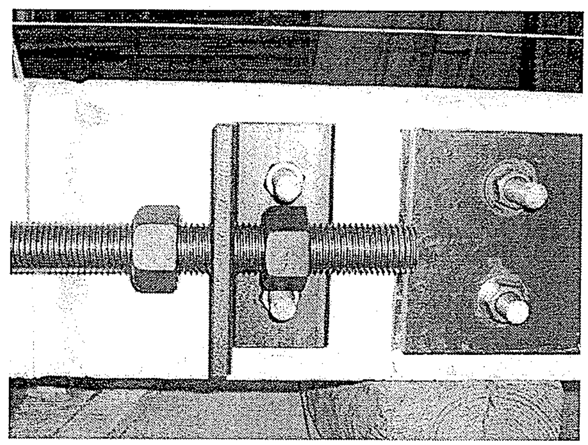

(d) Detail of restraint

Fig. 3.12: Details of prestressing

3.6.2. Freeze-thaw cycles

The freeze-thaw cycles were applied in accordance with ASTM C666-03 (2003). The cycles were from -25°C to +15°C. Such temperature range was chosen, because the environmental chamber available could not achieve lower temperatures than -25°C and +15°C was easily reaching the required +4°C inside the specimens. The environmental chambers allowed control of the moisture content in the air. Therefore, the relative humidity was forced to 50% during freezing and 95% during thawing. The freezing period was kept for 5 hrs and the thawing period for 3 hrs. The environmental chamber available in the structures laboratory is capable of providing a maximum rate of 1°C / 3 min, thus the required time to achieve the specified temperatures was 2 hrs. In other words, one cycle took 12 hrs. A total of 250 cycles were applied in approximately 4 months.

Four of the twelve specimens were instrumented with thermocouples to ensure that the specified temperatures were achieved. In addition, one thermocouple was used to measure the room temperature.

(a) Specimens inside chamber

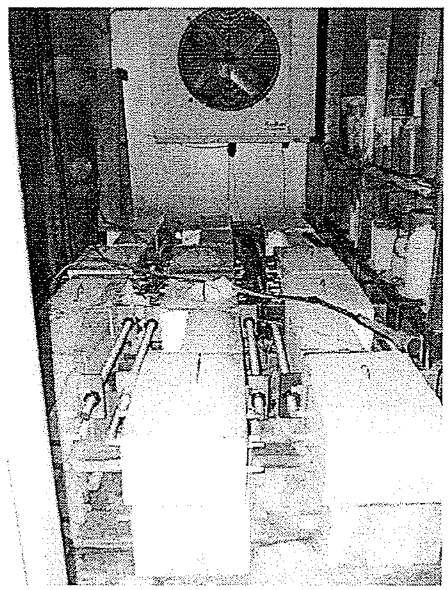

(b) Freezing

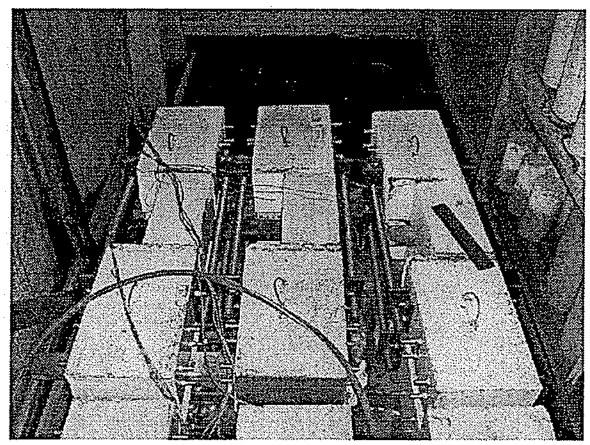

(c) Thawing

(d) Cylinders

Fig. 3.13: Specimens inside environmental chamber

3.6.3. Fatigue loading

In this part of the program, the specimens were conditioned to 1,000,000 cycles. The amplitude of the load was from 25% to 2.5% of the guaranteed tensile strength of the GFRP bar. This value is the maximum level of fatigue on GFRP bars permitted by the CAN/CSA-S6-06 (2006). The fatigue load was applied with a sinusoidal function, at a frequency of 1.5 Hz. A 1,000 kN MTS machine was used to perform the fatigue test.

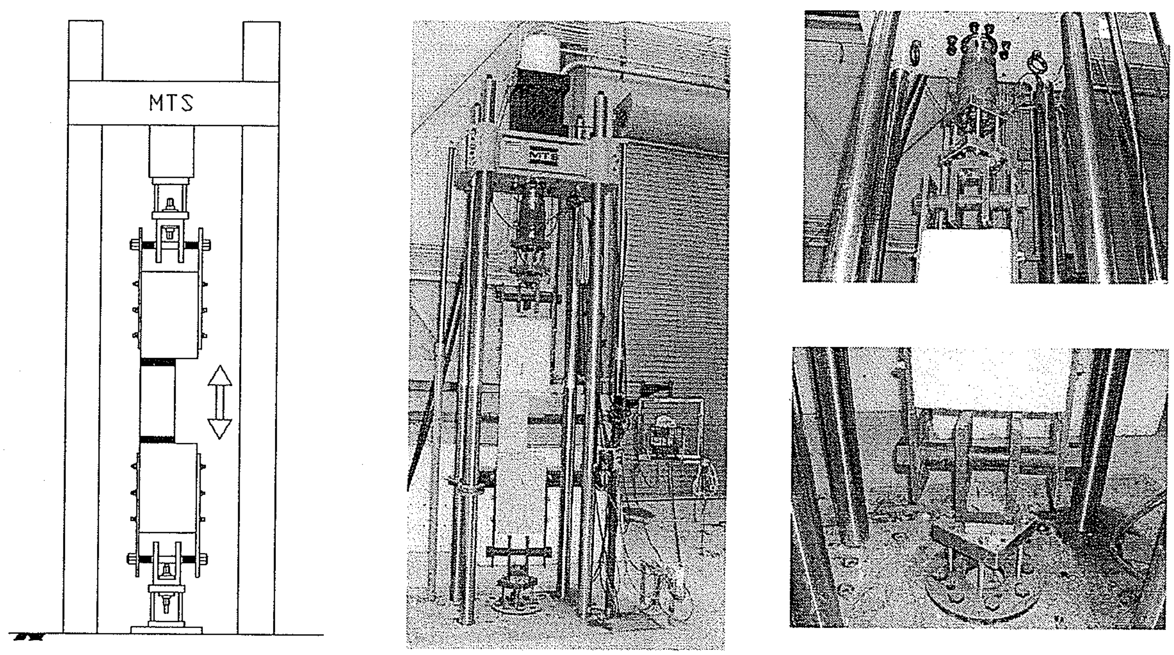

(a) Fatigue test (b) View of test set-up (c) Details of connections

Fig. 3.14: Details of fatigue test

3.7. Test Set-up and Procedure

The static/monotonic pullout tests were performed using the same 1,000 kN MTS machine used for fatigue loading. A set of two steel angles and two steel strips were used to tie the specimen to the strong floor. In the case of specimens of Series I, a wedge-type gripping system was used to hold the steel sleeve (anchor) and pull the GFRP bar, while in the other series the anchor blocks were pulled by the same set of steel plates used to apply the sustained load. The tests were performed under load control, at a rate of 10 kN/min.

A high accuracy LVDT was used to measure the free-end slip during pullout. The LVDT was glued to the free surface of the specimen before placing the specimen in the testing position.

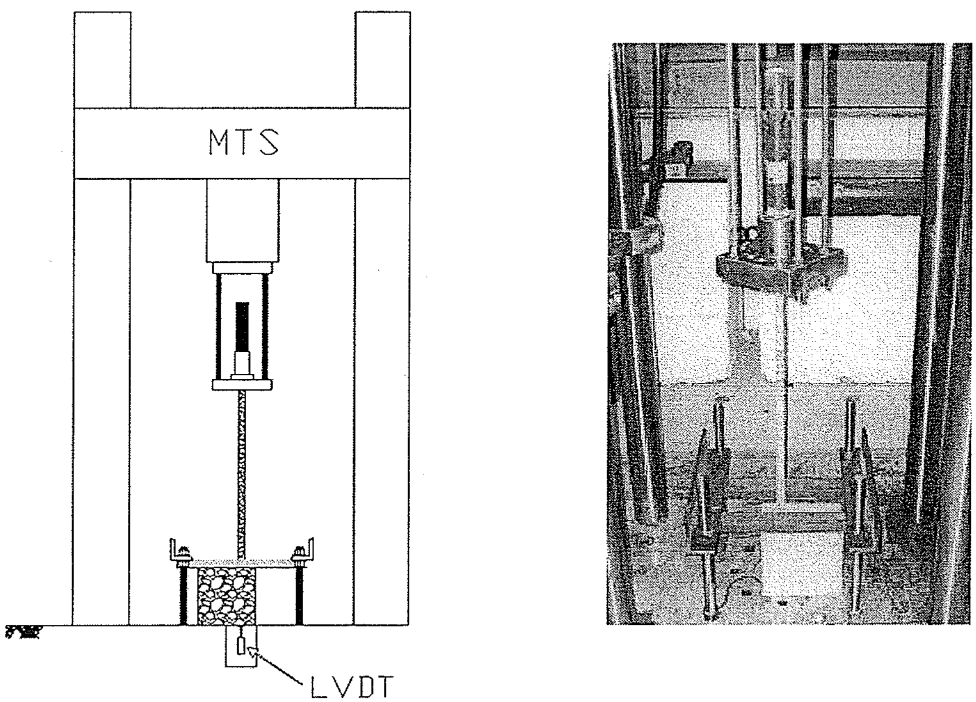

(a) Series I

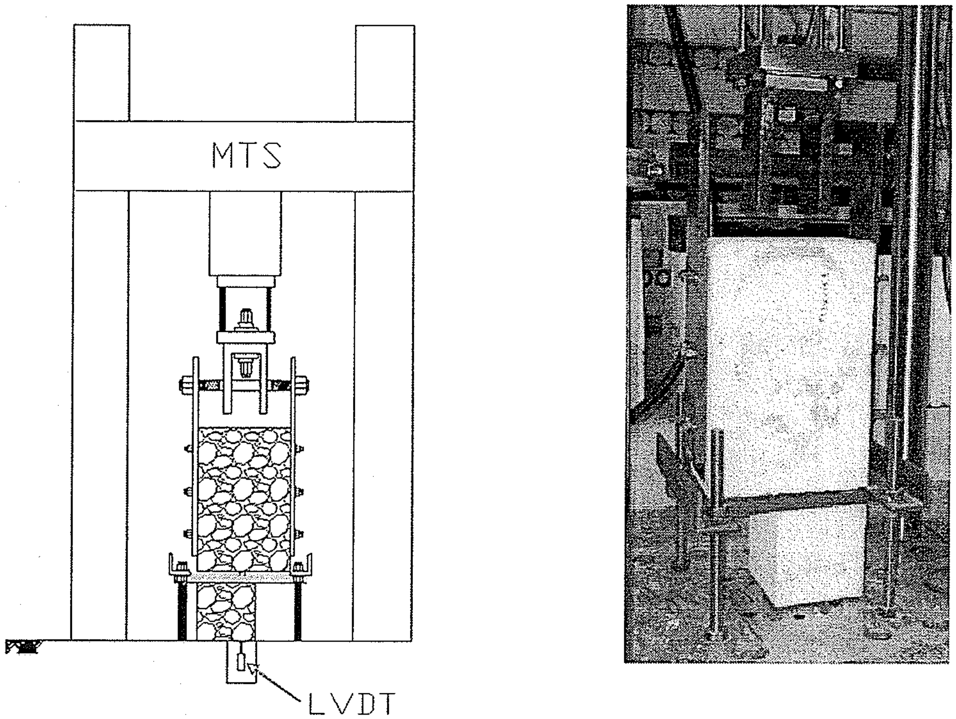

(b) Series II to IV

Fig. 3.15: Details of pullout test set-up

CHAPTER 4: ANALYSIS OF EXPERIMENTAL RESULTS

In this chapter, the experimental results along with observations are presented. Also an analysis of development length is performed and comparisons are made with Canadian standards.

4.1. Pullout Results

In this section the results regarding bond strength and slip measurements are presented in terms of the following relationships: bond stress versus free-end slip, bond strength versus concrete clear cover and peak slip versus different specimens. Also, a summary of results is presented in table format.

The term slip represents the relative displacement between the concrete and the GFRP bar. The slip can be measured at the free-end or at the loaded-end. Due to the specimen layout in Series II to IV, which didn't allow measurements at the loaded-end, only the free-end slip was measured.

The bond stress was assumed constant along the embedded length. Such assumption is very reasonable because the embedment length was only 5 d_b.

$$\tau = \frac{P}{\pi . d_b . l_e} \qquad \textbf{Equation 4-1}$$

In the following figures, the bond stresses versus free-end slip curves are presented. The curves are grouped by bar diameter and concrete clear cover. Figures 4.1 to 4.6 investigate the influence of the different conditionings in the bond stress versus slip curve (in terms of bond strength and slip values). Figures 4.7 to 4.18 the effect of the bar diameter is evaluated. Figures 4.19 to 4.21, evaluate the effect of the concrete clear cover.

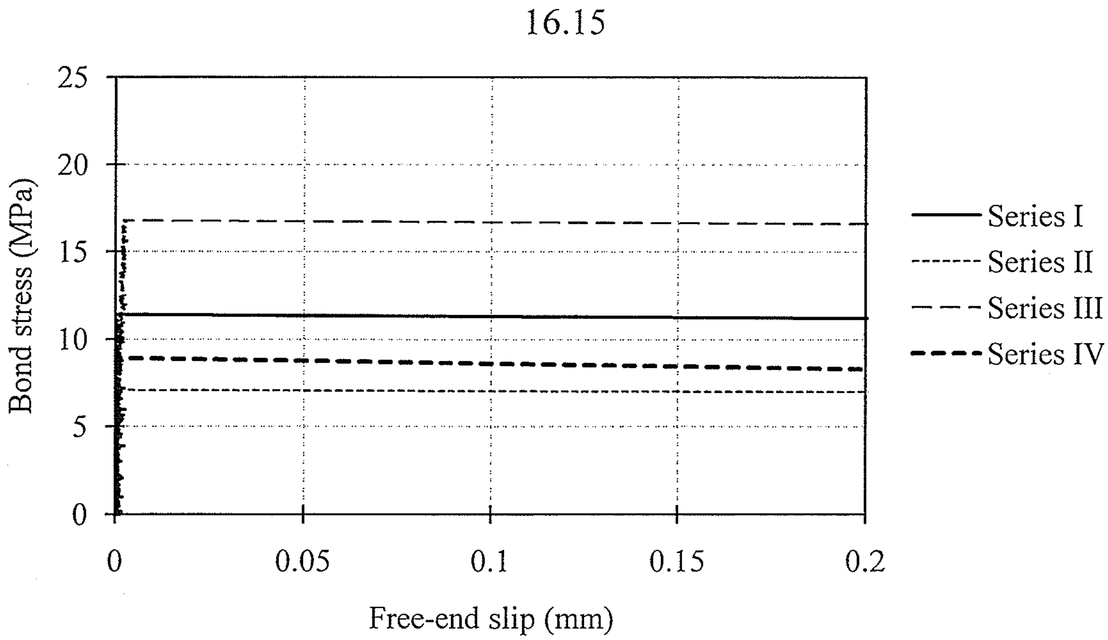

Fig. 4.1: Effect of conditioning: bar No. 16 and concrete clear cover of $1.5d_b$

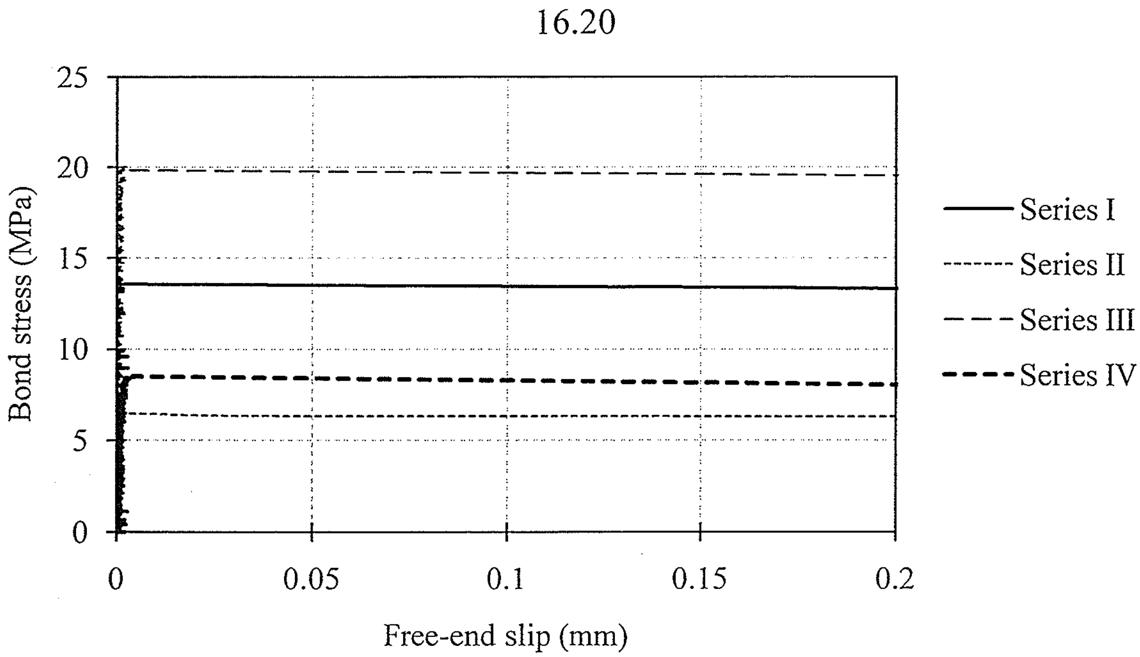

Fig. 4.2: Effect of conditioning: bar No. 16 and concrete clear cover of $2.0d_b$

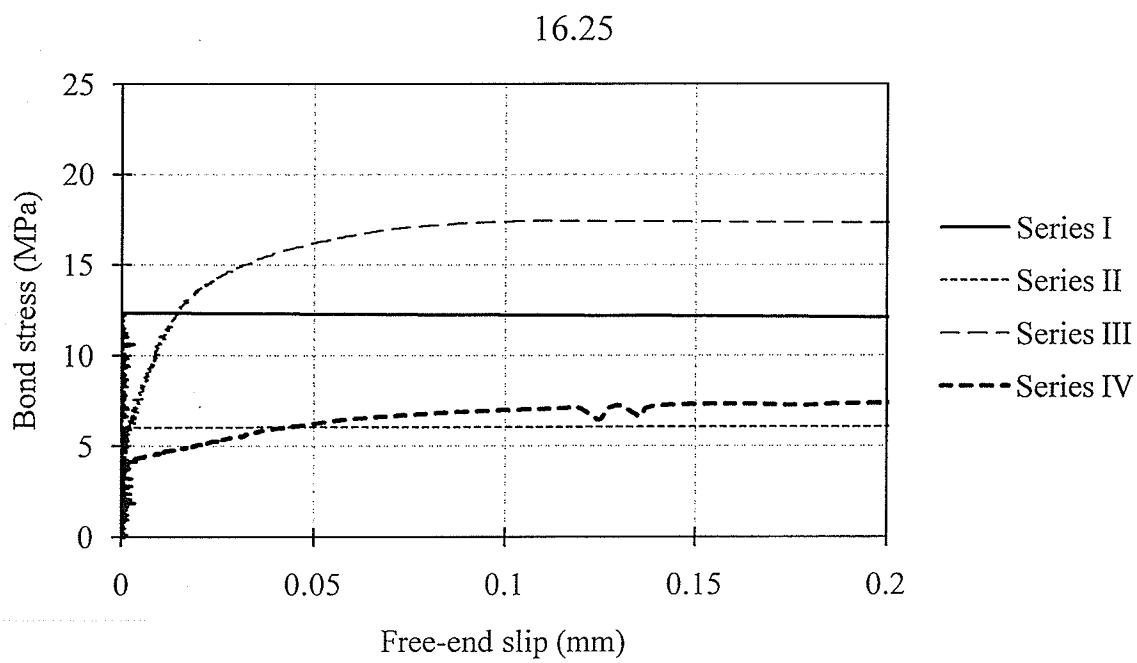

Fig. 4.3: Effect of conditioning: bar No. 16 and concrete clear cover of $2.5d_b$

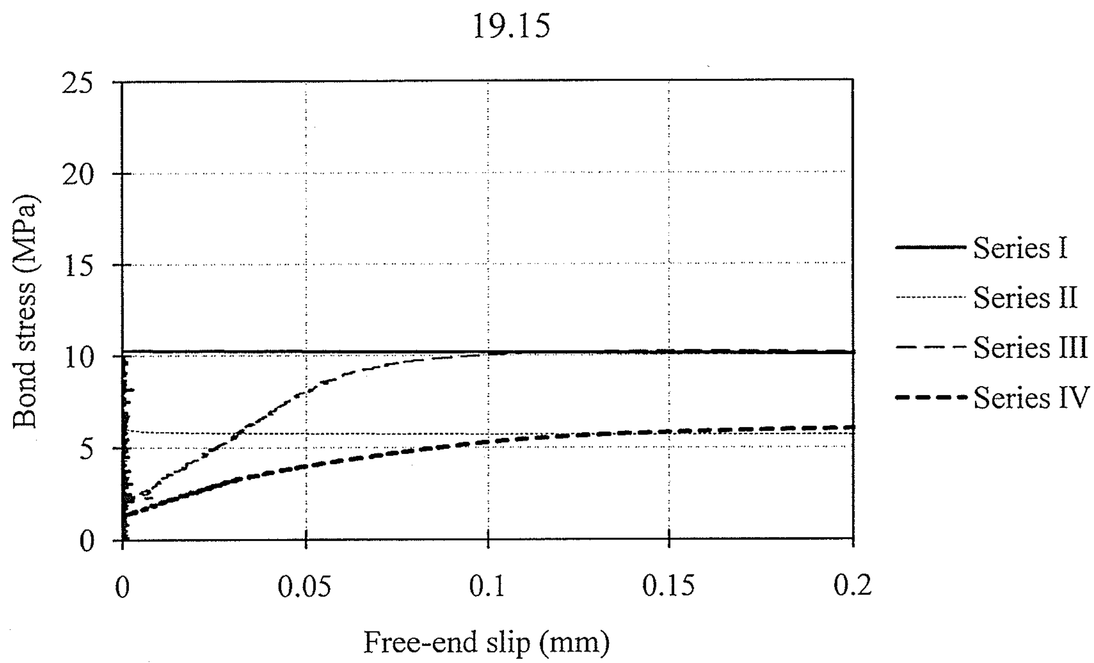

Fig. 4.4: Effect of conditioning: bar No. 19 and concrete clear cover of $1.5d_b$

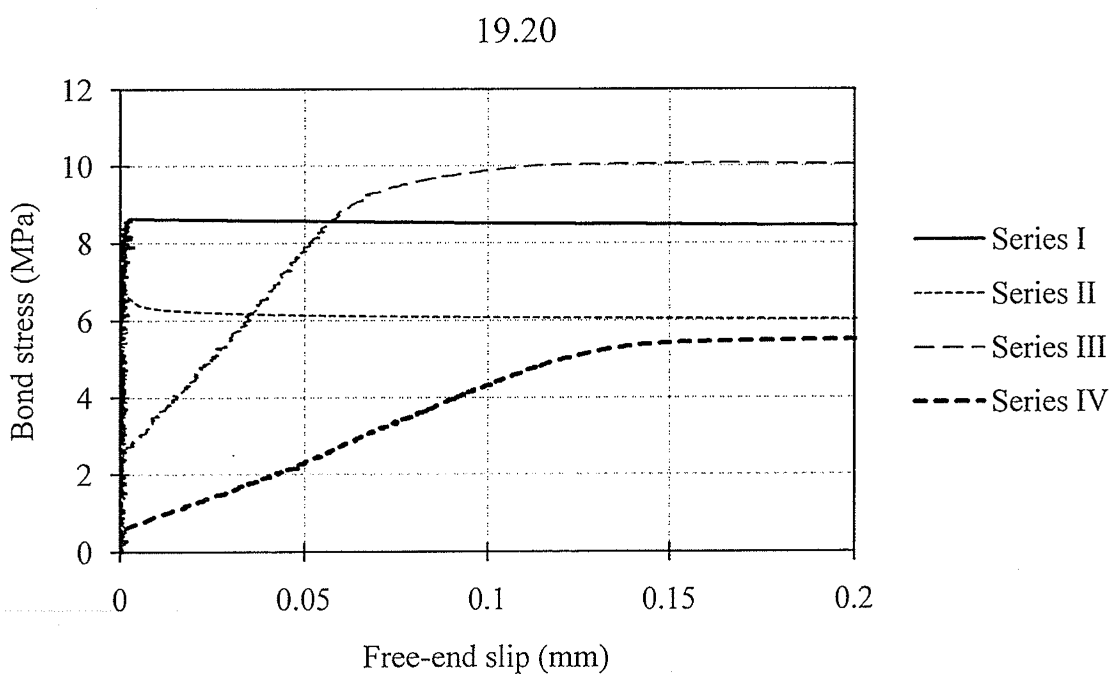

Fig. 4.5: Effect of conditioning: bar No. 19 and concrete clear cover of $2.0d_b$

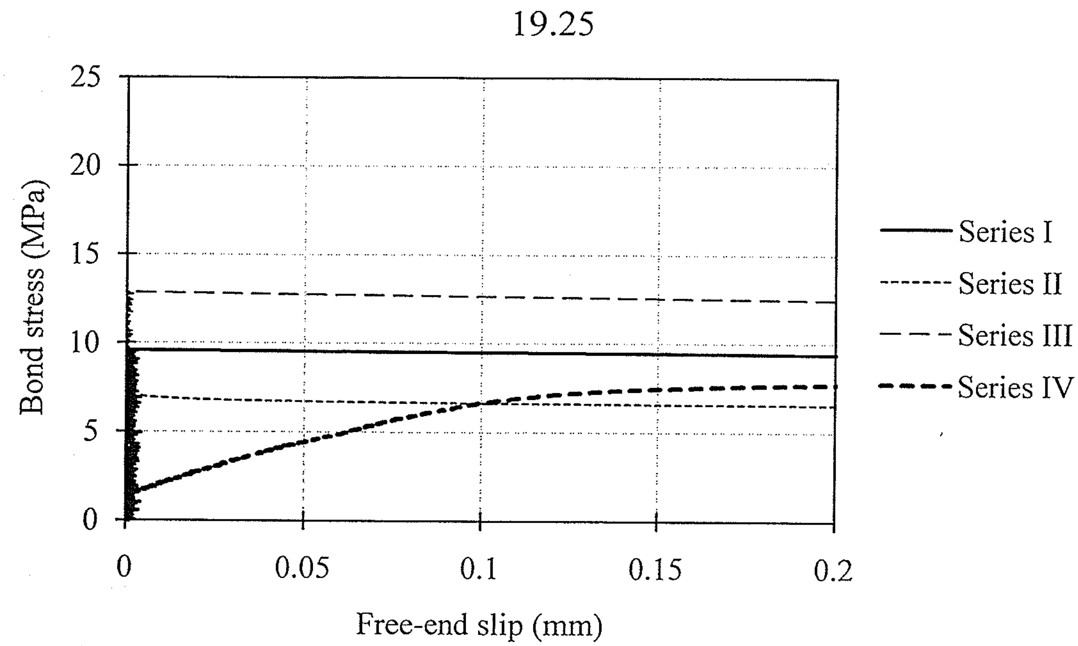

Fig.4.6: Effect of conditioning: bar No. 19 and concrete clear cover of $2.5d_b$

The curves presented in figures 4.1 to 4.6 show that the fatigue conditioning promoted great deterioration in the bond strength and no change in slip (or in the bond stiffness) for both bar diameters. As for the freeze-thaw cycles, it increased the bond strength for bars No. 16 considering all cover and No. 19 with concrete cover of $2.5d_b$. Such conditioning promoted great increase in the peak slip (decrease in bond stiffness) for bars No. 19, while for bars No. 16, only specimens with concrete clear cover of $2.5d_b$ presented an increase in slip.

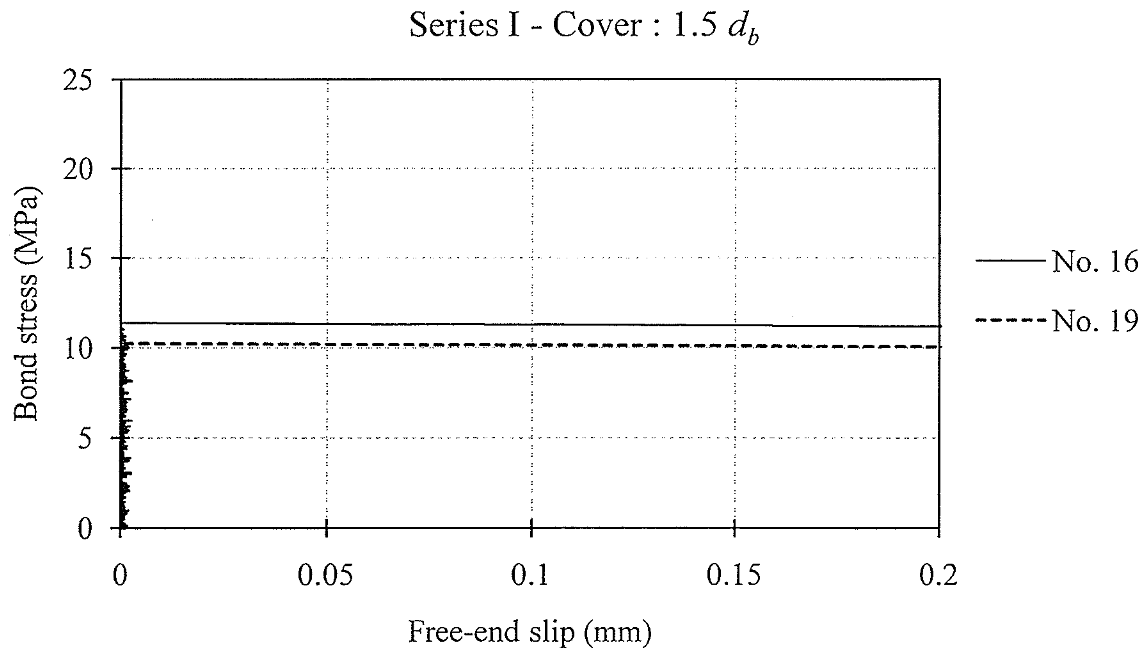

Fig. 4.7: Effect of bar diameter: Series I and concrete clear cover of $1.5d_b$

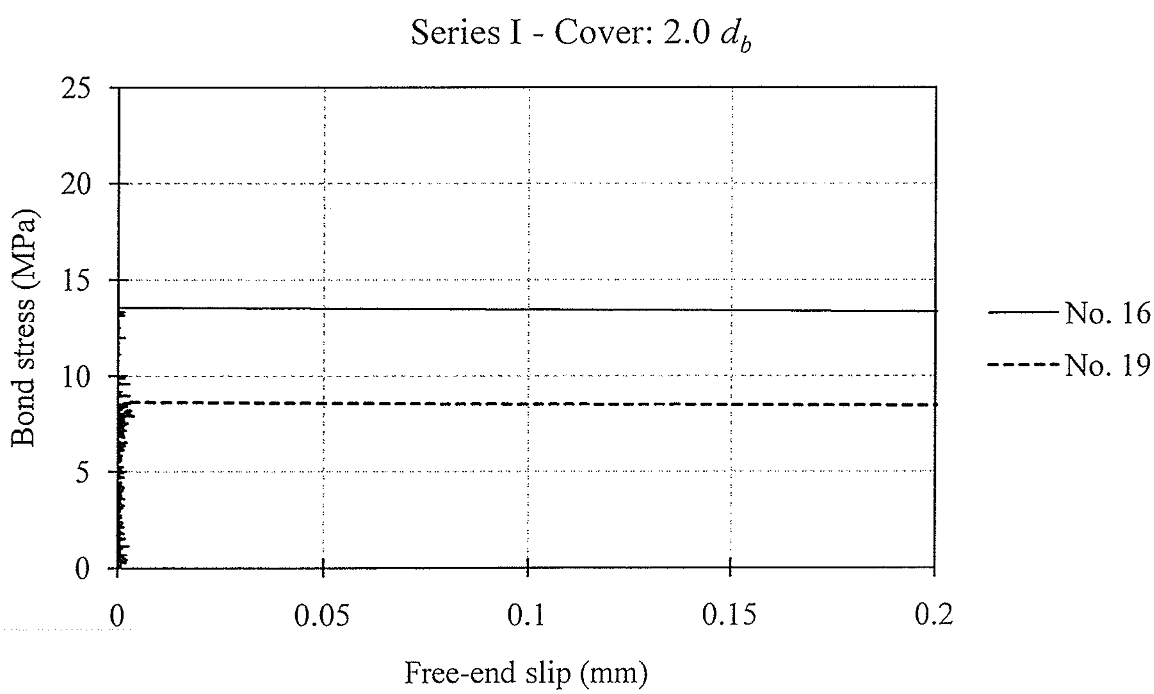

Fig. 4.8: Effect of bar diameter: Series I and concrete clear cover of $2.0d_b$

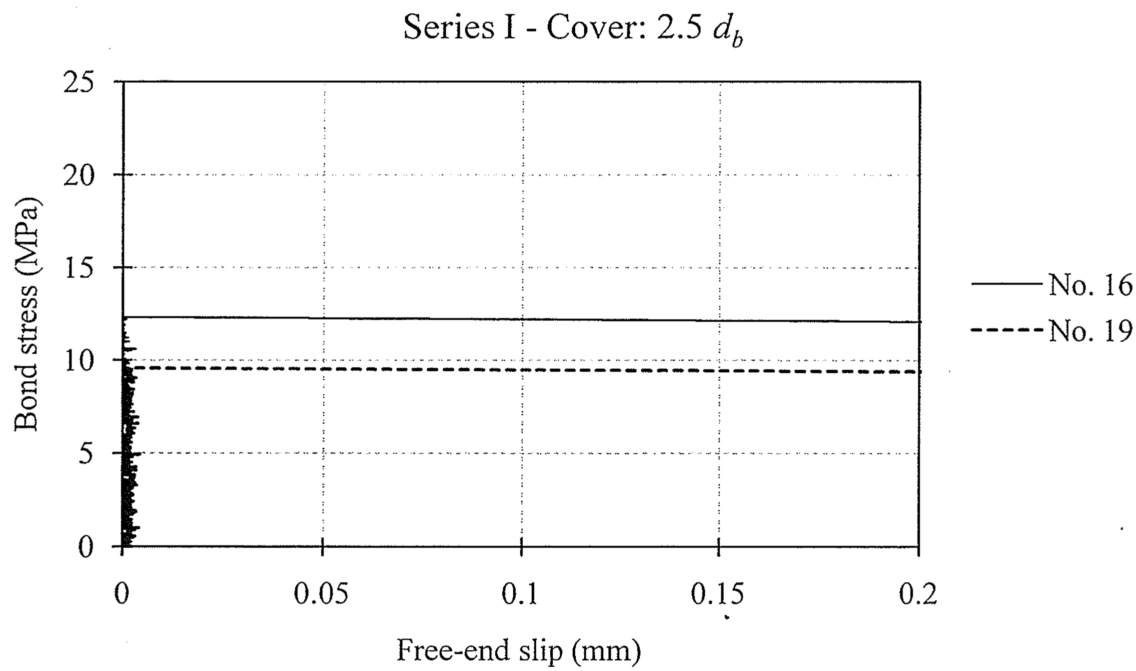

Fig. 4.9: Effect of bar diameter: Series I and concrete clear cover of $2.5d_b$

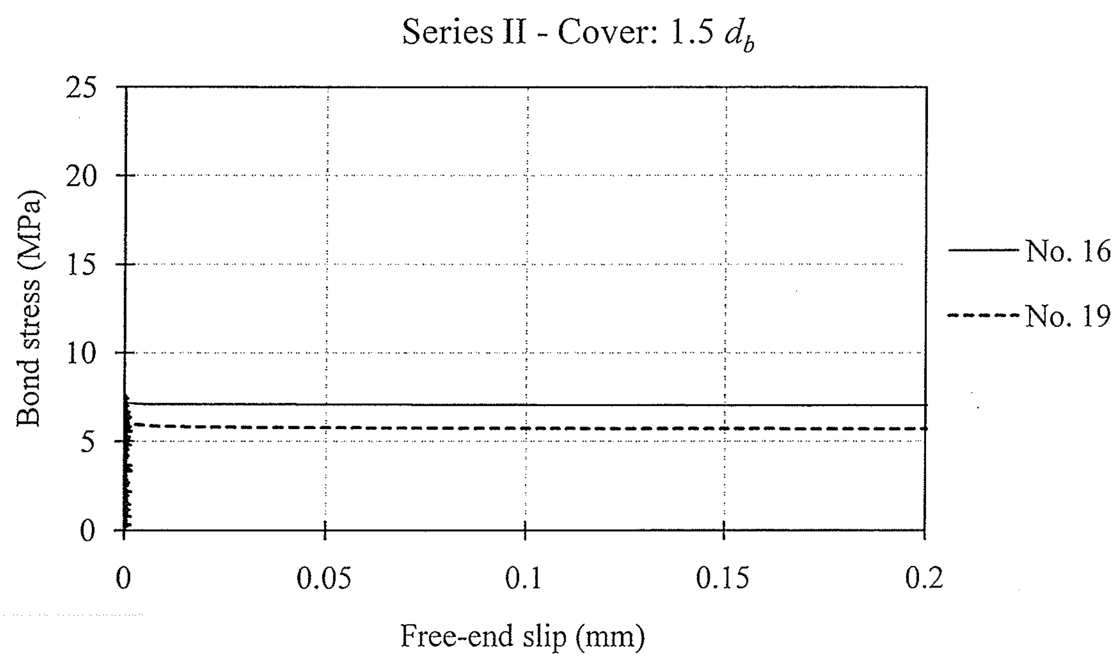

Fig. 4.10: Effect of bar diameter: Series II and concrete clear cover of $1.5d_b$

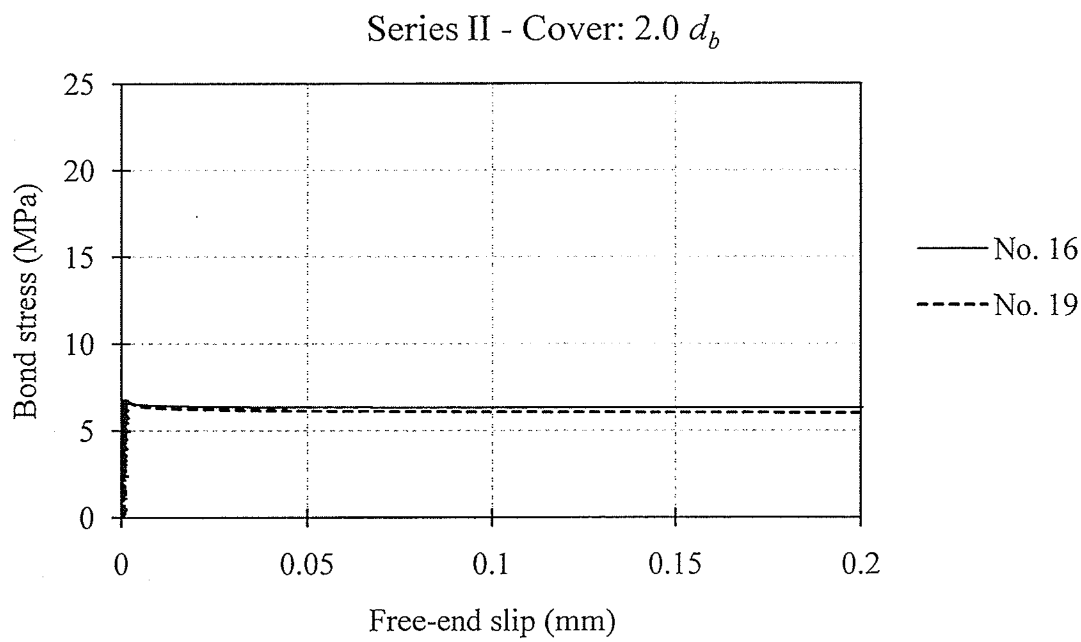

Fig. 4.11: Effect of bar diameter: Series II and concrete clear cover of $2.0d_b$

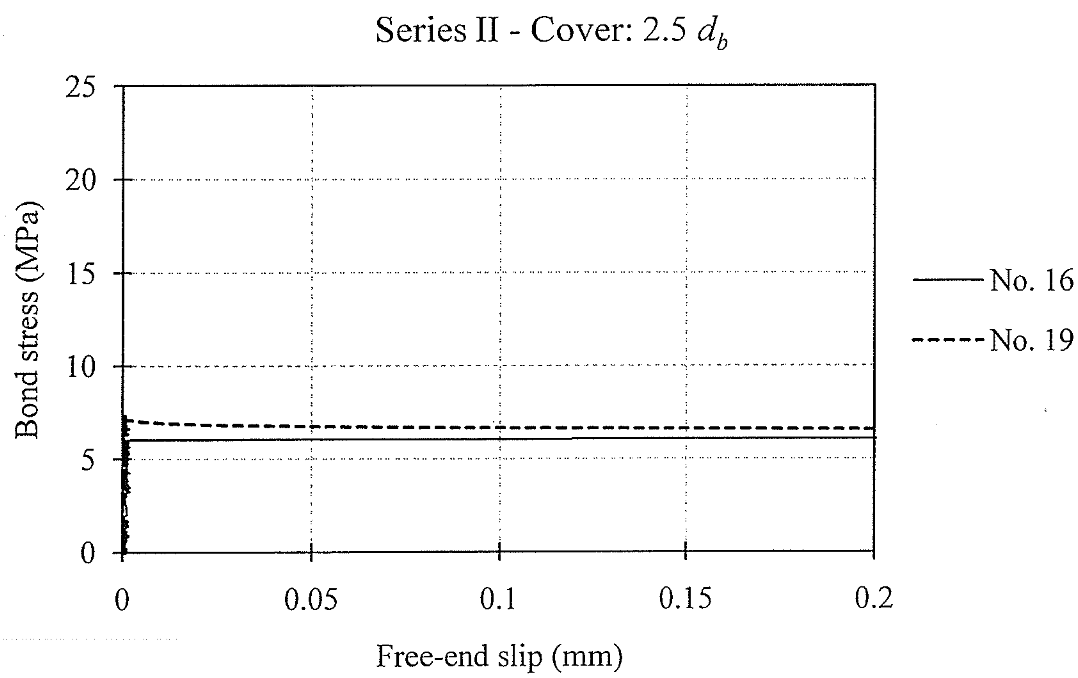

Fig. 4.12: Effect of bar diameter: Series II and concrete clear cover of $2.5d_b$

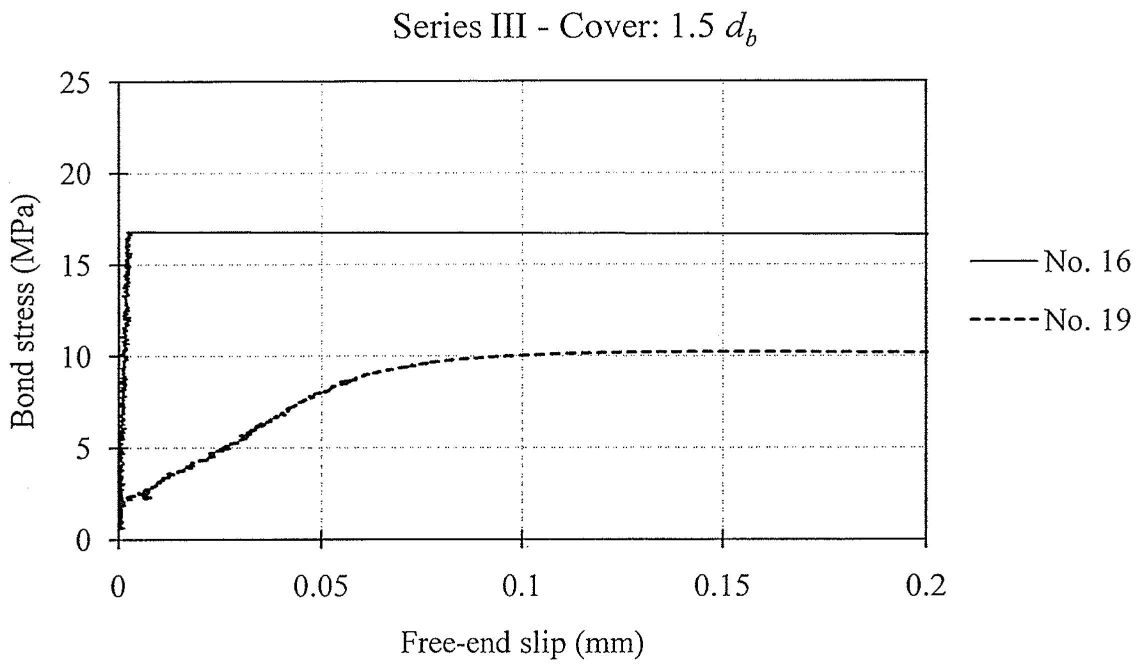

Fig. 4.13: Effect of bar diameter: Series III and concrete clear cover of 1.5d_b

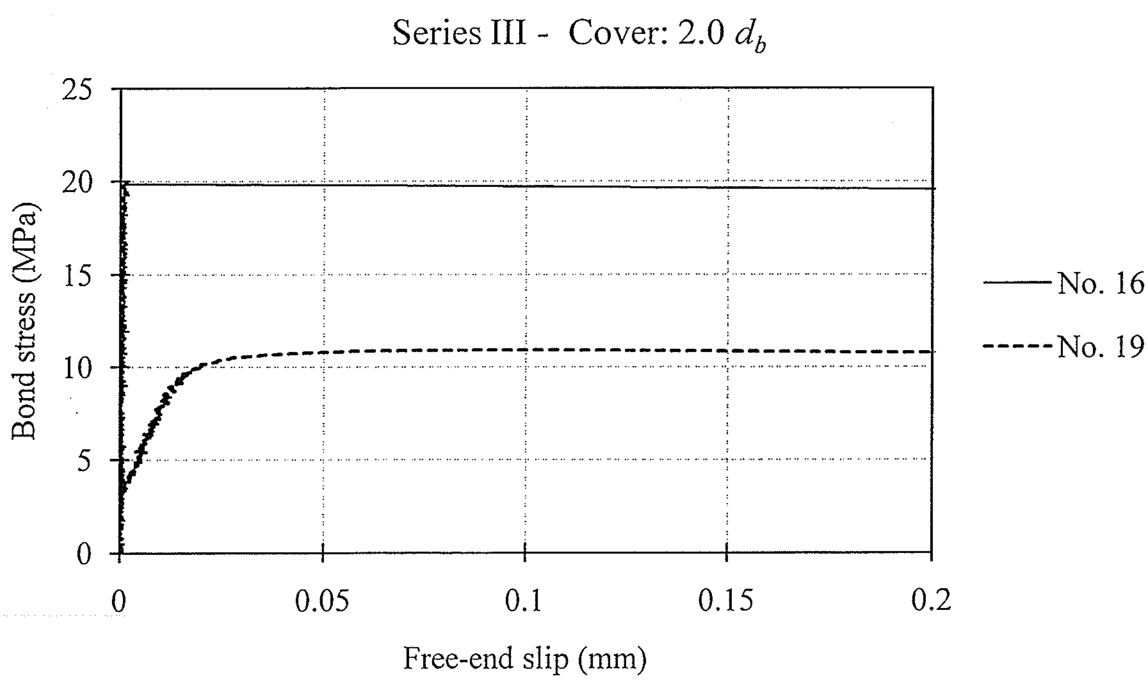

Fig. 4.14: Effect of bar diameter: Series III and concrete clear cover of 2.0d_b

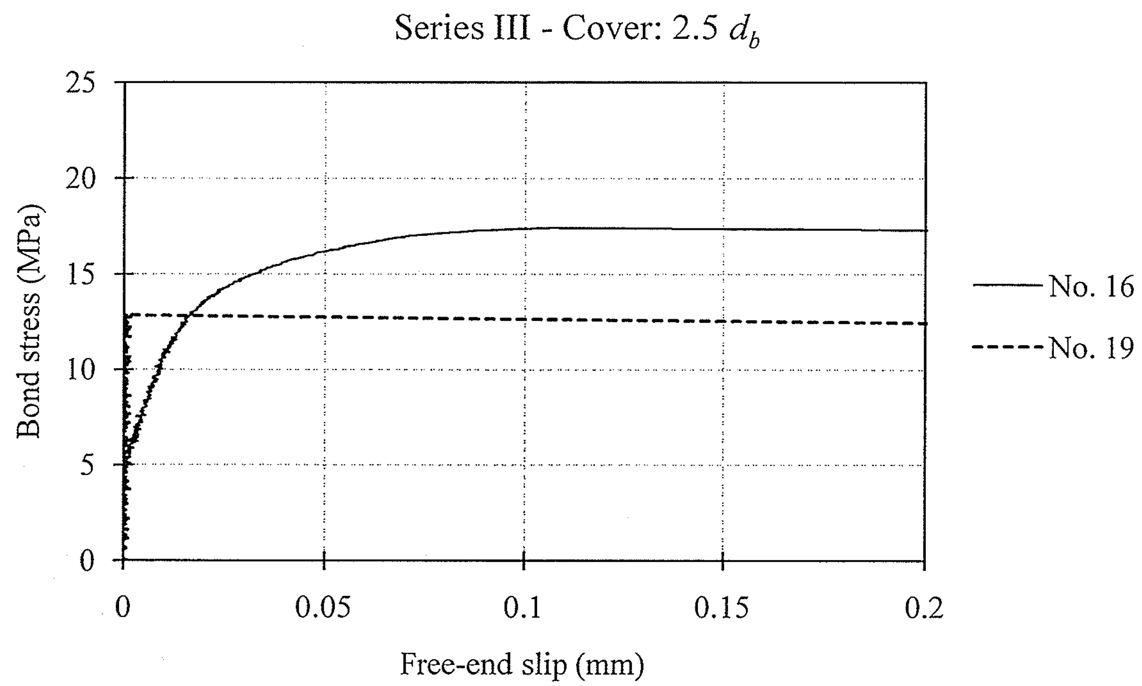

Fig. 4.15: Effect of bar diameter: Series III and concrete clear cover of $2.5d_b$

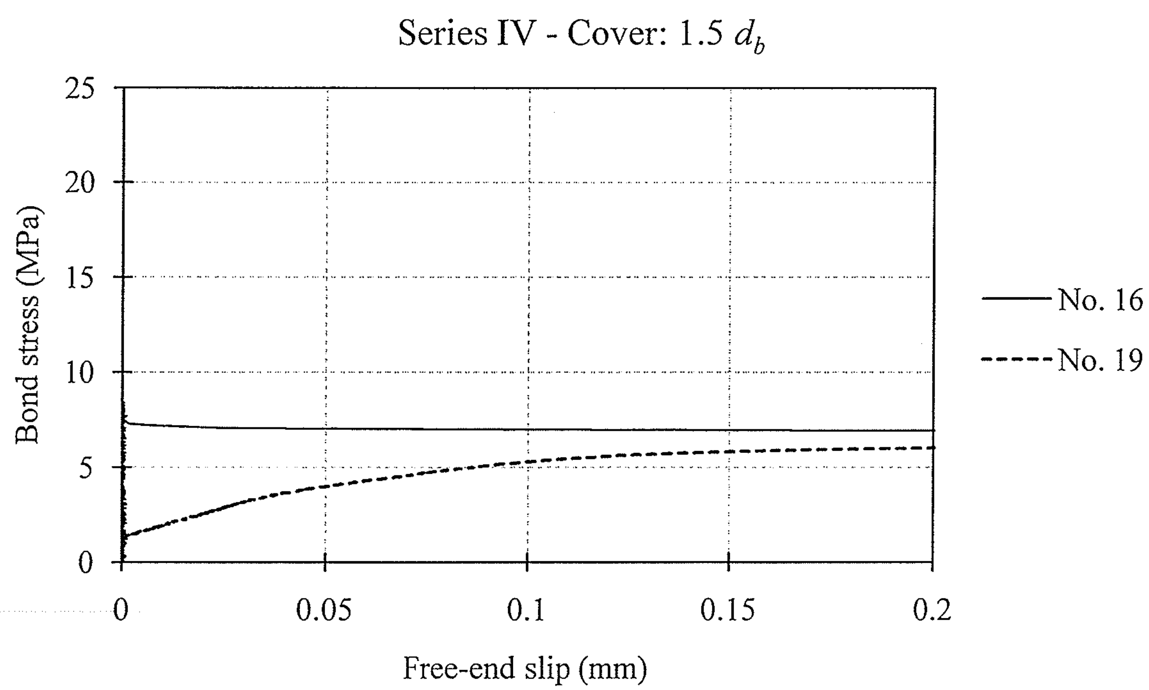

Fig. 4.16: Effect of bar diameter: Series IV and concrete clear cover of $1.5d_b$

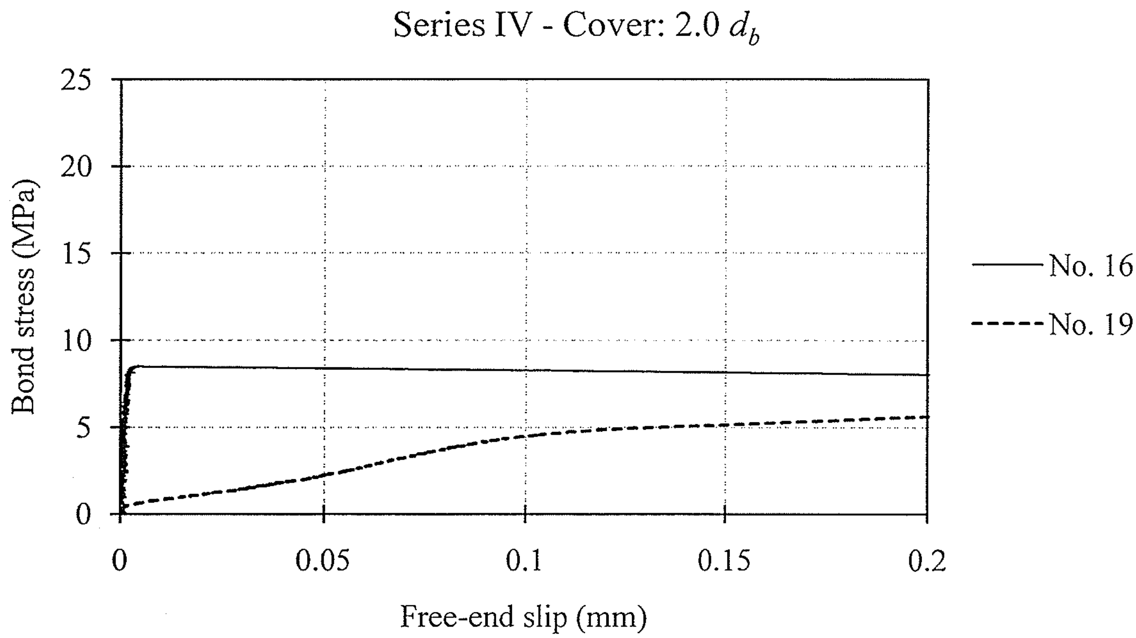

Fig. 4.17: Effect of bar diameter: Series IV and concrete clear cover of $2.0d_b$

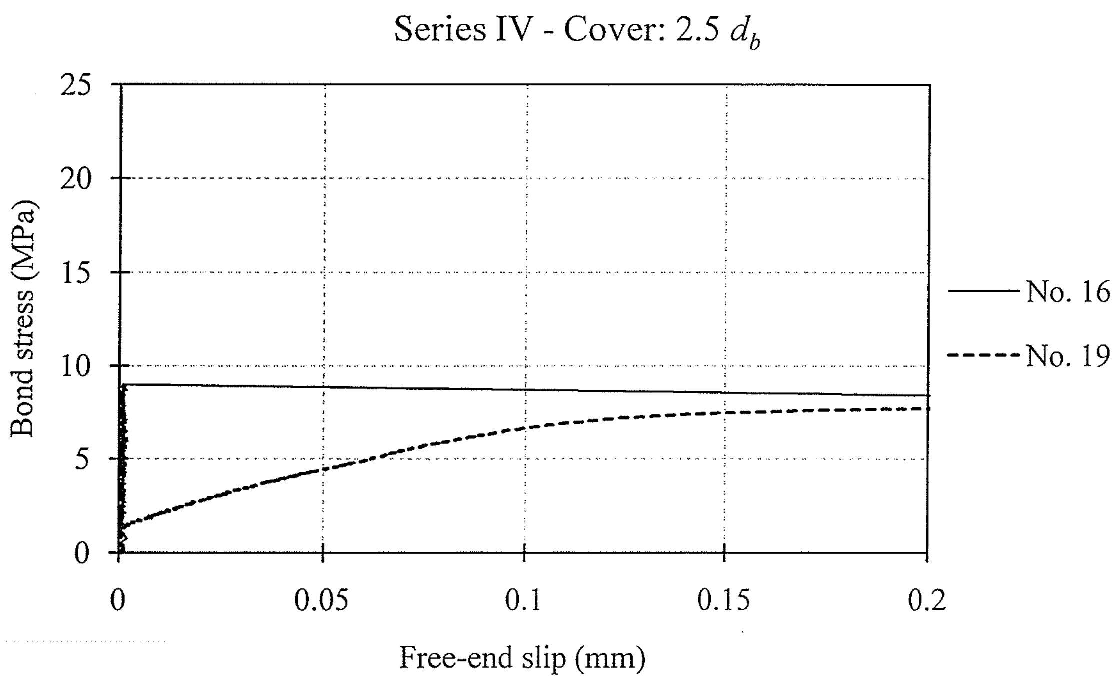

Fig. 4.18: Effect of bar diameter: Series IV and concrete clear cover of $2.5d_b$

In the figures 4.7 to 4.18, the values of bond strength for bar No. 19 are smaller than bar No. 16, which is in good agreement with previous findings in the literature. However, in the presence of fatigue load, the values of bond strength are approximately the same for both bar diameters. So, smaller bars seem to be more susceptible to fatigue load than larger bars.

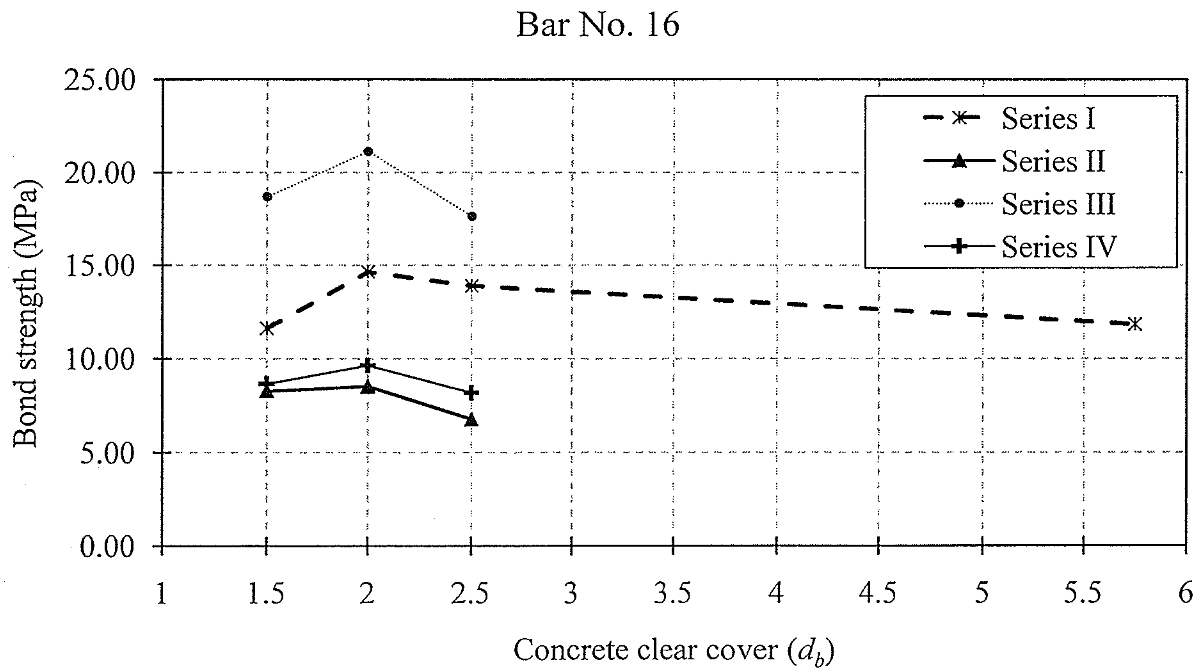

Fig. 4.19: Average bond strength versus concrete clear cover; bar No.16; for the centric placement of the bar, two out of three points where considered.

The experimental data obtained for specimens with bar No.16 is very consistent regarding the type of conditioning. Series III, which was subjected to the effects of freeze-thaw cycles along with sustained load, showed the highest bond resistance. Specimens in Series II and IV, which were conditioned to fatigue loading, showed the smallest bond resistance. However, values of bond strength obtained from Series IV are between 4 and 20 % higher than those in Series II.

This indicates the beneficial effects of the freeze-thaw cycles conditioning, in the case of bar No. 16. One of the reasons why the specimens subjected to the freeze-thaw cycles presented higher values of bond strength might be that the bar absorbed moisture and enlarged in cross-sectional area, thus enhancing the friction mechanism, which improves bond resistance. The thermal stresses probably degrade the concrete surrounding the bar. However, such deterioration was not so severe that it could not resist the shear forces in the interface - in the case of bar diameter No. 16.

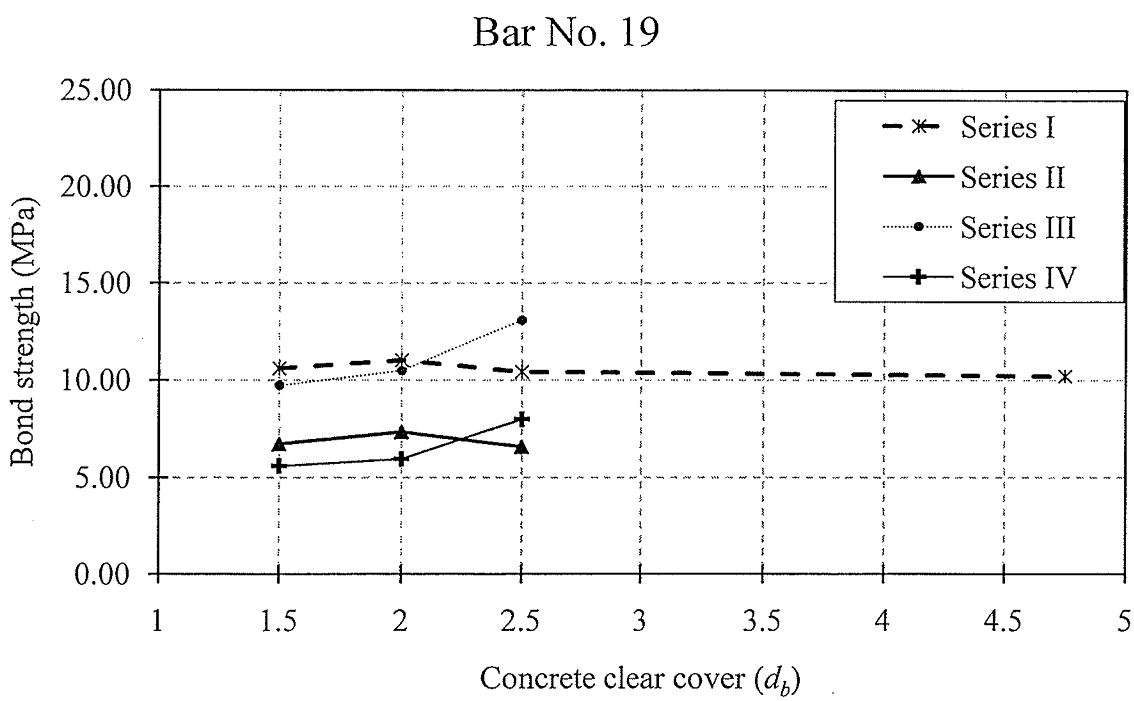

Fig. 4.20: Average bond stress versus concrete clear cover (d_b); bar No.19; for the centric placement of the bar, two out of three points where considered.

* Note: For the E.19.20 case, the value for bond strength from Series B was disregarded, since the difference in the values from A and B was significant. Also, the results for the specimens with concentric bars are presented, where two out of the three points were used.

Due to equipment deficiency, specimen S.FT.F.19.20 was subjected only to 4,000 cycles instead of 1,000,000. However, surprisingly, it seems that the deterioration caused by such a small number of cycles was as high as that of specimens subjected to 1,000,000 cycles.

In the case of specimens with No. 19 bars, the values obtained for Series III were similar to those obtained for Series I, for concrete clear covers of 1.5 and 2.0 d_b. However, for the concrete clear cover of 2.5 d_b, the bond strength values were higher than those from Series I. This may be due to the effect of thermal stresses on the expansion of the bar cross section, which is more pronounced for the larger bar diameter (No. 19) (see Appendix A). Therefore, the largest cover, 2.5 d_b, appears to have resisted the thermal loads and was capable of promoting significant increase in bond resistance. For smaller covers (1.5 and 2.0 d_b), the enlargement in the bar diameter may have caused damage in the surrounding concrete. For specimens of Series IV, the obtained results had similar trend to those of Series III, with values slightly smaller than the values obtained for Series II.

Also, it can be observed that with the increase in the concrete confinement represented by the concentric specimens, the bond strength seems to decrease or at the most stays constant. This behaviour was also observed by other researchers (Tepfers et al. 1998; Esfahani et al. 2005; Galati et al. 2005).

It was also shown by Malvar et al. (2003) that with increasing confinement – in his research represented by external pressure applied by a steel ring – no significant increase in bond strength could be seen for sand-coated GFRP bars. Malvar et al. (2003) explained that this was due to the sand-coating layer, which was not enough to provide an interlocking mechanisms.

Tepfers (2004) concluded that even under good confinement some FRP bars may show poor bond resistance, and due to their low splitting tendency, may behave well when the confinement is provided only by concrete covers. The author also added that some FRP bars may behave just the opposite, and provide better bond strength for higher confinement. It was also observed that for thinner concrete covers the concrete shows more plastic behaviour than for larger concrete covers (Tepfers 2003).

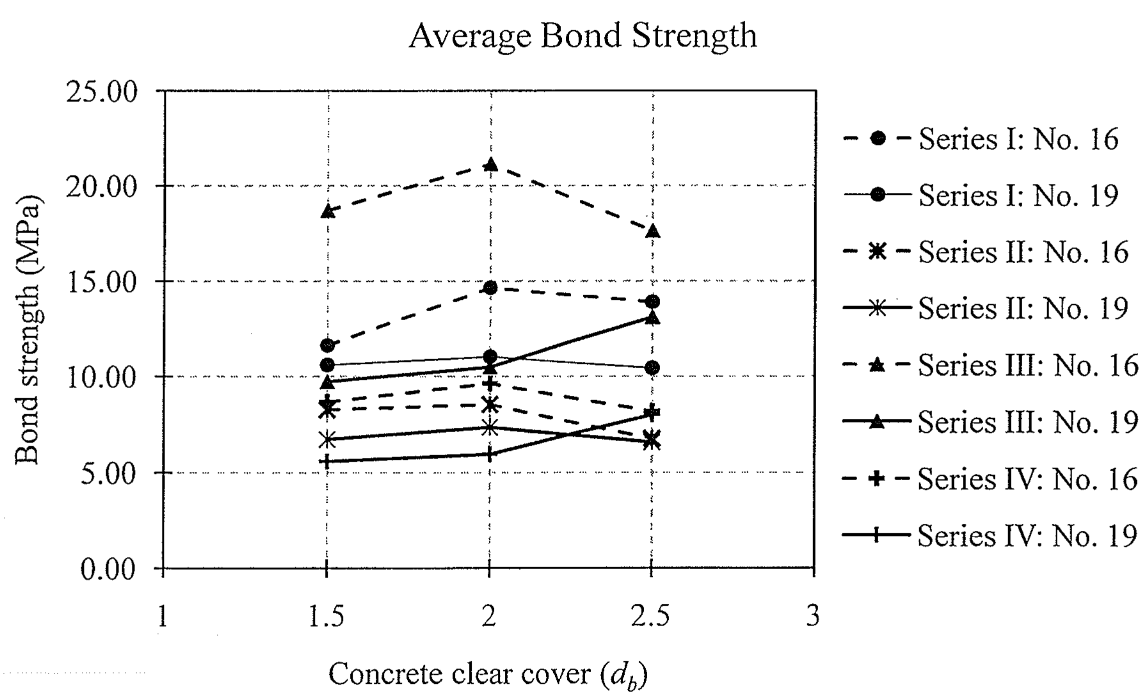

Fig. 4.21: Bond strength versus concrete clear cover – all series

It is interesting to note that both bars No. 16 and No. 19 presented approximately similar bond resistance for specimens in Series II, which indicates that bar No. 16 suffered more due to the fatigue loading than bar No. 19. The difference in the bond strength between specimens with No. 16 and No. 19 bars, for 1.5, 2.0 and 2.5 d_b cover was 23%, 16% and 3%, respectively. It seems that the 2.5 d_b cover is enough to avoid micro-cracks in the concrete near the bar surface, and thus causes higher degradation in the sand-coating layer, since the interface would be stronger. Also, in the case of specimens in Series IV with 2.5 d_b concrete cover, the bond strength for bars No. 16 and No. 19 was the same. Therefore, smaller bar diameters seems to be more susceptible to fatigue loading. The reason is probably because the surface area of bar No. 16 is smaller than that of No. 19 bar, so it is more difficult to redistribute the load in case of partial (local) loss of the sand-coating layer as a result of the cyclic loading.

Figure 4.22 presents average peak slip observed after the different types of conditioning.

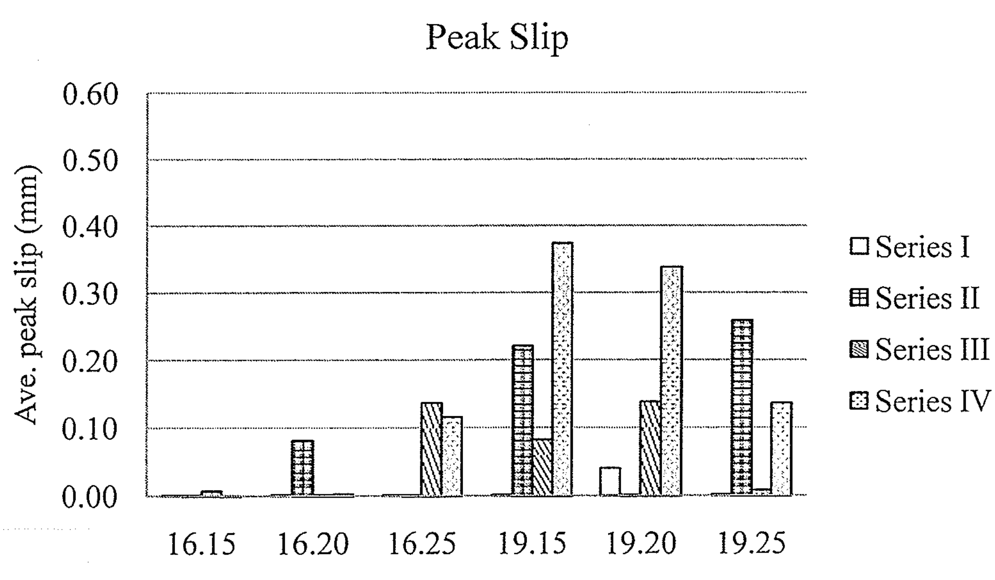

Fig. 4.22: Average peak slip

It seems that both conditionings, individually or combined, promoted the appearance and/or increase in the slip.

The producer's manual (Pultrall Inc. 2007) shows a value for moisture absorption of 0.42% for bars No. 16, while for No. 19 bars, it shows 0.21%. That is probably the reason why for specimens in Series III and IV with bar No. 16 and concrete clear cover of 2.5 d_b, where the moisture penetration wouldn't be so pronounced, the slip was greater than in the other series. In other words, the bar didn't swell due to moisture absorption but the interface was damaged by the thermal stresses. For No. 19 bars, the thermal stresses induced in the concrete surrounding the bar due to freeze-thaw cycles probably was more degrading to the bond resistance than the swelling of the bar due to moisture absorption was enhancing.

Greater number of specimens in Series IV exhibited slip compared to Series II and III. Also, the measured slip values were slightly higher (with the exception of specimen F.19.25), which indicates that the effects of the combined conditionings further promoted the appearance of slip and the increase in the peak slip. Tables 4.1 to 4.4 present the summary of results from individual series. Table 4.5 summarizes the results obtained, and provides a comparison with unconditioned specimens.

TABLE 4.1: Summary of results from Series I

Specimen name	Bond strength (MPa)	Ave. bond (MPa)	Peak slip (mm)
C.16-A	11.28	11.86	0.000139
C.16-B	12.43		0.002334
C.16-C	8.07	x	0.000959
C.19-A	8.99	x	0.001028
C.19-B	10.28	10.23	0.001013
C.19-C	10.17		0.000036
E.16.15-A	11.27	11.63	0.000174
E.16.15-B	11.99		0.000267
E.16.20-A	15.68	14.65	0.001113
E.16.20-B	13.63		0.001630
E.16.25-A	15.54	13.91	0.000914
E.16.25-B	12.27		0.000547
E.19.15-A	10.84	10.62	0.000771
E.19.15-B	10.39		0.001459
E.19.20-A	11.03	11.03	0.080349
E.19.20-B	8.73	x	0.000345
E.19.25-A	10.89	10.44	0.001995
E.19.25-B	9.99		0.000560

*The “x” illustrates the values which were not considered, once the difference between such values and its duplication (or triplication) were significant.

TABLE 4.2: Summary of results from Series II

Specimen name	Bond strength (MPa)	Ave. bond (MPa)	Peak slip (mm)
F.16.15-A	8.70	8.28	0.000571
F.16.15-B	7.86		0.000619
F.16.20-A	6.75	8.53	0.000613
F.16.20-B	10.32		0.162461
F.16.25-A	6.38	6.78	0.000017
F.16.25-A	7.18		0.001248
F.19.15-A	6.79	6.74	0.000403
F.19.15-B	6.68		0.442040
F.19.20-A	6.74	7.36	0.000621
F.19.20-B	7.98		0.000779
F.19.25-A	7.31	6.59	0.000192
F.19.25-B	5.86		0.517799

TABLE 4.3: Summary of results from Series III

Specimen name	Bond strength (MPa)	Ave. bond (MPa)	Peak slip (mm)
S.FT.16.15-A	17.56	18.71	0.000090
S.FT.16.15-B	19.85		0.014648
S.FT.16.20-A	21.21	21.15	0.000289
S.FT.16.20-B	21.09		0.001944
S.FT.16.25-A	18.29	17.65	0.142179
S.FT.16.25-B	17.00		0.131656

S.FT.19.15-A	9.25	9.74	0.000802
S.FT.19.15-B	10.23		0.164343
S.FT.19.20-A	10.91	10.50	0.105725
S.FT.19.20-B	10.08		0.170683
S.FT.19.25-A	12.85	13.10	0.000037
S.FT.19.25-B	13.35		0.017141

TABLE 4.4: Summary of results from Series IV

Specimen name	Bond strength (MPa)	Ave. bond (MPa)	Peak slip (mm)
S.FT.F.16.15-A	8.39	8.67	0.000293
S.FT.F.16.15-B	8.94		0.000330
S.FT.F.16.20-A	8.52	9.64	0.004236
S.FT.F.16.20-B	10.77		0.001532
S.FT.F.16.25-A	7.39	8.19	0.230716
S.FT.F.16.25-B	9.00		0.001354
S.FT.F.19.15-A	6.11	5.60	0.276388
S.FT.F.19.15-B	5.08		0.471223
S.FT.F.19.20-A	6.38	5.96	0.421186
S.FT.F.19.20-B	5.54		0.255202
S.FT.F.19.25-A	7.82	8.00	0.273625
S.FT.F.19.25-B	8.18		0.000021

TABLE 4.5: Summary of results

Specimens	Average bond strength (MPa)						
	Series I (control)	Series II (F.)	Difference Series II / I	Series III (S.FT.)	Difference Series III/I	Series IV (S.FT.F.)	Difference Series IV/I
16.15	11.63	8.28	-29%	18.71	61%	8.67	-25%
16.20	14.65	8.53	-42%	21.15	44%	9.64	-34%
16.25	13.91	6.78	-51%	17.65	27%	8.19	-41%
19.15	10.62	6.74	-37%	9.74	-8%	5.60	-47%
19.20	11.03	7.36	-33%	10.50	-5%	5.96	-46%
19.25	10.44	6.59	-37%	13.10	25%	8.00	-23%

It is clear from Table 4.5 that the fatigue loading conditioning significantly degraded the bond resistance of sand-coated GFRP bars, causing reductions of at least 29% in the bond strength. Also visible is the enhancement in the bond properties promoted by the freeze-thaw conditioning, which was more pronounced in No. 16 bar compared to No. 19. Investigating the results of Series IV, it can be concluded that the effect of fatigue loading is more dominant than the freeze-thaw cycles, since all specimens in Series IV showed significant losses of at least 23%. However, no loss was greater than the loss due to the individual effect of fatigue loading. For specimens with No. 16 bars, it seems that the effect of fatigue loading counteracts that of the freeze-thaw cycles. While for specimens with No. 19 bars and covers of 1.5 and 2.0 d_b, the adverse effects of both conditionings are added together.

The increase in the strains as well as the residual strains was evaluated. This increase in strain is represented by the difference in the readings from the specimen inside the chamber before and after the freeze-thaw cycles. The residual strains are defined as the remaining strains after the completion of the freeze-thaw cycles and the removal of the axial sustained load.

Table 4.6 presents the values obtained for each specimen and table 4.7 presents the average of the Series III and IV. Figure 4.23 presents the average values of increase and residual strains, which were obtained as the average of Series III and IV.

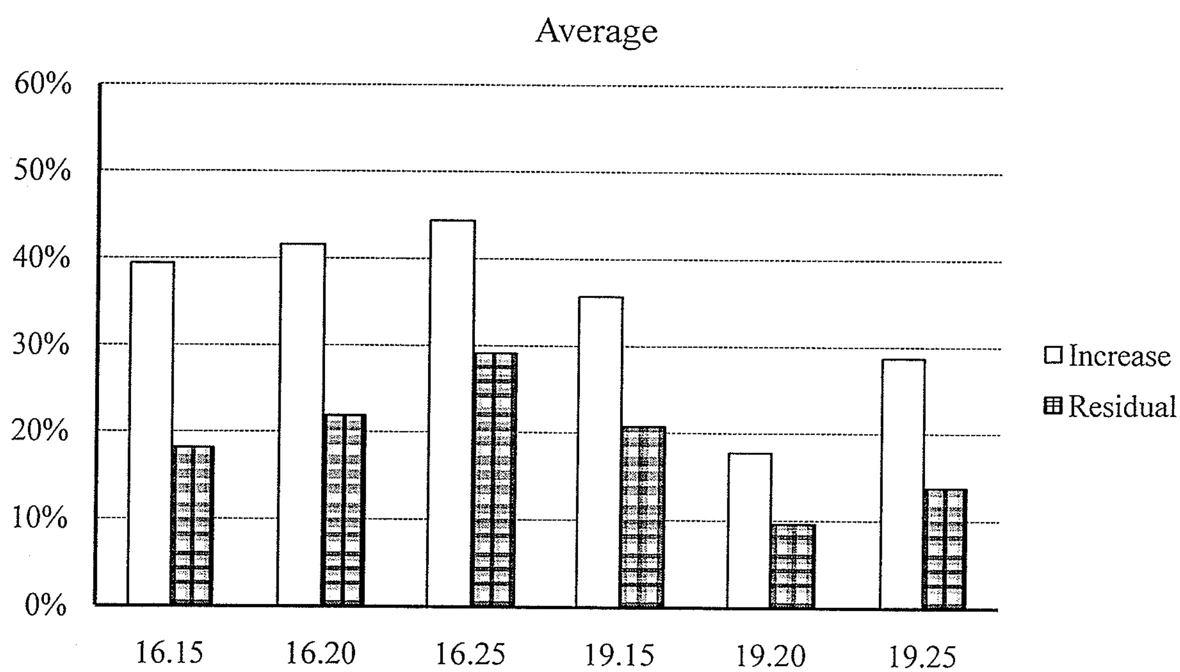

Fig. 4.23: Average increase and residual strains in specimens

It seems that No. 16 bars were affected more by the sustained load than No. 19 bars. For No. 16 bars, the residual strains increase with increasing concrete clear cover. However, for No. 19 bars, it seems that the concrete clear cover of 2.0 d_b is an optimum, since it presented the smallest increase in residual strains.

TABLE 4.6: Summary of increase and residual strains per specimen

Specimen	Increase	Residual	Specimen	Increase	Residual
S.FT.16.15	41%	26%	S.FT.F.16.15	37%	10%
S.FT.16.20	36%	19%	S.FT.F.16.20	47%	25%
S.FT.16.25	51%	45%	S.FT.F.16.25	38%	13%
S.FT.19.15	31%	23%	S.FT.F.19.15	41%	18%
S.FT.19.20	18%	8%	S.FT.F.19.20	17%	11%
S.FT.19.25	13%	9%	S.FT.F.19.25	44%	18%

Increases in the GFRP bar strain of up to 51% were observed, as well as residual strains of up to 45%. If increase in strain occurs at constant load, this means creep occurred.

TABLE 4.7: Average increase and residual strains

Specimen	Increase	Residual
16.15	39%	18%
16.20	42%	22%
16.25	44%	29%
19.15	36%	21%
19.20	18%	10%
19.25	29%	14%

4.2. Failure Modes

In this section, the failure mode was analyzed. The influence of the different conditioning schemes and parameters on the failure mode is investigated. Five types of failure could be observed in this experimental program. A brief description is presented as follows:

- Pure Pullout: Pullout failure is characterized by the bar being pulled out of the specimen without any splitting/cracking mechanism in the concrete. It is a progressive failure, which starts in the loaded-end and progresses to the free-end. It is a sudden and brittle failure caused by the abrasion of the sand-coating layer with immediate loss of bond resistance.

- Concrete Cover Failure: In this case a crack in the smallest cover is suddenly formed with immediate loss of bond resistance. If load can still be carried, it will be accompanied by increase in slip.

- V-Shape Concrete Cover Failure: In this case it is thought that a cover failure has already occurred, but the specimen was still able to carry more load. The final failure is observed with the v-shape failure.

- Concrete Block Split: In this case a crack, which started in the smallest cover, propagates through the whole concrete block.

- Diagonal Failure: Probably due to the lack of homogeneity of the concrete, a failure which should follow the v-shape, deviated and cracked the cover in the lateral direction.

The following figure presents the failure modes for specimens in Series I and Table 4.8 presents the summary of results for concentric specimens. Table 4.9 presents the summary of failure modes.

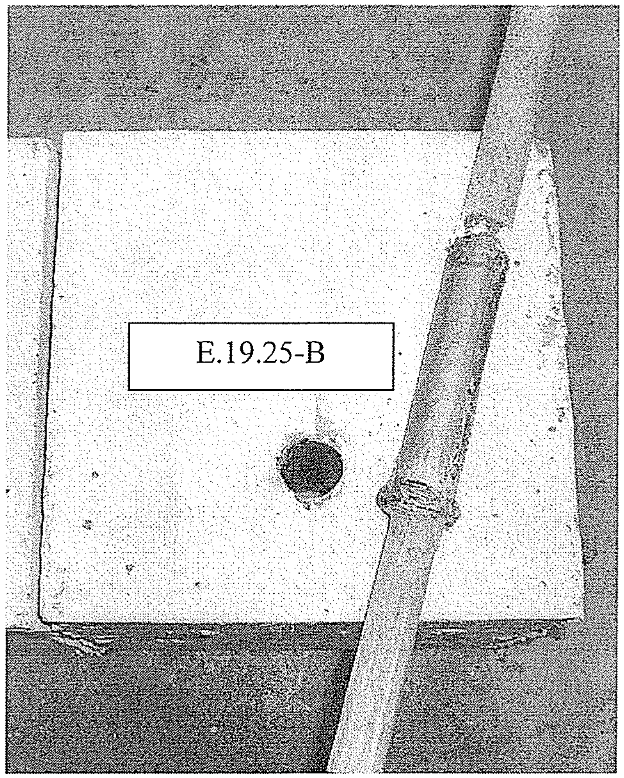

(a) Pure pullout

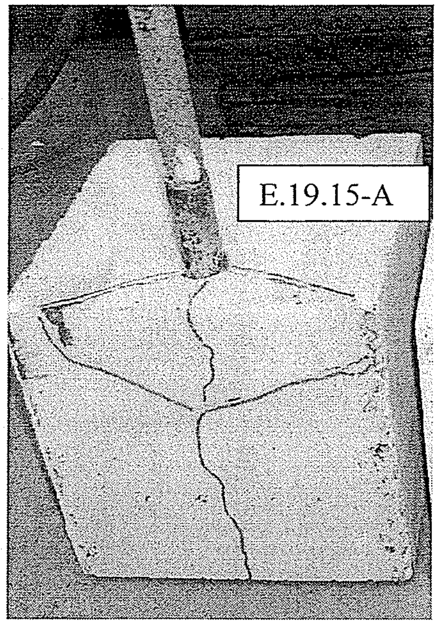

(b) V-Shape concrete cover

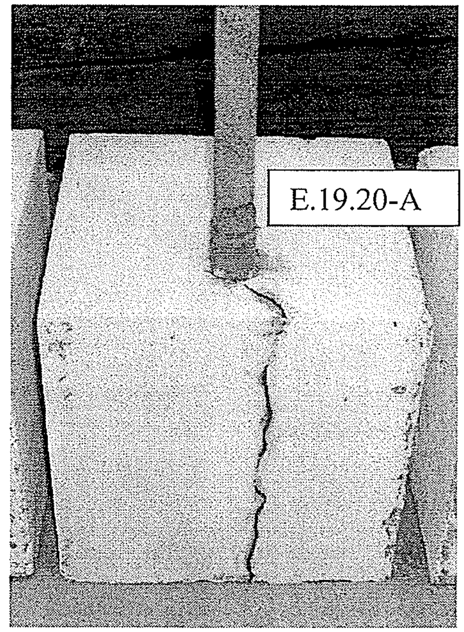

(c) Concrete cover

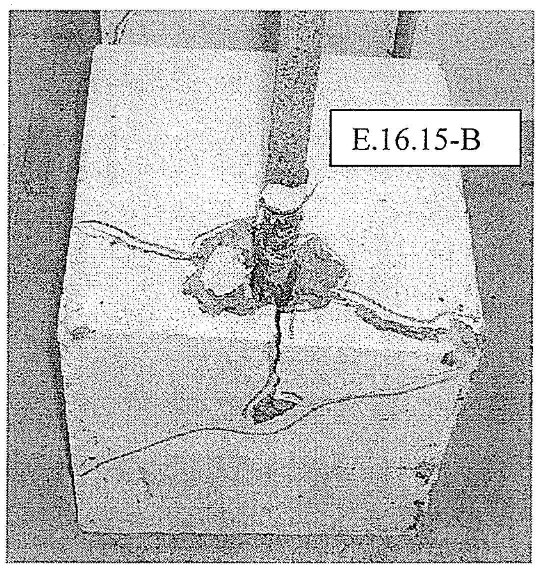

(d) Diagonal

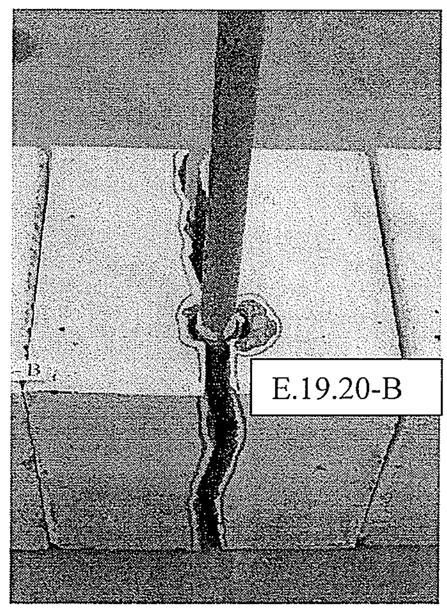

(e) Concrete block split

Fig. 4.24: Mode of failure of specimens is Series I.

TABLE 4.8: Mode of failure of concentric specimens in Series I

Specimen (No. 16)	Mode of failure	Specimen (No. 19)	Mode of failure
C.16-A	Pullout	C.19-A	Pullout
C.16-B	Pullout	C.19-B	Pullout
C.16-C	Pullout	C.19-C	Pullout

TABLE 4.9: Summary of failure modes

Specimen name	Series			
	I	II	III	IV
16.15 - A	Diagonal	Pullout	Diagonal	Diagonal
16.15 - B	Diagonal	Pullout	Diagonal	V-Shape
16.20 - A	Pullout	Diagonal	V-Shape	Pullout
16.20 - B	Pullout	Pullout	Cover	Diagonal
16.25 - A	Pullout	Pullout	Pullout	Pullout
16.25 - B	Pullout	Pullout	Cover	Pullout
19.15 - A	V-Shape	Diagonal	Diagonal	Cover
19.15 - B	Cover	Pullout	Pullout	Cover
19.20 - A	Cover	Pullout	Diagonal	Pullout
19.20 - B	Block Split	Pullout	V-Shape	Pullout
19.25 - A	Pullout	Pullout	Diagonal	Pullout
19.25 - B	Pullout	Pullout	Cover	Block Split

In Series I, it can be observed that by increasing the concrete clear cover, the failure mode changed. For specimens with No. 16 bars, the clear cover of 2.0 d_b was enough to ensure the pure pullout failure, while for No. 19 bar the same concrete clear cover ($2.0d_b$) was not enough to prevent cracking. The bond properties deterioration of specimens in Series II is presented in Table 4.5. This deterioration can also be identified by investigating the failure modes. It can be seen that the main failure mode was pure pullout, which further confirms the adverse effects of the fatigue loading on the bond strength. For specimens of Series III, only two pure pullouts occurred. This indicates that the developed bond stress was higher than that of specimens of Series I. However, in this case, the concrete condition also contributed to the splitting mechanism. The failure modes observed for specimens in Series IV appears to be a combination of Series II and III: half of the specimens failed in pure pullout and half failed by cracking. Figures 4.25 and 4.26 present a comparison between the series.

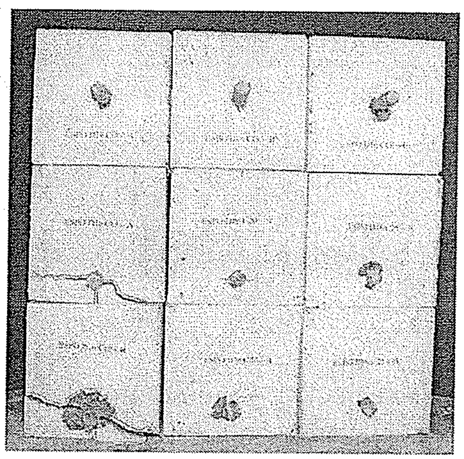

(a) Series I

(b) Series II

(c) Series III

(d) Series IV

Fig. 4.25: Failure mode of specimens with bar No. 16

The concrete deterioration is visible in both the specimens and cylinders subjected to freeze-thaw conditioning (see Appendix A).

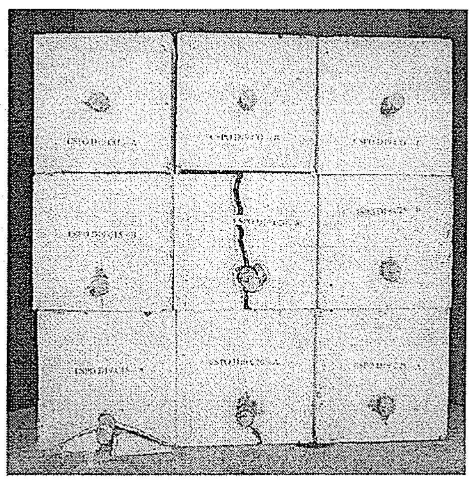

(a) Series I

(b) Series II

(c) Series III

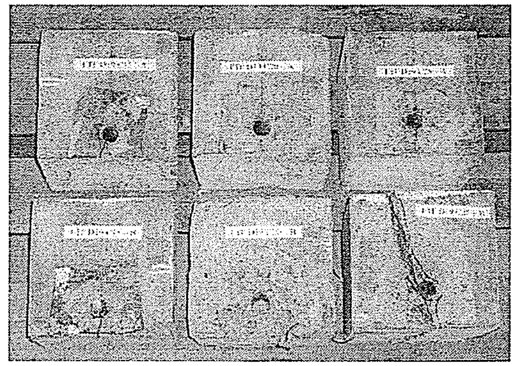

(d) Series IV

Fig. 4.26: Mode of failure of specimens with bar No. 19

On the other hand, in Series II, the pullout failure was progressive but smooth. No sound could be detected. The slip of the bar could sometimes be observed by the naked eye. This observation indicates that significant deterioration occurred in the sand-coating layer due to the fatigue loading. In some specimens, which failed by concrete block splitting, the print of the sand-coating layer on the concrete interface could be clearly seen as shown in Figure 4.27. An analytical study was carried out to investigate the cracking pattern (mode of failure) of all tested specimens. Through measuring the cracking pattern, a bond strength was calculated which was fairly close to the actual failure bond strength (deviations ranged from 0.5 to 19.9% as given in Appendix B).

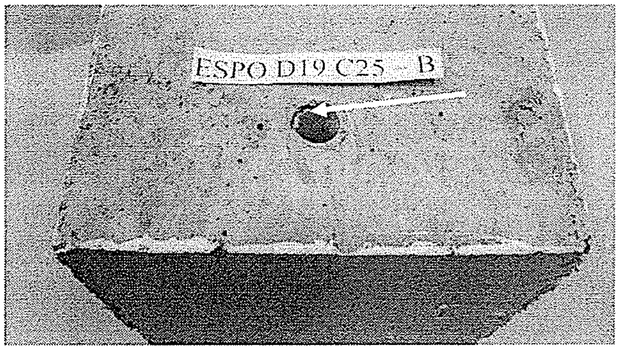

(a) Series I

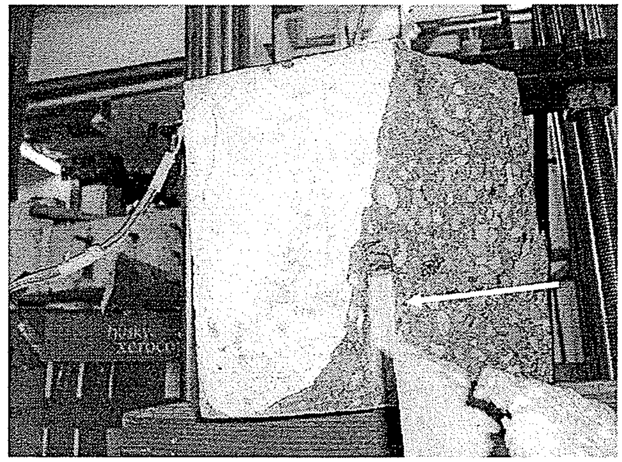

(b) Series III

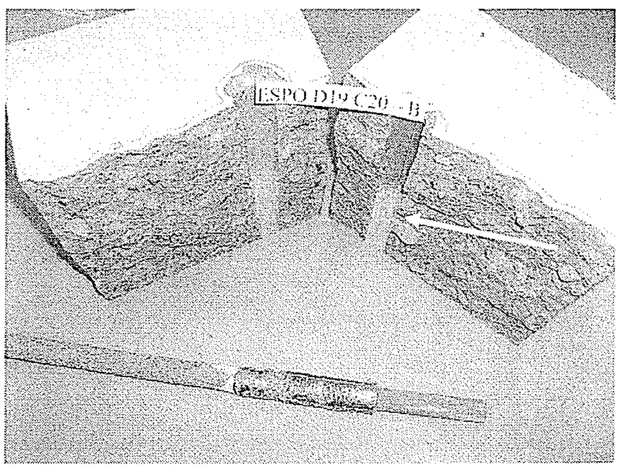

(c) Series I: bar after pullout

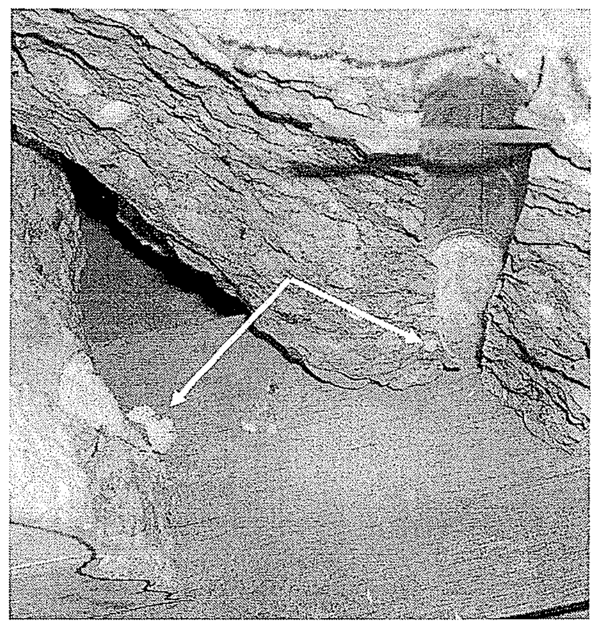

(d) Series IV

Fig. 4.27: After pullout test: sand-coating detachment

4.3. Development Length Analysis

In this section, an analysis of development length is conducted. Using the values obtained for bond strength considering each conditioning, development lengths were calculated by equilibrium of forces (equation 2-12). Such development lengths were compared to code provisions as described in, section 2.5.4. Table 4.8 presents the development length calculations summary.

TABLE 4.10: Summary of development length for Series I to IV

Specimen	Development length (mm)			
	Exp. Data	CAN/CSA-S6-06 (2006)	CAN/CSA-S802-02 (2002)	ACI 440.1R-06 (2006)
E.16.15	231.28	475.26	551.03	847.86
E.16.20	183.56	380.21	440.82	821.53
E.16.25	193.41	380.21	440.82	796.79
E.19.15	213.35	553.54	641.78	950.66
E.19.20	229.16	442.83	513.42	921.14
E.19.25	216.96	442.83	513.42	893.39
F.16.15	324.87	400.22	532.71	808.09
F.16.20	315.16	320.18	426.17	782.99
F.16.25	396.74	320.18	426.17	759.41
F.19.15	465.04	466.14	620.45	905.30
F.19.20	425.66	372.91	496.36	877.18
F.19.25	475.54	372.91	496.36	850.76

S.FT.16.15	143.77	482.81	578.23	906.92
S.FT.16.20	127.16	386.25	462.58	878.76
S.FT.16.25	152.41	386.25	462.58	852.29
S.FT.19.15	321.62	562.33	673.46	1018.02
S.FT.19.20	298.46	449.86	538.77	986.41
S.FT.19.25	239.14	449.86	538.77	956.70
S.FT.F.16.15	310.20	449.95	574.74	899.35
S.FT.F.16.20	278.99	359.96	459.79	871.42
S.FT.F.16.25	328.38	359.96	459.79	845.17
S.FT.F.19.15	559.36	524.06	669.40	1009.39
S.FT.F.19.20	525.53	419.25	535.52	978.04
S.FT.F.19.25	391.55	419.25	535.52	948.58

The CAN/CSA-S6-06 presented values slightly smaller than those obtained considering the experimental data from Series II and IV, which included fatigue loading. Therefore, the analysis will be focused on these two series. Figures 4.27 to 4.30 for development length versus concrete clear cover in terms of d_b are presented below for Series II and IV.

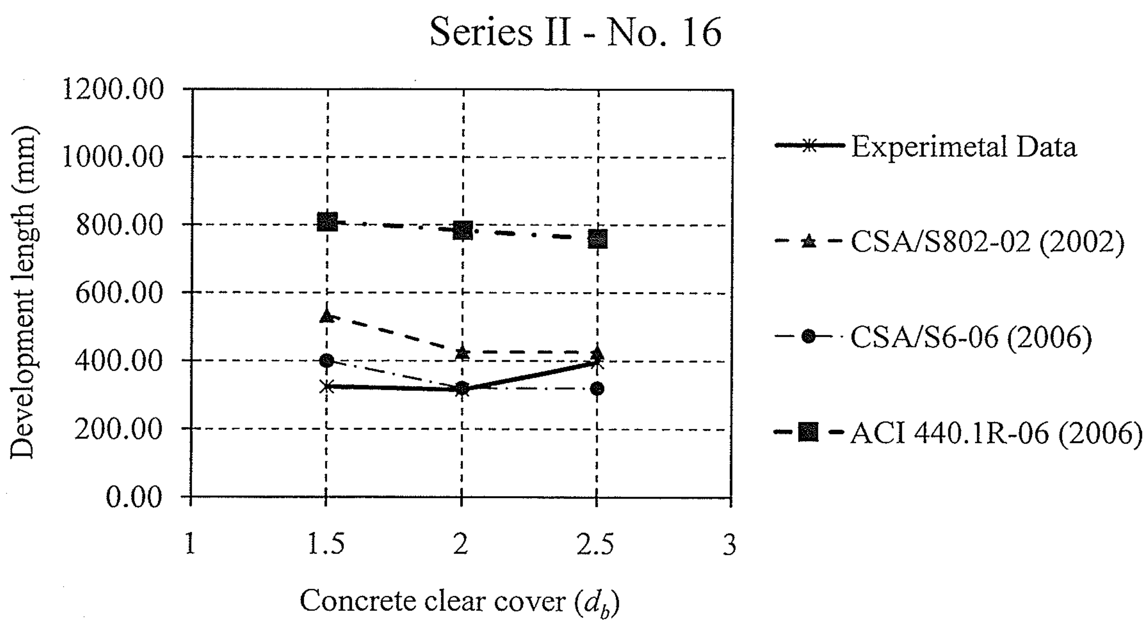

Fig. 4.28: Development length versus concrete clear cover; Series II and bar No. 16

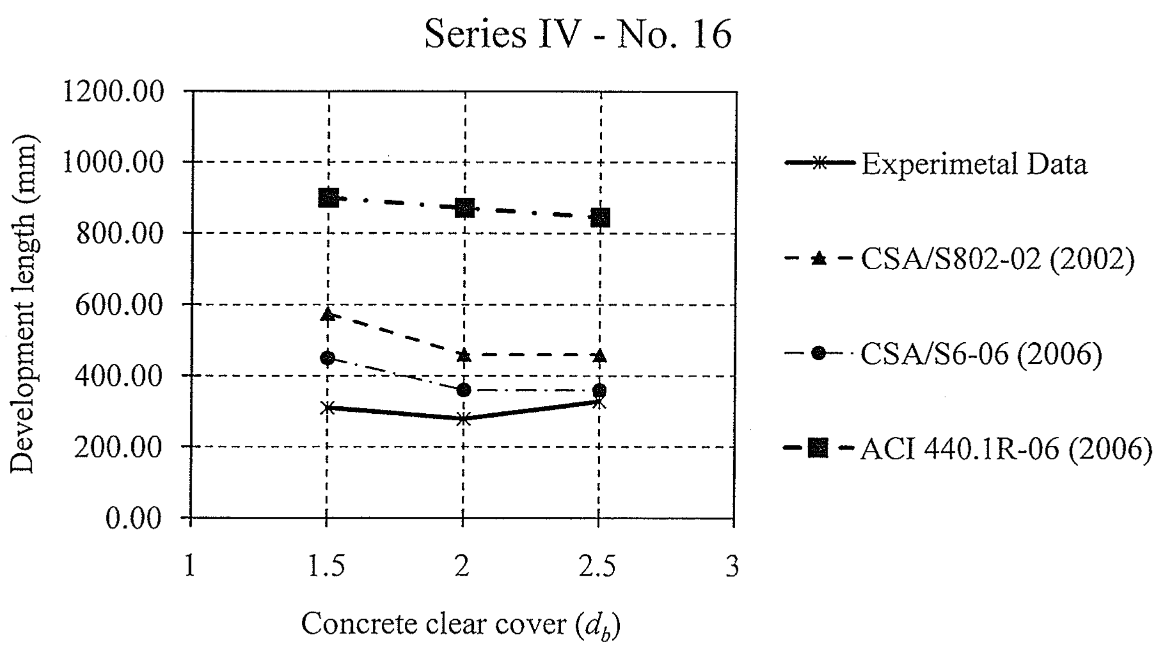

Fig. 4.29: Development length versus concrete clear cover; Series IV and bar No. 16

For No. 16 bars, it seems that, for higher confinement provided by concrete cover, the CAN/CSA-S6-06 (CSA 2006) gives smaller values for development length, becoming slightly un-conservative. It is interesting to observe that with the presence of the freeze-thaw conditioning, the bond strength was slightly higher providing smaller development length and, so, changing the CAN/CSA-S6-06 (CSA 2006) to more conservative values.

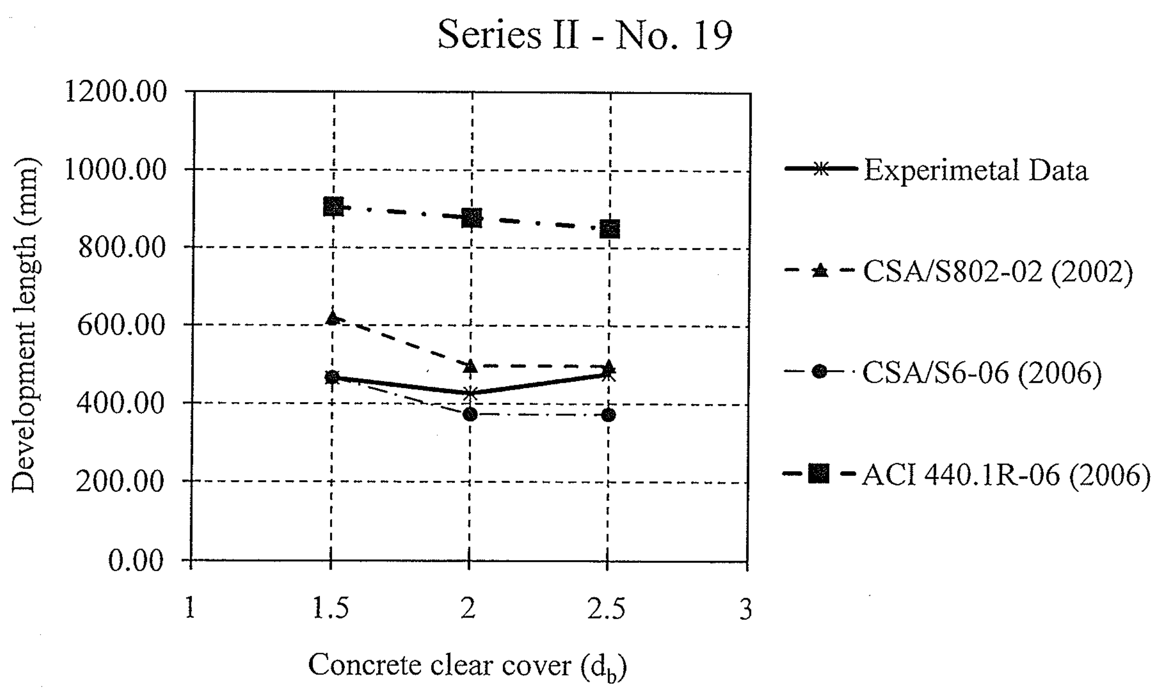

Fig. 4.30: Development length versus concrete clear cover; Series II and bar No. 19

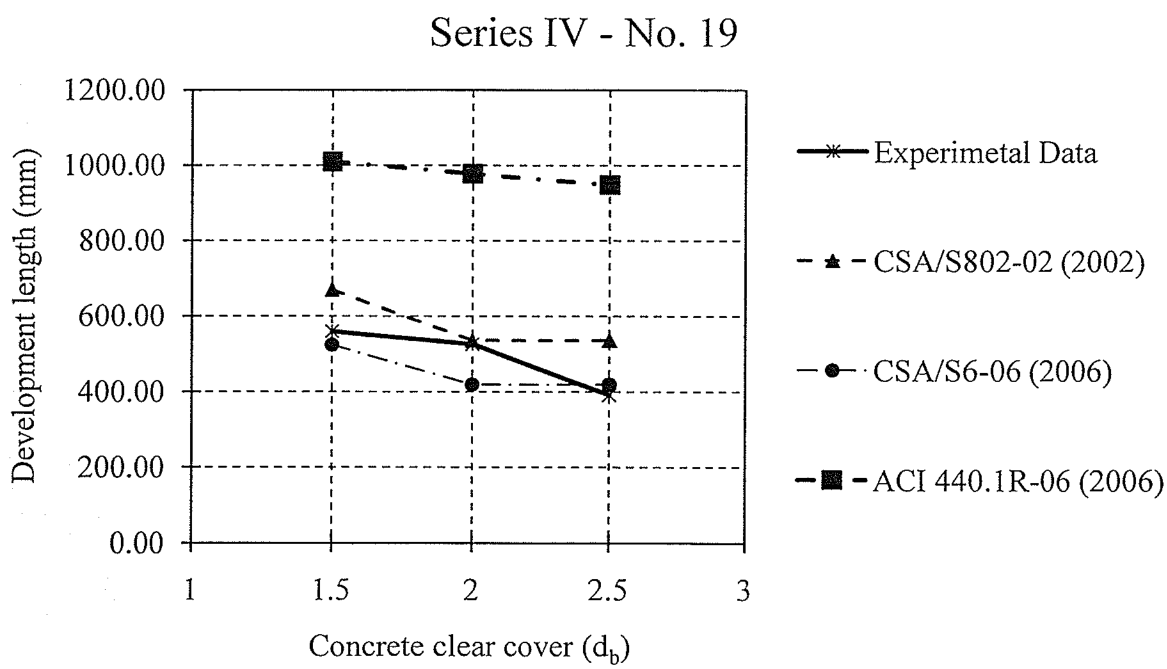

Fig. 4.31: Development length versus concrete clear cover; Series IV and bar No. 19

For No.19 bars, the values obtained for development length using the experimental data are higher than those calculated using the CAN/CSA-S6-06 (CSA 2006) equation. Table 4.11 presents a summary of the calculations and introduces the k_6 coefficient, which is the difference between the values of the CAN/CSA-S6-06 (CSA 2006) and the experimental data.

TABLE 4.11: Analysis of development lengths for Series II and IV

Specimen	Development length (mm)		
	CAN/CSA-S6-06 (CSA 2006)	Exp. Data	Exp. Data / CAN/CSA-S6-06 (CSA 2006) (%) (k_6)
F.16.15	400.22	324.87	81%
F.16.20	320.18	315.16	98%
F.16.25	320.18	396.74	124%
F.19.15	466.14	465.04	100%
F.19.20	372.91	425.66	114%
F.19.25	372.91	475.54	128%
S.FT.F.16.15	449.95	310.20	69%
S.FT.F.16.20	359.96	278.99	78%
S.FT.F.16.25	359.96	328.38	91%
S.FT.F.19.15	524.06	559.36	107%
S.FT.F.19.20	419.25	525.53	125%
S.FT.F.19.25	419.25	391.55	93%

Considering the obtained values, two relationships (graphs) for the difference between the values of the CAN/CSA-S6-06 (CSA 2006) and the experimental data can be interpreted. For each graph, a linear approximation can be obtained, considering best fitting.

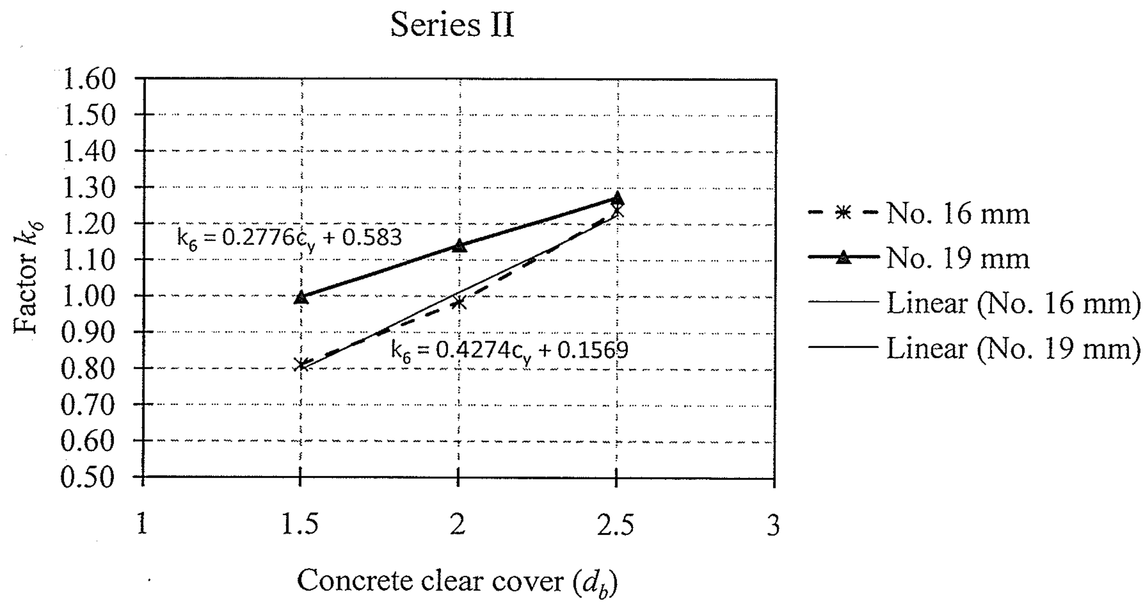

Fig. 4.32: Factor k_6 versus concrete clear cover: Series II

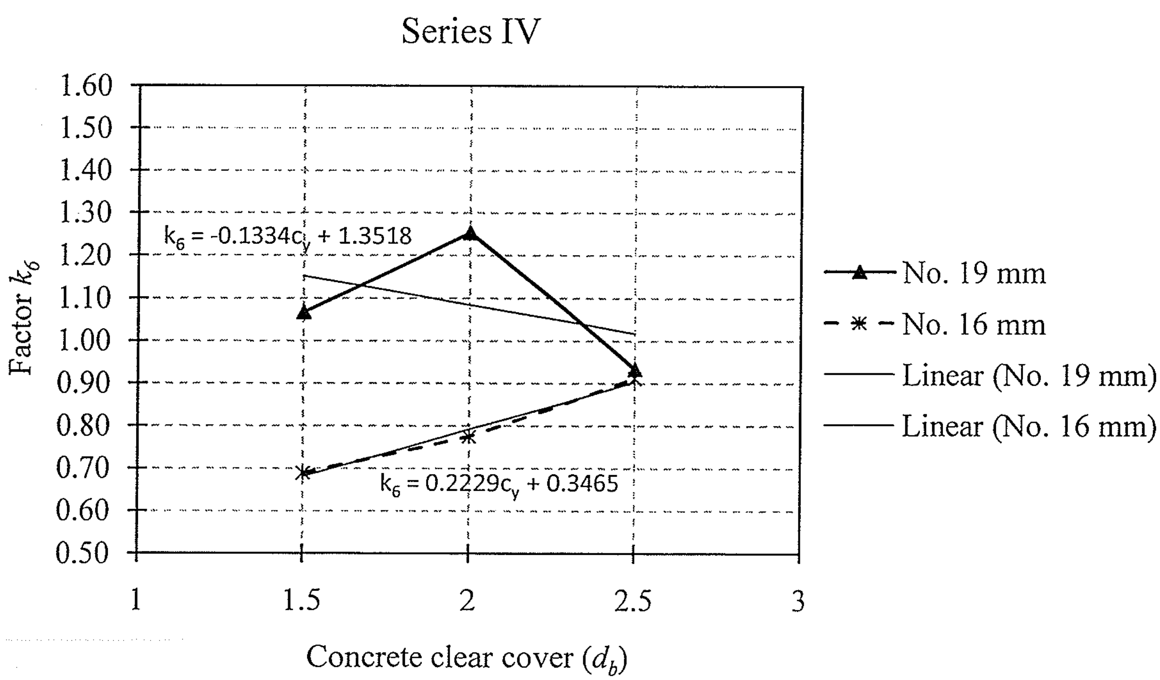

Fig. 4.33: Factor k_6 versus concrete clear cover: Series IV

Using mathematical manipulation, and solving a system of equations, the two approximation lines equations can be transformed into one, as follows:

Fatigue loading,

$$k_{6(d_b,c_y)} = (-0.0467d_b + 1.1667)c + (0.1367d_b - 2.0167)$$ **Equation 4-2**

Fatigue loading, freeze-thaw cycles and sustained loads

$$k_{6(d_b,c_y)} = (-0.1133d_b + 2.0333)c + (0.3267d_b - 4.8767)$$ **Equation 4-3**

Where c_y stands for concrete clear cover and d_b is the bar diameter. These equations are only valid for bars No. 16 and 19. Applying these equations, and multiplying these factors by the values obtained using the CAN/CSA-S6-06 (2006) the following curves can be plotted, where the term "Mod." in "CSA/S6-06 (2006) – Mod." stands for modified.

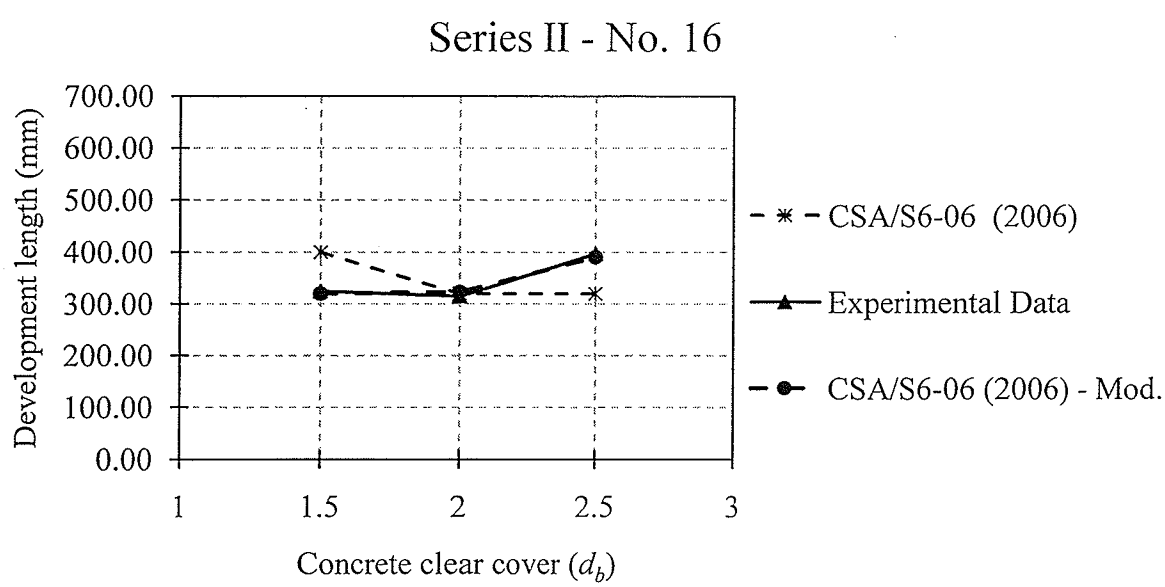

Fig. 4.34: Development length versus concrete clear cover: Series II and bar No. 16

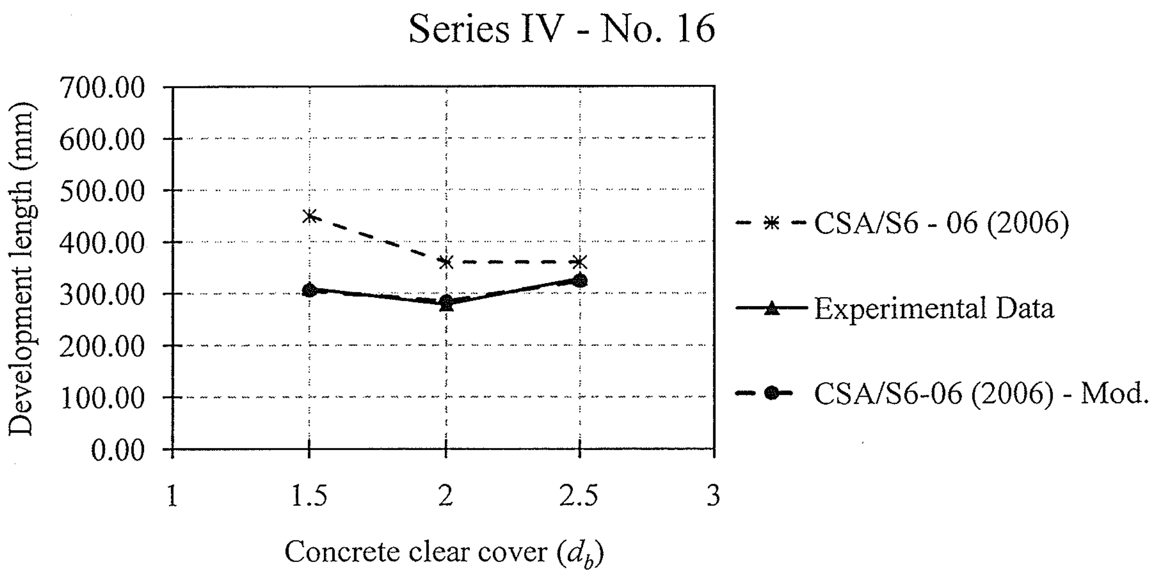

Fig. 4.35: Development length versus concrete clear cover: Series IV and bar No. 16

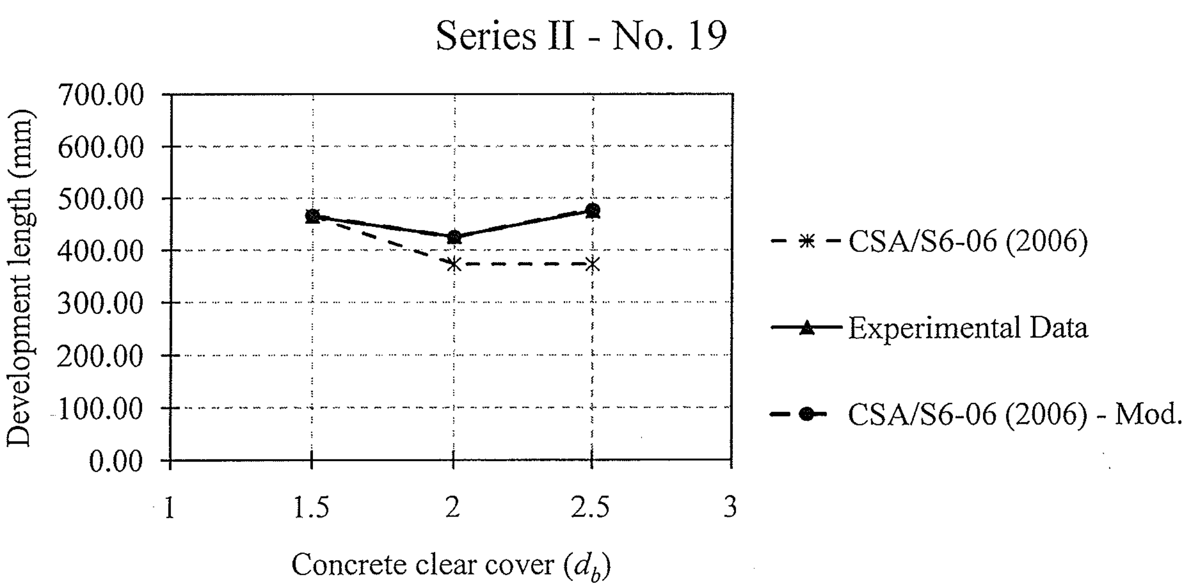

Fig. 4.36: Development length versus concrete clear cover; Series II and bar No. 19

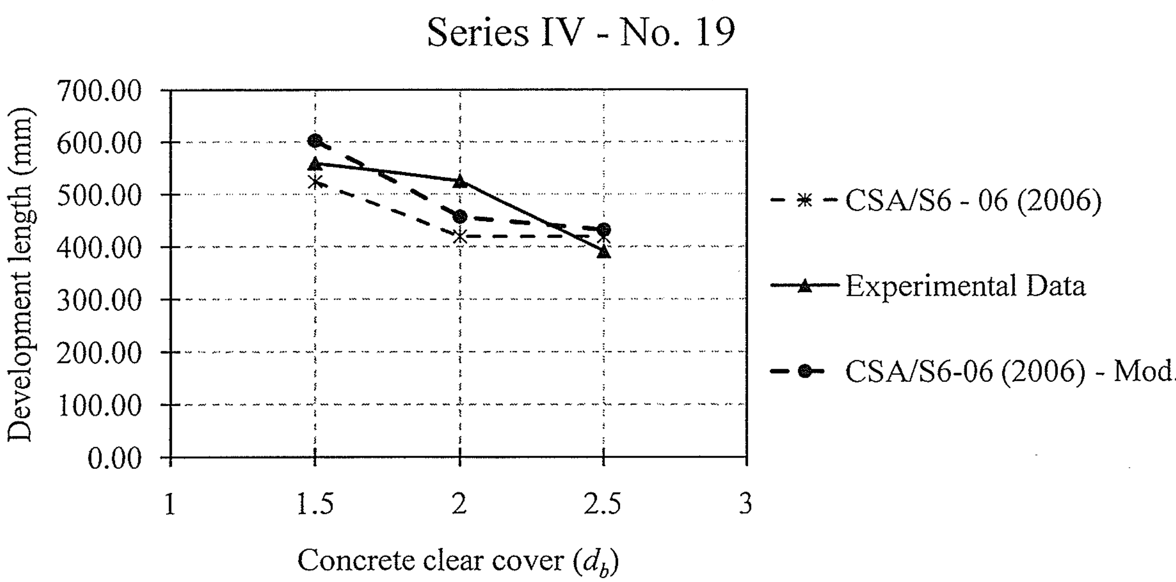

Fig. 4.37: Development length versus concrete clear cover: Series IV and bar No. 19

The best fitting curve for specimens with No. 19 bars in Series IV is not satisfactory. A more conservative approach would be to take factors k_6 greater than 1.0 and also to apply a safety coefficient prior to calculating equations 4.2 and 4.3.

The proposed equations are only valid for the tested bars No. 16 and 19. However, a flat (constant) value of 1.3 for the factor k_6 can be considered for structures subjected to fatigue loads, as shown in Figure 4.38, for S.FT.F.19. With the new coefficient, the modified equation from the CAN/CSA-S6-06 (2006) would be:

$$l_d = 0.45 . \frac{k_1 . k_4 . k_6}{\left(d_{cs} + k_{tr} . \dfrac{E_{frp}}{E_s} \right)} . \left(\frac{f_{frp,u}}{f_{cr}} \right) . A_{frp}$$

Equation 4-4

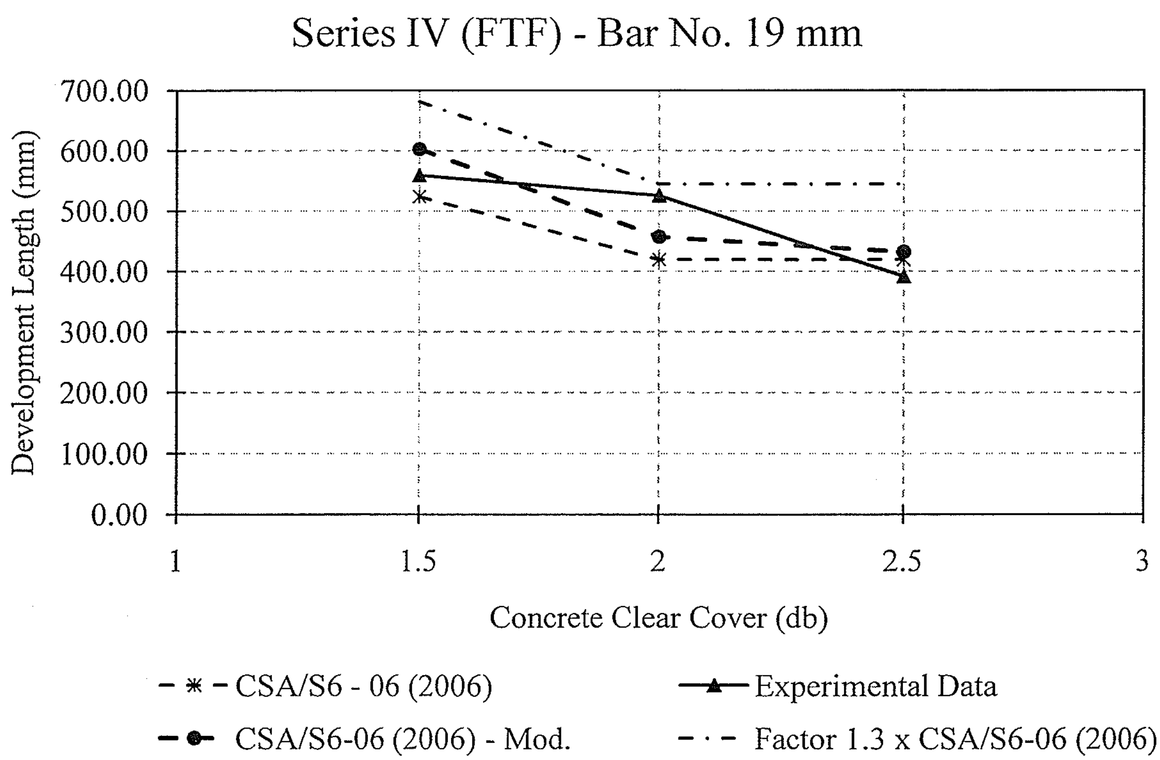

Fig. 4.38: Development length versus concrete clear cover: Series IV and bar No. 19

CHAPTER 5: SUMMARY AND CONCLUSIONS

5.1. Summary

In North America, bridge deck slabs and parking garages are prime examples where GFRP reinforcements are currently being used. These elements are continuously subjected to wide combinations of fatigue and/or sustained load from traffic as well as thermal loads due to freeze-thaw cycles and temperature fluctuations. Such environmental and loading conditions may affect the mechanical properties of the concrete itself, the FRP reinforcement, or bond between them. For reinforced concrete structures, the transfer of stresses between the concrete and the reinforcement, both at the serviceability and at the ultimate limit states, is strongly dependent on the quality of bond. Therefore, bond of FRP reinforcing bars to concrete elements subjected to harsh thermal and mechanical loads might be a critical design factor that needs to be investigated.

Currently, few to none experimental test data is available regarding the effects of freeze-thaw cycles, wet-dry cycles, high and low temperatures, as well as loading effects such as fatigue with constant and variable stress ranges, impact loads, sustained loads, among others (ISIS Canada 2006). To address these new necessities, this research presents an experimental study to investigate the influence of concrete cover and bar diameter on the bond strength and the failure mechanisms of glass FRP bars embedded in concrete after being conditioned by the individual or combined effects of freeze-thaw cycles, sustained loads, and fatigue loads.

The experimental program in this study, which contains 36 specimens, is divided into four series according to the conditioning scheme. Series (I) Control, unconditioned, specimens;

Series (II) Fatigue loading; Series (III) Freeze-thaw cycles along with sustained loads; Series (IV) Freeze-thaw cycles along with sustained loads followed by fatigue loading.

The conditioning of the specimens includes 250 freeze-thaw cycles, a sustained axial tensile load (30% of the guaranteed tensile strength of the GFRP bar, GTS) and 1,000,000 cycles of tensile fatigue loading (maximum stress of 25% of the GTS and a frequency of 1.5 Hz). Two bar sizes (No. 16 and 19) and three concrete clear covers (1.5, 2.0 and 2.5d_b) were investigated.

In addition, an analytical study was carried out to compare the experimental results to the available code predictions for the development length, ℓ_d, of FRP bars embedded in concrete. A coefficient factor, k_6, is proposed to be applied to the CHBDC (CSA 2006) predictions for ℓ_d taking into account the different environmental and loading conditions used in this study.

5.2. Conclusions

Based on the experimental results and analytical study, the following categorized conclusions can be drawn:

(a) Effect of conditioning:

1- Investigating the results of Series IV (freeze-thaw cycles and sustained load followed by fatigue loading), it can be concluded that the effect of fatigue loading is more dominant than the freeze-thaw cycles, since all specimens in Series IV showed significant loss in bond strength of at least 23%. However, no loss was greater than the loss due to the individual effect of fatigue loading. For specimens with No. 16 bars, it seems that the effect of fatigue loading counteracts that of the freeze-thaw cycles. While for specimens with No. 19 bars and covers of 1.5 and 2.0d_b, the adverse effects of both conditionings are added together.

2- In Series I (control specimens), it can be observed that by increasing the concrete clear cover, the failure mode changed. For specimens with No. 16 bars, the clear cover of 2.0d_b was enough to ensure the pure pullout failure, while for No. 19 bar the same concrete clear cover (2.0d_b) was not enough to prevent cracking. In Series II, the main failure mode was pure pullout, which further confirms the adverse effects of the fatigue loading on the bond strength. For specimens of Series III, only two pure pullouts occurred. This indicates that the developed bond stress was higher (23 to 47%) than that of specimens of Series I. However, in this case, the concrete condition also contributed to the splitting mechanism. The failure modes observed for specimens in Series IV appears to be a combination of those of Series II and III: half of the specimens failed in pure pullout and half failed by cracking.

(b) Effect of bar diameter:

3- It is interesting to note that both No. 16 and No. 19 bars exhibited approximately the same bond resistance for specimens in Series II. The difference in the bond strength between specimens with No. 16 and No. 19 bars, for 1.5, 2.0 and 2.5d_b cover was 23%, 16% and 3%, respectively, with No. 16 bars presenting the higher values of bond resistance. It seems that the 2.5d_b cover is enough to avoid micro-cracks in the concrete near the bar surface, and thus causes higher degradation in the sand-coating layer, since the concrete interface would be stronger. Also, in the case of specimens in

Series IV with $2.5d_b$ concrete cover, the bond strength for bars No. 16 and No. 19 was the same, with only a 2% difference, where No. 16 bars presenting the higher values. Therefore, smaller bar diameters seems to be more susceptible to fatigue loading. The reason is probably because the surface area of No. 16 bar is smaller than that of No. 19 bar, so it is more difficult to redistribute the load in the case of partial (local) loss of the sand-coating layer as a result of the cyclic loading.

4- Specimens with No. 19 bars were affected more by the freeze-thaw cycling and sustained loading compared to specimens with No. 16 bars. That is due to the fact that only No. 19 bars with the larger cover of 2.5 d_b were able to resist the thermal loads and present enhancement of bond resistance (25%), while all No. 16 bars presented higher values of bond resistance than unconditioned specimens (61, 44 and 27% for 1.5, 2.0 and $2.5d_b$, respectively). This is mainly due to the thermal expansion, which was more pronounced in the larger diameter bar. Therefore, the freeze-thaw conditioning promoted great deterioration in the bond stiffness and an increase in slip.

5- The values of bond strength obtained for No. 16 bars are higher than those for No. 19 (at least 10, 3, 35 and 2% for Series I; II, III and IV, respectively). This observation is also in agreement with previous research (Benmokrane et al. 1996; Larralde and Silva-Rodriguez 1993; Nanni et al. 1995; Achillides and Pilakoutas 2004).

(c) Effect of concrete clear cover:

6- It seems that a concrete clear cover of $2.0d_b$ is an optimum for sand-coated GFRP bars. However, if subjected to the effect of freeze-thaw cycles, bar No. 19 presented 25%

higher bond resistance than unconditioned specimens for the larger concrete cover of $2.5d_b$.

7- In Series I, it was observed that an increase in the concrete confinement provided by the large concrete cover (more than $3.5d_b$) resulted in a decrease in the bond resistance of up to 23%. The reason for such decrease is thought to be due to concrete behaviour, where the plasticity is less pronounced in larger concrete covers. These observations are in agreement with the findings of other researchers (Tepfers et al. 1998; Tepfers 2003; Tepfers 2004; Malvar et al. 2003; Esfahani et al. 2005; Galati et al. 2005).

(d) Effect of sustained load:

8- Significant increase in the GFRP bars strain of at least 18% was observed for all specimens that were subjected to sustained loading. These findings differ from the findings of Hattori et al. (1995) and Laoubi et al. (2006), who tested beam specimens. They concluded that the effects of sustained load in flexural elements are negligible and mainly controlled by the concrete creep behaviour. Therefore, it seems that the effects of sustained axial tension loads are more severe than flexural sustained loads. Also, residual strains of at least 10% were observed after the sustained load was removed.

9- It seems that No. 16 bars were more affected by the sustained load than No. 19 bars. The increase in strains for No. 16 bars was at least 39% while for No. 19 bars it was only 18%. As for the residual strains, No. 16 bars presented up to 29% compared to 21% for No. 19 bars. The increase in strains and residual strains became more significant as the concrete cover increases for No. 16 bars. For No. 19 bars, it seems that the concrete clear cover of $2.0d_b$ is an optimum, presenting the smallest increase in strain and residual strains.

(e) Development Length Analysis:

10- For specimens in Series II and IV with No. 16 bars, it seems that, for higher confinement provided by the large concrete clear cover of $2.5d_b$, the CAN/CSA-S6-06 (CSA 2006) gives up to 24% smaller values for development length, becoming slightly un-conservative. It is interesting to observe that with the presence of the freeze-thaw conditioning, the bond strength was slightly higher (21%) providing smaller development length and, thus, changing the CAN/CSA-S6-06 (CSA 2006) to more conservative values. In case of No.19 bars, the values obtained for development length using the experimental data are up to 28% higher than those calculated using the CAN/CSA-S6-06 (CSA 2006) equation.

11- Two equations are proposed to calculate a conditioning coefficient k_6 to be used with the current equation in the CAN/CSA-S6-06 (CSA 2006). These equations are only valid for the tested bars No. 16 and 19. However, a flat (constant) value of 1.3 for the factor k_6 can be considered for structures subjected to fatigue loading.

(f) General:

12- Conditioning with freeze-thaw cycles and sustained loading resulted in significant deterioration in the concrete itself. This was confirmed by standard compressive and splitting tests on cylinder samples. The concrete compressive and tensile strengths were reduced by 10.7 and 15.8%, respectively.

13- An investigation was carried out to analyse the cracking pattern of all specimens. Bond strength values were calculated considering the cracks penetration depths and angles along with the plastic behaviour of concrete. The obtained bond strength values were fairly close to those obtained experimentally (variation ranged from 0.5 to 19.9% as in Appendix B).

5.3. Recommendations for Future Work

Based on the performed experimental and analytical studies, recommendations for futures work would be to investigate:

- A wider range of FRP bars sizes (No. 2 to No. 25),
- Other types of fibre (carbon and aramid),
- Bar surface patterns (wrapped, deformed, wrapped with sand-coating),
- Embedment lengths ($5d_b$ to $20d_b$),
- Scheme of fatigue loading (amplitude, frequency, reversal or tension-compression cycles),
- Wet-dry cycles along with sustained loads.

REFERENCES

Abrishami, H. and Mitchel, D. (1993). "Simulation of uniform bond stress." *ACI Materials Journal*, Vol. 89, No. 2, pp. 161-168.

Achillides, Z. and Pilakoutas, K. (2004). "Bond behaviour of fibre reinforced polymer bars under direct pullout conditions." ASCE, *Journal of Composites for Construction*, Vol. 8, No. 2, pp. 173-181.

ACI Committee 440. (1996). "State-of-the-art report on fibre reinforced plastic (FRP) reinforcement for concrete structures." *ACI 440R-96*, American Concrete Institute, Farmington Hills, Detroit, p. 65.

ACI Committee 440. (2006). "Guide for the design and construction of structural concrete reinforced with FRP bars." *ACI 440.1R-06*, American Concrete Institute, Farmington Hills, Detroit, 44 p.

Aiello, M., Foccaci, F., Hunag, P. and Nanni, A. (1999). "Cracking of concrete cover in FRP reinforced concrete elements under thermal loads." *Proceedings of the 4th International Symposium on FRP for Reinforcement of Concrete Structures,* FRPRCS4, Baltimore, MD, Nov. , pp. 233-243.

Aiello, M. (1999). "Concrete cover failure in FRP reinforced beams under thermal loading." ASCE, *Journal of Composites for Construction*, Vol. 3, No. 1, pp. 46-52.

Aiello, M., Focacci, F. and Nanni, A. (2001). "Effects of thermal loads on concrete cover of fibre reinforced polymer reinforced elements: theoretical and experimental analysis." *ACI Materials Journal*, Vol. 98, No. 4, pp 332-339.

Aly, R. (2007). "Stress along tensile lap-spliced fibre reinforced polymer reinforcing bars in concrete." *Canadian Journal of Civil Engineering*, Vol. 34, pp. 1149-1158.

Al-Dulaijan, S., Nanni, A., Al-Zahrani, M., Bakis, C. and Boothby, T. (1996). "Bond evaluation of environmentally conditioned GFRP/concrete systems." *Advanced Composites Materials in Bridges and Structures*, Canadian Society for Civil Engineering, CSCE, Quebec, pp. 845-852.

Al-Zahrani, M. Al-Dulaijan, S., Nanni, A., Bakis, C. and Boothby, T. (1999). "Evaluation of bond using FRP rods with axisymmetric deformations." Elsevier, *Construction and Building Materials*, Vol. 13, pp. 299-309.

ASM International (1987). "Engineered materials handbook. Volume 1 – Composites." *Metals park*, Ohio, USA, 983 p.

ASM International (1988). "Engineered materials handbook. Volume 2 – Composites." *Metals park*, Ohio, USA, 883 p.

Bakis, C., Al-Dulaijan, S., Nanni, A., Boothby, T. and Al-Zahrani, M. (1998). "Effect of cyclic loading on bond behaviour of GFRP rods embedded in concrete beams." *Journal of Composites Technology and Research*, JCTRER, Vol. 20, No. 1, pp. 29-37.

Bank, L., Puterman, M. and Katz, A. (1998). "The effect of material degradation on bond properties of fibres reinforced plastic reinforcing bars in concrete." *ACI Materials Journal*, Vol. 95, No. 3, pp. 232-243.

Benmokrane, B., Tighiouart, B. and Chaallal, O.(1996). "Bond strength and load distribution of composite GFRP reinforcing bars in concrete." *ACI Materials Journal*, Vol. 93, No. 3, pp. 246-253.

Canadian Standards Association (CSA). (2002). "Design and construction of building components with fibre reinforced polymers." *CAN/CSA-S806-02*, Canadian Standards Association, Toronto, 206 p.

Canadian Standards Association (CSA). (2006). "Canadian highway bridge design code-section 16, updated version for public review." *CAN/CSA-S6-06*, Canadian Standards Association, Toronto, 33 p.

Chaallal, O. and Benmokrane, B. (1993). "Pullout and bond of glass-fibre rods embedded in concrete and cement grout." RILEM, *Materials and Structures Journal*, Vol. 26, pp. 167-175.

Cosenza, E., Manfredi, G. and Realfonzo, R. (1996). "Bond characteristics and anchorage length of FRP rebars." *Advanced Composites Materials in Bridges and Structures*, Canadian Society for Civil Engineering, CSCE, Quebec, pp. 909-916.

Cosenza, E., Manfredi, G. and Realfonzo, R. (1997). "Behaviour and modeling of bond of FRP rebars to concrete." ASCE, *Journal of Composites for Construction*, Vol. 1, No. 2, pp.40-51.

Edwards, A. and Yannopoulos, P. (1978). "Local bond-stress-slip relationships under repeated loading." *Magazine of Concrete Research*, Vol. 30, No. 103, pp. 62-72.

Esfahani, M., Kianoush, M. and Lachemi, M. (2005). "Bond strength of glass fibre reinforced polymer reinforcing bars in normal and self consolidating concrete." *Canadian Journal of Civil Engineering*, Vol. 32, pp. 553-560.

Faoro, M.(1996). "The influence of stiffness and bond of FRP bars and tendons on the structural behaviour of reinforced concrete members." *Advanced Composites Materials in Bridges and Structures*, Canadian Society for Civil Engineering, CSCE, Quebec, pp. 885-892.

Focacci, F., Nanni, A. and Bakis, C. (2000). "Local bond-slip relationship for FRP reinforcement in concrete." ASCE, *Journal of Composites for Construction*, Vol. 4, No. 1, pp. 24-31.

Galati, N., Nanni, A., Dharani, L., Focacci, F. and Aiello, A. (2005). "Thermal effects on bond between FRP rebars and concrete." *Elsevier – Composites: Part A*, pp. 1223-1230.

Gentry, T. and Husain, M. (1999). "Thermal compatibility of concrete and composite reinforcements." ASCE, *Journal of Composites for Construction*, Vol. 03, No. 02, pp. 82-86.

Hattori, A., Inoue, S., Miyagawa, T. and Fujii, M. (1995). "A study on bond creep behaviour of FRP rebars embedded in concrete." *Non-Metallic (FRP) Reinforcement for Concrete Structures*, pp. 172-179.

He, Z. and Sun, Y. (2006). "Experimental study on bond behaviour of GFRP rod in concrete subjected to stress reversal." *Federation Internationale du Beton* (FIB), Session 10. ID 10-29.

ISIS Canada. (2006). "Durability of fibre reinforced polymers in civil infrastructure" Technical Report, *The Canadian Network of Centres of Excellence on Intelligent Sensing for Innovative Structures*. ISIS Canada, Winnipeg, Manitoba, 213 p.

ISIS Canada. (2007). "Reinforcing concrete structures with fibre reinforced polymers." ISIS-Manual No.3, version 2, *The Canadian Network of Centres of Excellence on Intelligent Sensing for Innovative Structures*, ISIS Canada, Winnipeg, Manitoba, 98 p.

ISIS Canada. (2008). "Strengthening reinforced concrete structures with externally-bonded fibre reinforced polymers." ISIS-Manual No.4, version 2, *The Canadian Network of Centres of Excellence on Intelligent Sensing for Innovative Structures*, ISIS Canada, Winnipeg, Manitoba, 88 p.

Katz, A., Berman, N. and Bank, L. (1999). "Effect of high temperatures on bond strength of FRP rebars." ASCE, *Journal of Composites for Construction*, Vol. 3, No 2, pp. 73-81.

Katz, A. (2000). "Bond to concrete of FRP rebars after cyclic loading." ASCE, *Journal of Composites for Construction,* Vol. 4, No. 3, pp. 137-144.

Klowak, C., Memon, A. and Mufti, A. (2007). "Static and fatigue investigation of innovative second-generation steel-free bridge decks." *Canadian Journal of Civil Engineering*, Special Issue on Intelligent Sensing for Innovative Structures, Vol. 34, pp. 331-339.

Koller, R., Chang, S. and Xi, Y. (2007). "Fibre-reinforced polymer bars under freeze-thaw cycles and different loading rates." *Journal of Composite Materials*, Vol. 41, No. 1, pp. 5-25.

Laoubi, K., El-Salakawy, E. and Benmokrane, B. (2006). "Creep and durability of sand-coated glass FRP bars in concrete elements under freeze/thaw cycling and sustained loads." Elsevier, *Cement and Concrete Composites*, Vol.28, pp. 869-878.

Larralde, J. and Silva-Rodriguez (1993). "Bond and slip of FRP rebars in concrete." ASCE, *Journal of Materials in Civil Engineering*, Vol. 5, No. 1, pp 30-40.

Mac Gregor, J. and Wight, J. (2005). "Reinforced concrete: mechanics and design." 4th Edition, Prentice Hall, NY.

Malvar, J. (1995). "Tensile and bond properties of GFRP reinforcing bars." *ACI Materials Journal*, Vol. 92, No. 3, pp. 276-285.

Malvar, L., Cox, J. and Cochran, K. (2003). "Bond between carbon fibre reinforced polymer bars and concrete I: experimental study."ASCE, *Journal of Composites for Construction*, Vol. 7, No. 2, pp. 154-163.

Mashima, M. and Iwamoto, K. (2004). "Bond characteristics of FRP rod and concrete after freezing and thawing deterioration." *ACI Structural Journal*, Vol. 138, pp. 51-70.

Micelli, F. and Nanni, A. (2004). "Durability of FRP rods for concrete structures." Elsevier, *Construction and Building Materials*, Vol. 18, pp. 491-503.

Nanni, A., Al-Zaharani, M., Al-Dulaijan, S., Bakis, C. and Boothy, T. (1995). " Bond of FRP reinforcement to concrete – experimental results." *Non-Metallic (FRP) Reinforcement for Concrete Structures*. London, ISBN 0 419 20540 3.

Park, R. and Paulay, T. (1975). "Reinforced concrete structures." Wiley-Interscience, 769 p.

Pecce, M., Manfredi, G., Realfonzo, R. and Cosenza, E. (2001). "Experimental and analytical evaluation of bond properties of GFRP bars." ASCE, *Journal of Materials in Civil Engineering*, Vol. 13, No. 4, pp. 282-290.

Pulltral Inc. (2007). V-ROD "Product guide specification." Thetford Mines, Quebec, March 2007.

Rossetti, A. and Galeota, D. (1995). "Local bond stress-slip relationship of glass fibre reinforced plastic bars embedded in concrete." RILEM, *Materials and Structures*, Vol. 25, pp. 340-344.

Shahidi, F., Wegner, L. and Sparting, B. (2006). "Investigation of bond between fibre-reinforced polymer bars and concrete under sustained loads." *Canadian Journal of Civil Engineering*, Vol. 33, pp.1426-1437.

Soudki, K., El-Salakawy, E., and Craig, B. (2007). "Behaviour of CFRP strengthened reinforced concrete beams in corrosive environment." ASCE, *Journal of Composites for Construction,* Vol. 11, No. 3, pp. 291-298.

Tastani, S., Pantazopoulou, S. and Karvounis, P. (1984). "Local bond–slip characteristics of GFRP bar." *ACI Structural Journal*, Vol. 2, No. 230, pp 1481-1496.

Tepfers, R. (1973). "A theory of bond applied to overlapped tensile reinforcement splices for deformed bars." *Doctoral Thesis*. Work No. 723, Publ 73:2. Division of Concrete Structures, Chalmers University of Technology, Göteborg, May 1973, 328 p.

Tepfers, R. (1983). "Lapped tensile reinforcement splices." *Journal of the Structural Division*, Proceedings of the American Society of Civil Engineers, ASCE, Vol. 108, No. ST1, pp. 289-301.

Tepfers, R., Hedlund, G. and Rosinski, B. (1998). "Pull-out and tensile reinforcement splice tests with GFRP bars." *Second International Conference on Composites in Infrastructure*, ICCI-98, Tucson, Arizona, January 1998, pp. 37-51.

Tepfers, R., Tamuzs, V., Apinis, R. and Modniks, J. (2000). "Centric and eccentric pull-out tests for estimation of bond splitting tendency of FRP reinforcement." Nordic Concrete Research, Vol. 23, pp. 152-154.

Tepfers, R. (2003). "Bond of FRP reinforcement in concrete – a challenge." *Mechanics of Composite Materials*, Vol. 39, No. 4, pp. 315-328.

Tepfers, R. (2004). "Bond clause proposal for FRP-bars/rods in concrete based on CEB/FIP model code 90 with discussion of needed tests." *Department of Structural Engineering and Mechanics - Concrete Structures*, Chalmers University of Technology, Sweden, Report no. 04:2, Archive No. 120.

Toutanji, A. and Gomez, W. (1997). "Durability characteristics of concrete beams externally bonded with FRP composite sheets." Elsevier, *Cement and Concrete Composites*, Vol. 19, No. 4, pp. 351-358.

Wanbeke, B. and Shield, C. (2006). "Development length of glass fibre-reinforced polymer bars in concrete." *ACI Structural Journal*, Vol. 103, No. 1, pp. 11-17.

Weber, A. (2005). "Bond properties of newly developed composite rebar." *Proceedings of the International Symposium on Bond Behaviour of FRP in Structures,* BBFS 2005, International Institute for FRP in Construction, Hong Kong, China, December, pp. 379-384.

Won, J. and Park, C. (2006). "Effect of environmental exposure on the mechanical and bonding properties of hybrid reinforcing bars for concrete structures." *Journal of Composite Materials*, Vol. 40, No. 12, pp. 1063-1074.

APPENDICES

APPENDIX A

A.1. TEMPERATURE AND STRAINS

Series III and IV where submitted to 250 freeze-thaw cycles along with a sustained load of 30% of the GFRP bar guaranteed tensile strength. Two specimens from each series presented thermocouples at bar level and all of them had a strain gauge connected to the GFRP bar. The figure bellow presents two cycles of freezing and thawing. The temperature ranged between -16°C to +16°C inside the specimens. One of the thermocouples was lost.

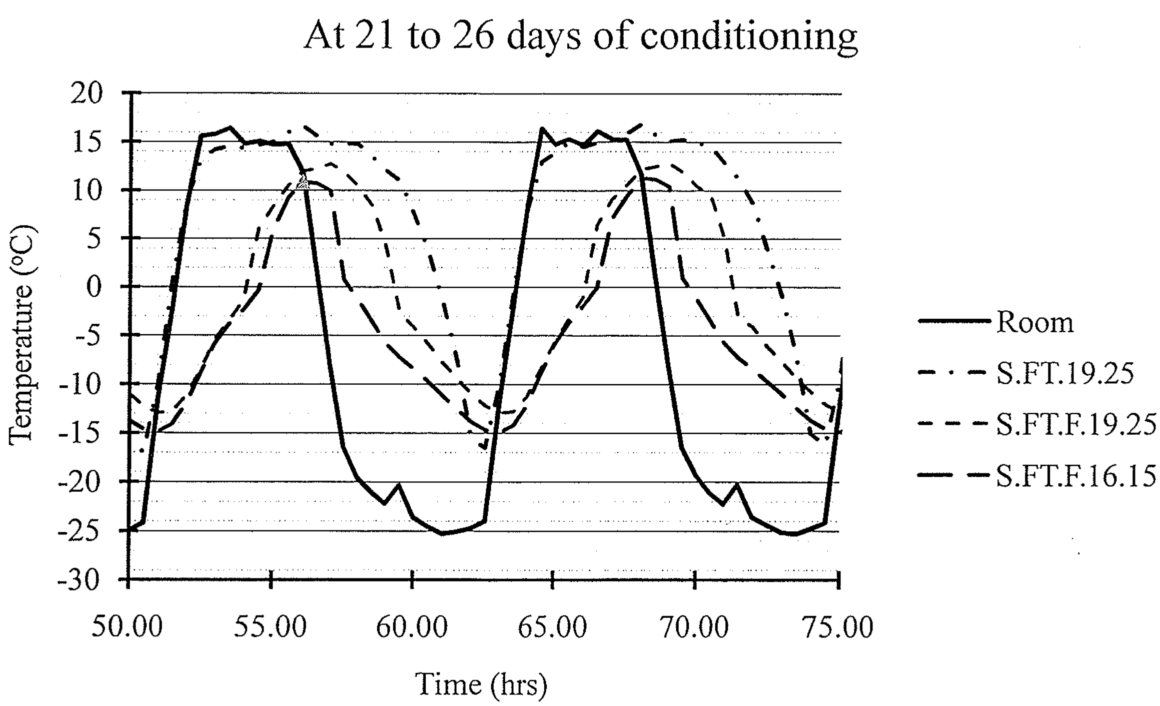

Fig. A.1: Specimen behaviour under freeze-thaw cycles at 21 to 26 days of conditioning

A.2. Concrete Deterioration

The freeze-thaw conditioning along with sustained axial tensile load promoted significant deterioration in the concrete matrix of specimens in Series III and IV. In figures A.3 and A.4 it is possible to see the degraded concrete.

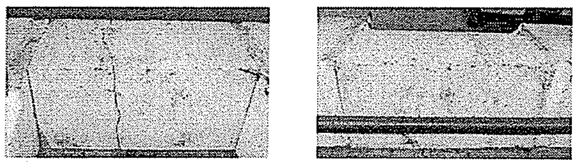

S.FT.16.15

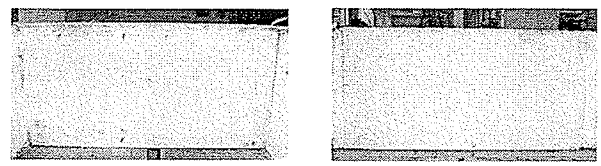

S.FT.19.15

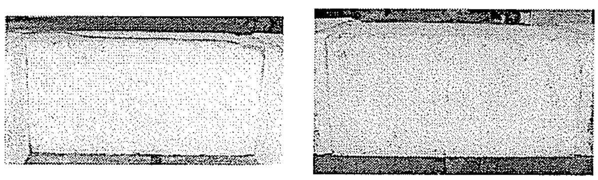

S.FT.16.20

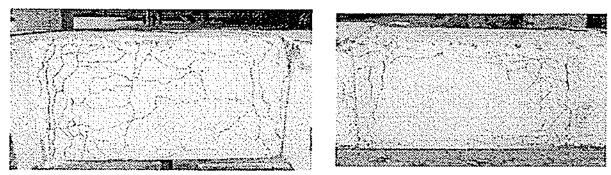

S.FT.19.20

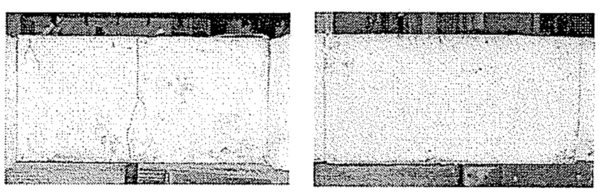

S.FT.16.25

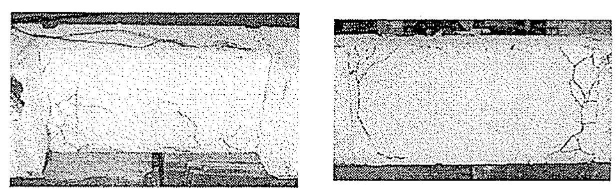

S.FT.19.25

Fig. A.2: Concrete deterioration: Series III

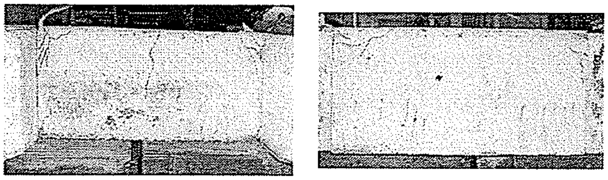

S.FT.F.16.15

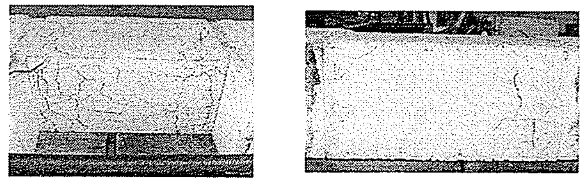

S.FT.F.19.15

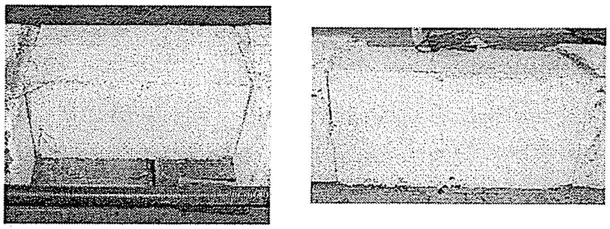

S.FT.F.16.20

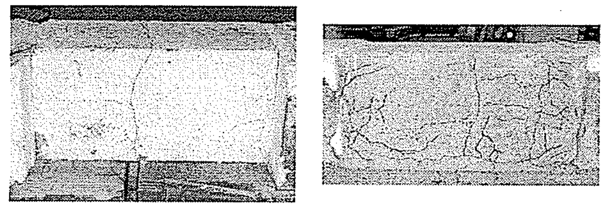

S.FT.F.19.20

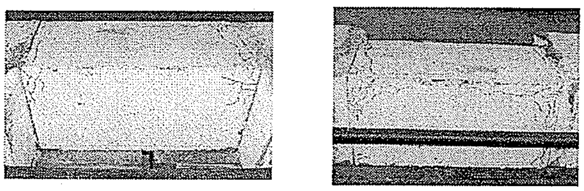

S.FT.F.16.25

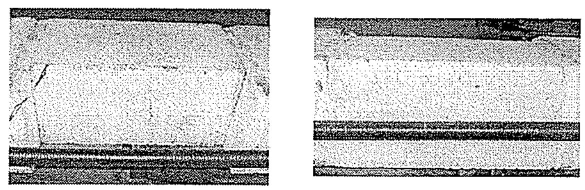

S.FT.F.19.25

Fig. A.3: Concrete deterioration: Series IV

It can be noticed in the figures above that greater deterioration was observed in the specimens with bar No. 19 rather than in the specimens with bar No. 16 for both Series III and IV. This fact is related to the difference in the coefficients of thermal expansion (CTE) and Poisson ratio encountered between the concrete and GFRP bars. The cross-sectional area of bars No. 19 is larger than bars No. 16, and therefore, will lead to more expansion and, consequently more damage in the surrounding concrete. Such thermal stresses may lead to longitudinal cracks, as is observed in specimens with bar No. 19.

Also great deterioration was observed in the concrete cylinders, which were submitted to the same freeze-thaw cycles as the specimens. These were used to obtain the values for the concrete compressive strength as well as the tensile strength.

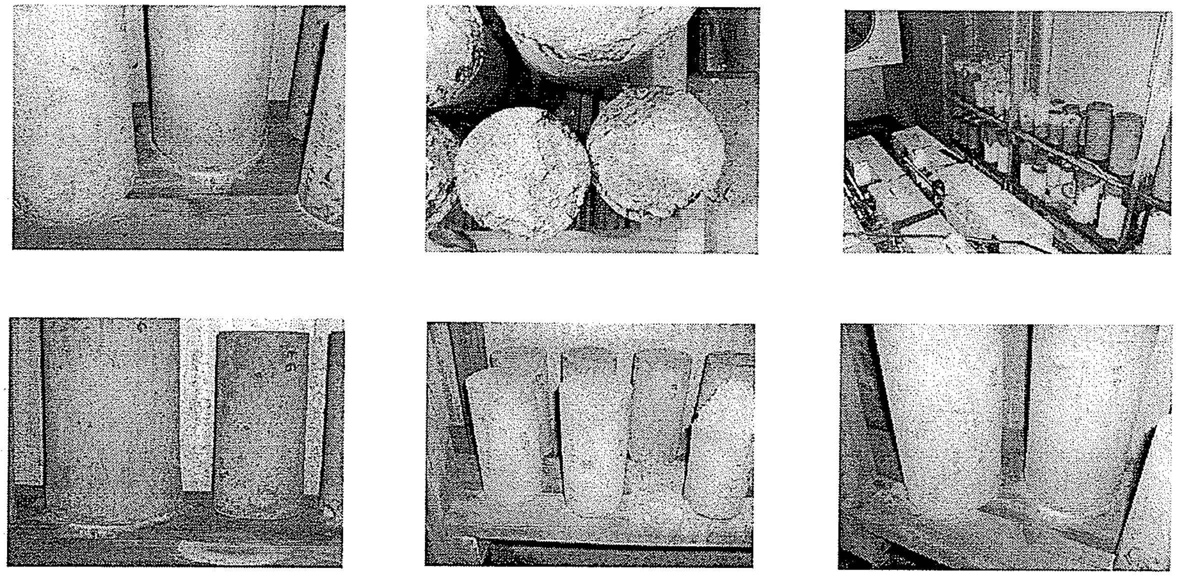

Fig. A.4: Cylinders deterioration

Some of the cylinders were so deteriorated that it couldn't be tested. Others had major circumferential cracks as can be seen in the figure above.

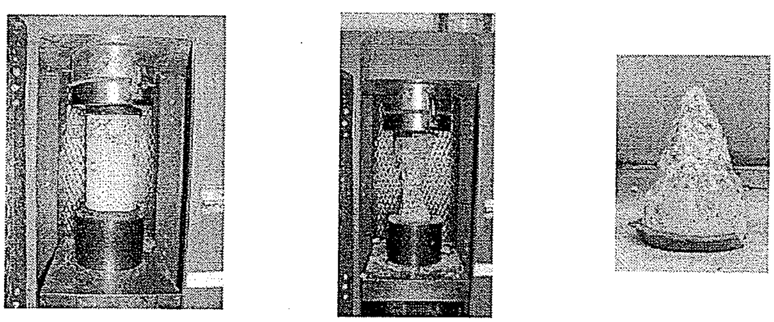

Fig. A.5: Testing of conditioned cylinders

The following tables present the values for concrete compressive and tensile strength obtained for the different series. The 28-days strength as well as strength at testing is provided.

TABLE A.1: Cylinders: Series I

Period	Compressive strength (MPa)	Tensile strength (MPa)
At 28 day*	48.6	3.2

*Same as testing

TABLE A.2: Cylinders: Series II

Period	Compressive strength (MPa)	Tensile strength (MPa)
Before conditioning (at 28 day)	50.3	3.2
After conditioning (at testing)	53.2	3.8

It can be noticed that the concrete compressive strength presented 5.8 % increase while in the tensile strength the increase reached 18.8 %.

TABLE A.3: Cylinders: Series III

Period	Compressive strength (MPa)	Tensile strength (MPa)
Before conditioning (at 28 day)	50.6	3.8
After conditioning (at testing)	45.2	3.2

It can be noticed that the concrete compressive strength presented 10.7 % degradation while in the tensile strength the degradation reached 15.8 %.

TABLE A.4: Cylinders: Series IV

Period	Compressive strength (MPa)	Tensile strength (MPa)
Before conditioning (at 28 day)	50.2	2.9
After conditioning (at testing)	46.1	3.4

It can be noticed that the concrete compressive strength presented 8.2 % degradation while in the tensile strength there was an increase of 10.3 %.

APPENDIX B

ANALYTICAL INVESTIGATION

In this appendix, the crack pattern was investigated. By considering the state of concrete – as elastic, partly cracked or plastic – and the dimension of the cracks, an analytical investigation was done.

The Figure B.1 presents the moment in which failure occurs. It considers that there was a previous crack, in the smaller concrete cover and it also considers the full plasticization of the concrete, where the crack will appear once the stress in the entire crack path is equal to the concrete tensile strength (Tepfers 2004).

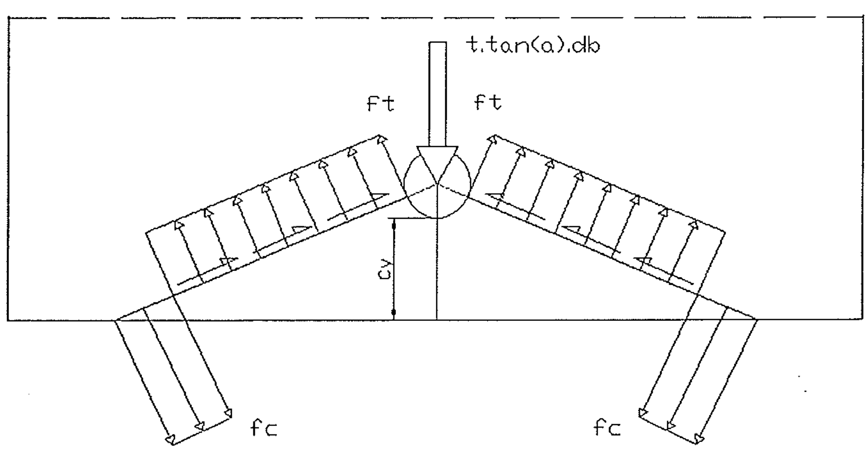

Fig. B.1: Stresses at failure; plastic stage

This formulation is rather complex and impractical. Besides, the concrete rarely achieves full plasticization. This formulation can be substituted disregarding the compression and the shear stresses, and also the first crack. A Partly cracked stage is considered, which is more reasonable and a linear stress distribution is considered. The simplification is presented in the Figure B.2.

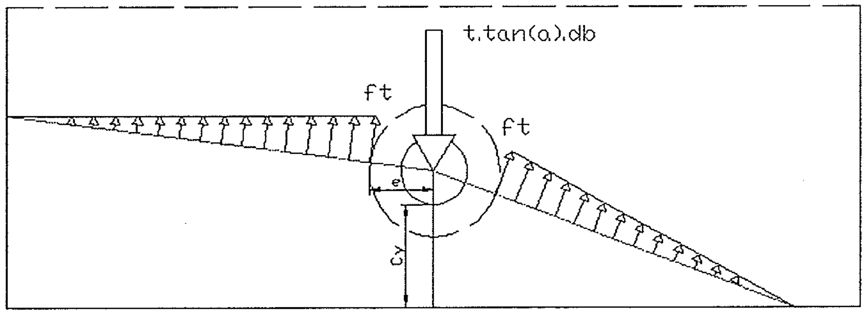

Fig. B.2: Stresses at failure – simplified model; partly cracked behaviour

The depth of the cracked concrete ring can be obtained through differential equations and is given by,

$$e = 0.486.\left(c_y + \frac{d_b}{2}\right)$$ **Equation B-1**

In the above equation c_y is the concrete clear cover and d_b is the bar diameter. The figure bellow presents the crack patter of control specimens.

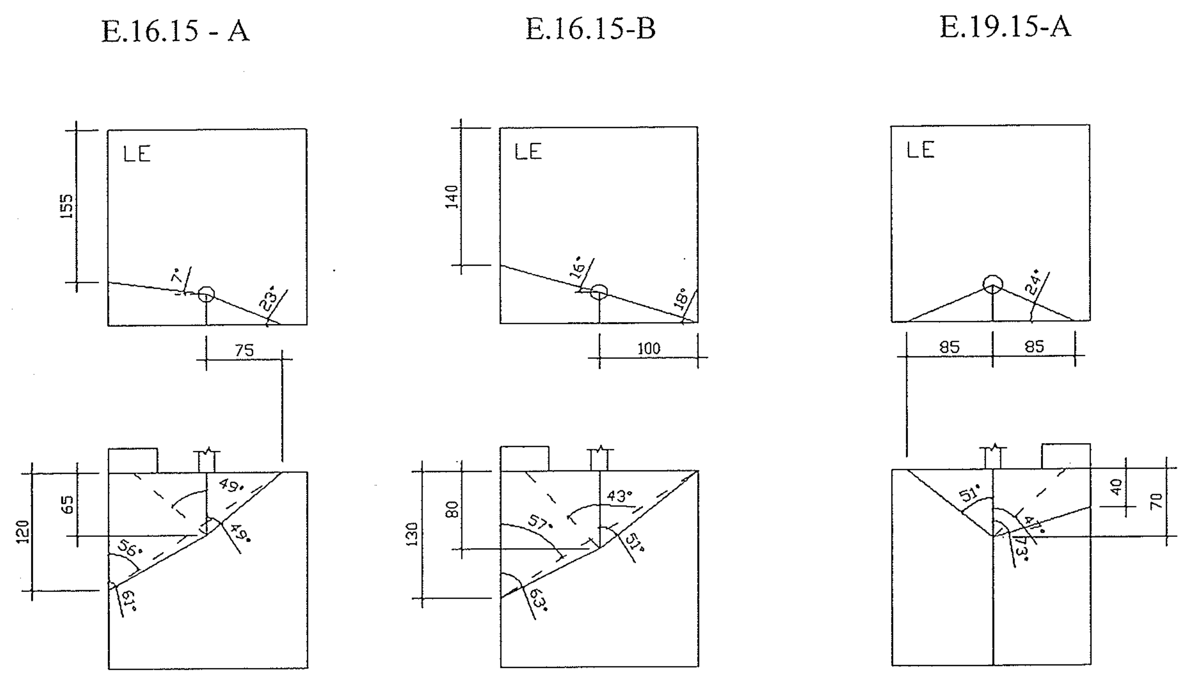

Fig. B.3: Crack pattern of specimens in Series I: top view from loaded-end (LE) and side view

TABLE B.1: Calculated bond strength: Series I

Specimen	Exp. bond strength (MPa)	α (^{o})*	τ (MPa)	Error (%)
E.16.15-A	11.27	49	12.59	11.70
E.16.15-B	12.00	57	11.05	7.92
E.19.15-A	10.84	47	10.71	1.20

*Obs.: Measured values (see Fig. B.3)

Through the presented errors in Table B.1, it can be seen that such method for calculating the final load from the crack pattern is very reasonable and very simple.

F.16.20-A F.19.15-A

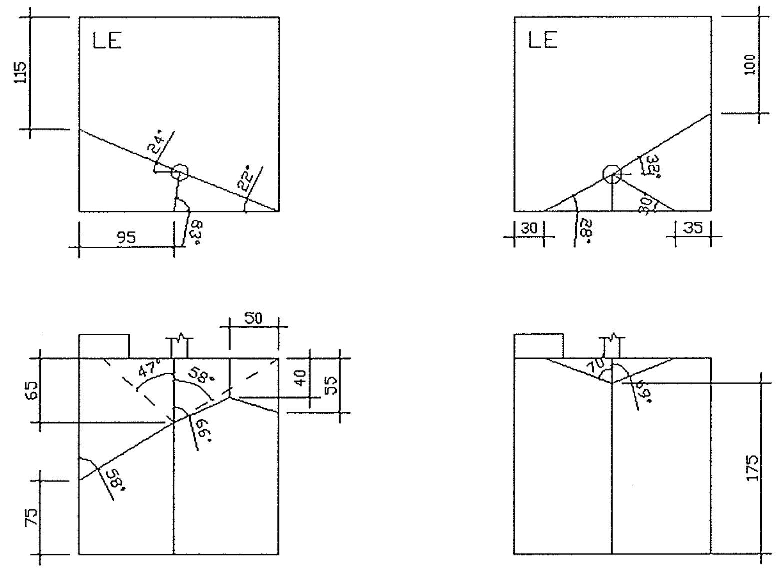

Fig. B.4: Crack pattern of specimens in Series II: top view from loaded-end (LE) and side view

TABLE B.2: Calculated bond strength: Series II

Specimen	Exp. bond strength (MPa)	α (^{o})	τ (MPa)	Error (%)
F.16.20-A	6.75	66	8.75	30.00
F.19.15-A	6.79	70	6.76	0.49

S.FT.15-A S.FT.16.15-B S.FT.16.20-A

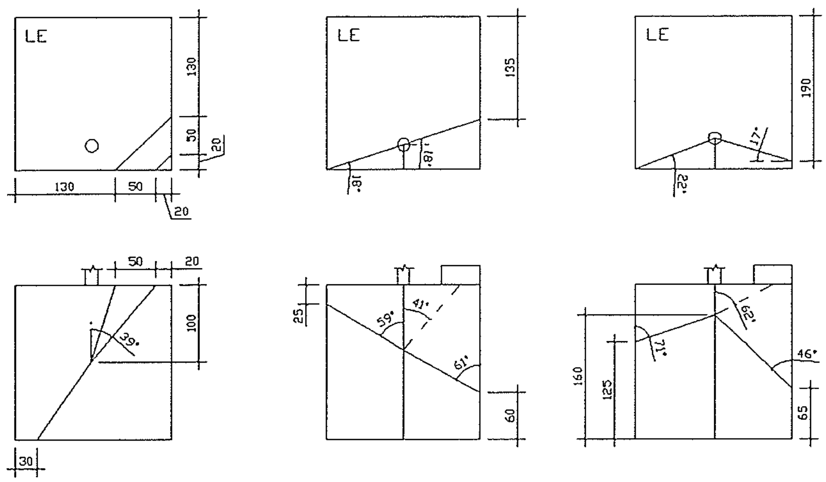

Fig. B.5: Crack pattern of specimens in Series III: top view from loaded-end (LE) and side view; bar No. 16

S.FT.19.15-A S.FT.19.20-A S.FT.19.20-B S.FT.19.25-A

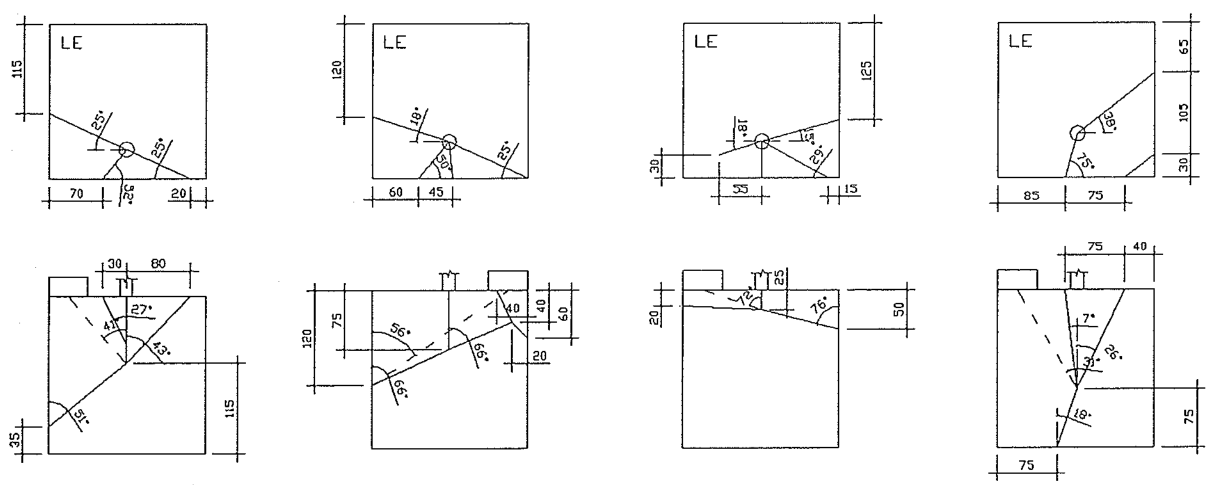

Fig. B.6: Crack pattern of specimens in Series III: top view from loaded-end (LE) and side view; bar No. 19

TABLE B.3: Calculated bond strength: Series III

Specimen	Exp. bond strength (MPa)	Concrete behaviour					
		Partly cracked			Plastic		
		α (^{o})	τ (MPa)	Error (%)	α (^{o})	τ (MPa)	Error (%)
S.FT.16.15-A	17.56	39	18.37	4.66			
S.FT.16.15-B	19.85	41	18.97	4.40			
S.FT.16.20-A	21.21				62	19.40	8.54
S.FT.19.15-A	9.25	51	11.09	19.86			
S.FT.19.20-A	10.91	56	10.08	7.61			
S.FT.19.20-B	10.08				72	11.80	17.06
S.FT.19.25-A	12.85	31	11.88	7.55			

Table B.3 shows the results for Series III. It can be observed that apart from considering the partly cracked stage, the plastic behaviour of concrete was also investigated, once the results for partly cracked behaviour were not accurate.

S.FT.F.16.15-A S.FT.F.16.15-B S.FT.F.16.20-B S.FT.F.19.20-B

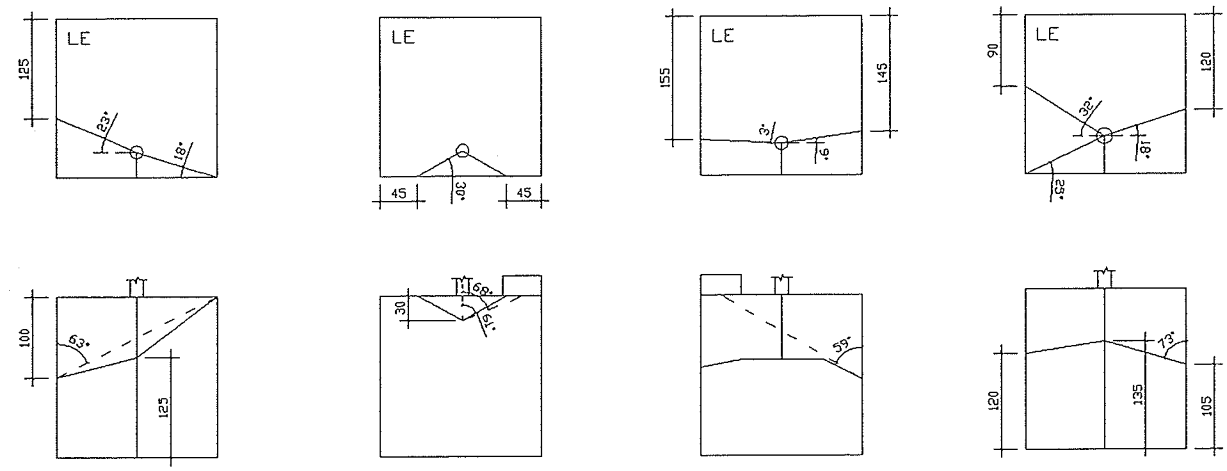

Fig. B.7: Crack pattern of specimens in Series IV: top view from loaded-end (LE) and side view

TABLE B.4: Calculated bond strength: Series IV

Specimen	Exp. bond strength (MPa)	Concrete behaviour: Partly cracked α (°)	τ (MPa)	Error (%)	Plastic α (°)	τ (MPa)	Error (%)
S.FT.F.16.15-A	8.39	63	9.08	8.22			
S.FT.F.16.15-B	8.94				68	9.40	5.15
S.FT.F.16.20-B	10.77	59	10.31	4.27			
S.FT.F.19.20-B	5.54	73	6.38	15.00			

The same observations which were made for Series III, apply here.